National Library of Canada

Acquisitions and Bibliographic Services Branch

395 Wellington Street
Ottawa, Ontario
K1A 0N4

Bibliothèque nationale du Canada

Direction des acquisitions et des services bibliographiques

395, rue Wellington
Ottawa (Ontario)
K1A 0N4

Your file Votre référence

Our file Notre référence

NOTICE

The quality of this microform is heavily dependent upon the quality of the original thesis submitted for microfilming. Every effort has been made to ensure the highest quality of reproduction possible.

If pages are missing, contact the university which granted the degree.

Some pages may have indistinct print especially if the original pages were typed with a poor typewriter ribbon or if the university sent us an inferior photocopy.

AVIS

La qualité de cette microforme dépend grandement de la qualité de la thèse soumise au microfilmage. Nous avons tout fait pour assurer une qualité supérieure de reproduction.

S'il manque des pages, veuillez communiquer avec l'université qui a conféré le grade.

La qualité d'impression de certaines pages peut laisser à désirer, surtout si les pages originales ont été dactylographiées à l'aide d'un ruban usé ou si l'université nous a fait parvenir une photocopie de qualité inférieure.

Canada

Finite-Element Time-Domain Analysis of Axisymmetrical Radiating Structures

by
Hassan O. Ali

A thesis
submitted to the school of Graduate Studies and Research
in partial fulfillment of the requirements for the degree of
Master of Applied Science.

Ottawa-Carleton Institute for Electrical Engineering,
Department of Electrical Engineering,
Faculty of Engineering,
University of Ottawa.

ISBN 0-315-80069-0

Canada

UNIVERSITÉ D'OTTAWA
UNIVERSITY OF OTTAWA

I hereby declare that I am the sole author of this document. I authorise the University of Ottawa to lend this document to other institutions or individuals for the purporse of scholarly research.

Hassan O. Ali

I further authorize the University of Ottawa to reproduce this document by photocopying or by other means, in total or in part, at the request of other institutions or individuals for the purpose of scholarly research.

Hassan O. Ali

Abstract

A method of computation based on the finite element method was used to solve axisymmetrical electromagnetic wave propagation problems directly in the time-domain. The finite element method, employing first order triangular elements, was used to generate a system of second order linear differential equations. The system of differential equations was solved for the magnetic field using a suitable differential equation solving algorithm written in the course of this work. The method was used to model several situations involving axisymmetrical radiating structures directly in the time domain and the results compared well with the published data. Situations involving pulses, which are of particular interest to EMI/EMC field, were successfully studied. Conclusions were drawn on the suitability of the method in modeling radiated emissions from printed circuit board configurations, under the influence of transient exciting fields.

Acknowledgements

I would like to express my heart-felt gratitude to my supervisor Dr. G. Costache for the precious guidance he offered me while doing this work. I wish also to thank all my colleagues for the enlightning discussions we shared and the moral support they were ever ready to give me. The work would never be fully successful without a harmonized working environment made possible by all the department support and technical staff, for whom I owe a debt of gratitude. Special gratitude is for my wife, Sabra, for her incredible patience, encouragement and understanding. Finally, I wish to express my sincere thanks to the Canadian Commonwealth Scholarship Committee for the financial support, without which, this work would never be accomplished.

Contents

List of Figures

List of Symbols

Vector quantities are indicated by bold characters both in frequency and time domain.

E electric field intensity

H magnetic field intensity

J_s surface current density

V voltage, volt

Y admittance

Z impedance

a diameter of the inner conductor of a coaxial line

b inner diameter of the external conductor of a coaxial line

c velocity of light in free space

f frequency, right hand side vector

Δt time step

h antenna length

r,ϕ,z cylindrical coordinates

$\boldsymbol{a}_r$ unit vector in the r-direction

$\boldsymbol{a}_\phi$ unit vector in the ϕ-direction

$\boldsymbol{a}_z$ unit vector in the z-direction

$\boldsymbol{n}$ unit vector normal

n number of element nodes

$N_j^{(k)}$ finite element interpolatory function of the jth node for element k

ω radian frequency

ϵ permittivity

μ permeability

σ conductivity

Γ reflection coefficient

∇ the nabla operator

η intrinsic impedance of a medium

λ wavelength

β phase constant

t time

Ω domain of the problem

S surface of the problem domain

C boundary of the problem domain

ASIC application-specific integrated circuit

CCW counter clockwise

EMC electromagnetic compatibility

EMI electromagnetic interference

EMP electromagnetic pulse

ESD electrostatic discharge

FD-TD finite-difference time-domain

FEM finite element method

PCB printed circuit board

max maximum

TEM transverse electromagnetic

tan tangential

VLSI very large scale integration

Chapter 1

1 Introduction

1.1 Motivation

With the present technological advancements in the design of telecommunication and other electronic equipment, newer and more complex devices such as 32-bit microprocessors, digital signal processors, and a variety of ASIC's (application-specific integrated circuits), are widely used. These devices, represent a very important source of electromagnetic energy due to their higher clock speeds, greater dynamic current consumption and increased size and complexity. The devices themselves are efficient radiators of the electromagnetic energy which when coupled into nearby structures may be amplified to levels high enough to cause electromagnetic interference (EMI) problem within and outside the electronic equipment. The existence of extensive internal clock distribution networks along with repetitive simultaneous switching of many parallel outputs, only worsens the problem. Indeed, these result in transient voltages of considerable magnitudes on the integrated circuits and the nearby components. When subjected to these internal transients as well as external transients caused by lightning, electrostatic discharge (ESD) or nuclear explosion (EMP), the components act as monopole antennas and radiate very effectively. The combined radiated electromagnetic energy can sometimes exceed allowable radiated emission limits and may adversely affect the functioning of the equipment.

Some very few works have been done to model the radiated emissions from electronic equipment right at the component level. One of these [1], characterizes the radiated emissions from printed circuit board components in the frequency domain,

using integral methods employing the magnetic and electric dipole moments. Another one [2], uses the finite-difference time domain (FD-TD) method to characterize the radiated emissions from a VLSI package and heatsink configuration. Unfortunately all these methods handle with difficulty inhomogeneities and variation of material properties quite often encountered in the situation in question. The finite element method (FEM) is quite suitable for those situations as it treats inhomogeneities and materials with quite an ease. Infact, the FEM has not been used much in modeling problems directly in the time domain. Indeed, little if any has been done to model driven antenna problems directly in the time domain using the FEM. Thus, the motive is to exploit the vast advantages of the FEM to model transient radiation of axisymmetrical radiating structures. As a result of the development of the method of computation, simple radiating structures such as cylindrical and conical monopoles of finite dimensions will be investigated under different forms of excitation. The method may also be used for the time-domain prediction of radiated emissions from electronic equipment components and hence a cost effective design of electronic equipment for EMI compliance will be made possible.

1.2 Objectives

The fact is, components within alectronic equipment, differ in shapes, sizes, material composition, functional characteristics and even their behaviour when subjected to electromagnetic field. This makes the task of modeling the radiated emission extremely difficult. However, simplified models can be used to model the emissions fairly well. For simplicity, the components are assumed to be of axisymmetrical shapes, thus making the problem virtually a two-dimensional one.

The primary objective of the work is to develop a method of computation based on the finite element method which will model an axisymmetrical wave propagation problem directly in the time domain. More specifically, the work should

be able to predict the radiated field from axisymmetrical radiating structures driven by both time-harmonic and transient voltages as these would be true representatives of the real situation encountered in electronic equipment situations.

The method has to be applied to already solved problems for its validation. Once validated, the method will find extensive application to problems not only of particular interest to EMI/EMC but also generally to all axisymmetrical radiation problems.

1.3 Accomplishments

A novel method of computation based on the FEM which can solve axisymmetrical electromagnetic wave propagation problems directly in the time domain, is introduced.

A new method of implementing absorbing boundary conditions at the position of the antenna feed, is suggested.

Accurate computation of driving-point current, input admittance and far field values of the magnetic field for cylindrical and conical monopole antennas excited by different forms of time-varying voltages is made possible and results are obtained.

The formulation has the following advantages over the FD-TD when applied to same problem situations:

- Only half of the problem domain needs to be solved hence less computer memory is required.

- Only one unknown (azimuthal component of the magnetic field) is solved at a time as compared to three (all field components) for the case of FD-TD. This provides a further reduction in the computer memory requirement.

- Steady state solution for monochromatic voltage excitation is possible without an unnecessary prolongation of the computation time.

- Complicated problem configurations can be easily handled and results made reliable at sensitive, most important regions by only locally changing the node density around the regions. Although this is possible with FD-TD, it is not with the ease provided by FEM.

In the course of this work, two main computer programs have been written. The first program formulates the problem, creates a system of linear second order differential equations. The equations are solved by the second program. The realization of the differential equation solver is counted as another major achievement of this work, for its efficiency, accuracy and liniency.

The scope of application of the formulation is too wide to fathom. Here below are only a few situations for which the method can be successfully used:

- direct time domain computation of the input admittance, current distribution and far field of any axisymmetrical antenna driven by a sinusoidal or non-sinusoidal voltage either directly or through a coaxial line.

- prediction of radiated emissions from integrated circuits and heat sinks within a PCB under the influence of sinusoidal or non-sinusoidal exciting fields.

- prediction of inter-PCB electromagnetic interference.

- the method can be used along side other methods to accurately study inter-component electromagnetic interference within PCB configurations.

Chapter 2

2 Literature Review

2.1 Background Material

Solution to the transient response of axisymmetrical radiating structures has been dealt with by many researchers using different techniques and set-ups. The most widely investigated radiating structure is a linear antenna. Among the earliest works is that done by Schelkunoff [3] which uses a linear current element as the source of radiation. Transient transmission and reception characteristics of thin cylindrical dipoles excited by step voltage of rectangular pulses of different durations were investigated both theoretically and experimentally in [4-7]. The results obtained, however, have a major drawback of premature termination and hence less value in frequency domain. Biconical antennas have been investigated in [8] by using an approximate input impedance function and neglecting the higher order modes.

Numerical techniques have also been used extensively in linear antenna investigations. Transient radiated field is computed for Gaussian-pulse-excited infinitely long linear antenna in [9] using Fourier transform techniques. The same techniques have been used in [10,11] for the computation of the transient fields produced by thin cylindrical antennas driven by dc pulses and in [12] for step-voltage-excited non-uniformly loaded finite linear antennas. The method applying the space-time integral equation for the antenna current distribution has been used in the time domain in [13,14] for the study of both unloaded and uniformly loaded finite linear antennas. The moments method has also been used directly in the time domain in [15] to compute field radiated by dipole antennas excited by step voltage. Another method worth mentioning is the singularity expansion method which has been discussed in [16] and used to compute radiated field from linear antennas through Laplace transform techniques.

After the introduction of the finite-difference time domain (FD-TD) algorithm [17] in 1966, it was not immediately used towards modeling antenna radiation problems until recently [18,19]. In [18] the radiated fields from coaxially-driven cylindrical and conical antennas were accurately computed directly in the time domain for a set-up which is experimentally realizable. On the other hand, the use of the finite element method in modeling radiation problems directly in the time domain, is very rare in literature. Little if any has been done to model driven antenna problems directly in the time domain using the finite element method. This present work is considered to be one of the earliest investigations of the transient response of experimentally realizable, axisymmetrical driven antenna configurations, using the finite element method directly in the time domain.

2.2 The Finite-Element Method for Time-Dependent Problems

As this work was mainly done using the finite element method as a computational tool, it is intended in this section to provide a brief discussion on the method, so that the foregoing analysis will be clearly understood. As the finite element method as used in frequency domain problems might be already well understood by many, the emphasis here will be put on the time-domain aspect of the formulation.

In a general situation involving electromagnetic wave propagation, the well-known time-dependent Maxwell's equations are used. When the electric field E, is eleminated from the two Maxwell's curl equations,

$$\nabla \times \boldsymbol{E} = -\mu \frac{\partial \boldsymbol{H}}{\partial t} \tag{2.1}$$

$$\nabla \times \boldsymbol{H} = \sigma \boldsymbol{E} + \epsilon \frac{\partial \boldsymbol{E}}{\partial t} \tag{2.2}$$

the following double-curl equation results,

$$\nabla\times\nabla\times\boldsymbol{H}+\left(\sigma\mu\frac{\partial \boldsymbol{H}}{\partial t}+\epsilon\mu\frac{\partial^2 \boldsymbol{H}}{\partial t^2}\right) = 0 \tag{2.3}$$

where the magnetic field H, is a function of space and time and σ, μ, ϵ are material constants which are here assumed to be independent of time. From here on, only one component of H will be considered for simplicity, and it will be denoted as H. The analysis is the same for other components of H. The cylindrical coordinate system will also be used all through and the problem is assumed to be two-dimensional.

When only one component is considered at a time, equation (2.3) can be written in a scalar form as,

$$f(H)+\left(\sigma\mu\frac{\partial H}{\partial t}+\epsilon\mu\frac{\partial^2 H}{\partial t^2}\right) = 0 \tag{2.4}$$

where $f(H)$ is a scalar function of H resulting from the double curl operation.

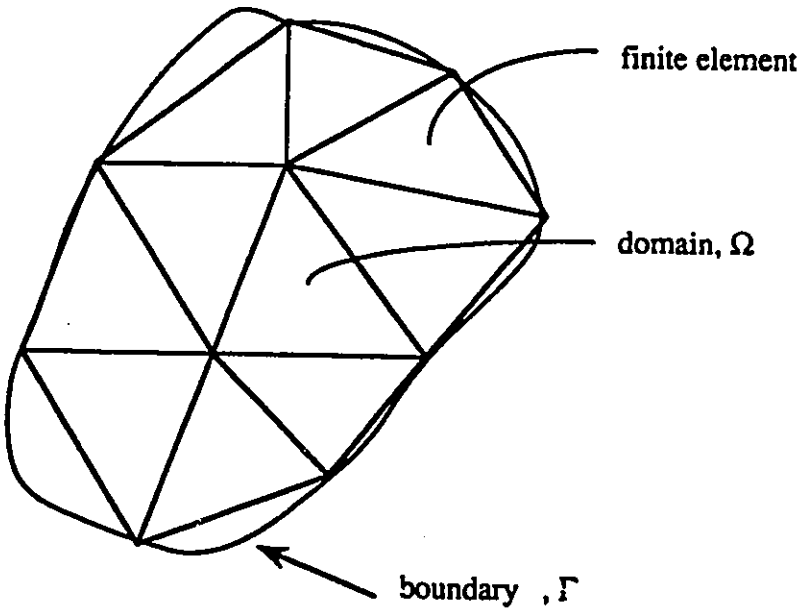

Fig. 2.1 Finite element discretization of the problem domain

The implementation of the finite element method towards solving equation (2.4) starts with the discretization of the problem domain, Ω, into small triangular elements to cover the whole problem domain as shown in Fig. 2.1. Over each finite element (triangle) the unknown magnetic field component H, is approximated as,

$$H \approx \sum_{j=1}^{3} u_j N_j \tag{2.5}$$

where $u_j = u_j(t)$, are the time-dependent unknown coefficients to be determined, and $N_j = N_j(r,z)$, are the finite element interpolatory functions, (functions of the space coordinates, r and z), which for linear (first order) approximation, can be written as

$$\begin{bmatrix} N_1 \\ N_2 \\ N_3 \end{bmatrix} = \frac{1}{2A} \begin{bmatrix} r_2 z_3 - r_3 z_2 & z_2 - z_3 & r_3 - r_2 \\ r_3 z_1 - r_1 z_3 & z_3 - z_1 & r_1 - r_3 \\ r_1 z_2 - r_2 z_1 & z_1 - z_2 & r_2 - r_1 \end{bmatrix} \begin{bmatrix} 1 \\ r \\ z \end{bmatrix} \tag{2.6}$$

where A is the area of the element.

As can be evident in (2.6), the N_j's have the property that, $N_j = 1$ at node j of the element and $N_j = 0$ at the other nodes (different of j) making up the finite element. This is an important property of the interpolatory functions since exactly at the nodes, the u_j's will assume the approximate values of H at those nodes. Thus, solution of the u_j's will mean solution of H at the corresponding nodes.

When equation (2.5) is used in (2.4) the required expansion will be accomplished. Next, the weighted residual (Galerkin) method [21], is used, which requires the weighted residual (difference between the exact and the approximate solution) to be zero when the expanded (2.4) is tested using the weighting functions same as those used in the expansion. The expansion and the testing process will yield the following,

$$\sum_{j=1}^{3} \int_{\Omega} \left[N_i F(N_j) u_j + \sigma \mu N_i N_j \frac{\partial u_j}{\partial t} + \varepsilon \mu N_i N_j \frac{\partial^2 u_j}{\partial t^2} \right] d\Omega = 0, \qquad i = 1,2,3. \tag{2.7}$$

where $F(N_j)u_j = f(N_j u_j)$.

As the integration in (2.7) is with respect to spacial variables, the u_j's and their time derivatives will not be affected when the integration is performed and there will result a subsystem of second order partial differential equations with respect to time. When the above process is performed for every element in the problem domain, several such subsystems of differential equations will result. The subsystems when assembled in the usual manner well known in the finite element method, a large system of second order differential equations will result.

Now the system of differential equations has to be solved for the unknown time-dependent coefficients, u_j's, which correspond to the magnetic field component approximated in (2.5). There are several ways of solving the system of second order differential equations. However for a given problem, not all the methods will be suitable. The methods have to be chosen after considering the computational effort required, computer memory requirement, flexibility with regard to sample sizes (spacial and temporal) and stability, and above all accuracy and reliability. The method used in this work is discussed in Chapter 5.

Chapter 3

3 Finite-Element Frequency-Domain Problem Formulation

Although the main concern of this work is to formulate the electromagnetic radiation problem directly in the time domain, here below the frequency domain formulation is presented mainly for two purposes. Firstly, to acquaint the reader with what has been previously done in the frequency domain relating the problem so that a smooth transition to the time-domain formulation is made possible and hopefully one may see the differences between the two formulations. Secondly, to introduce several suggestions and changes to the previously published [22] frequency domain formulation. Certainly, time-domain results may be obtained from the frequency-domain data via the Fourier transform techniques but in a less economical way.

Reference will be made quite often to the work done by Sumbar *et al* [22] which is the frequency domain finite element analysis of a driven antenna radiation problem. For reasons which will unfold later in this chapter, the frequency domain formulation presented here, will slightly differ from the original formulation [22], but basically the principle is the same.

3.1 General Formulation

Consider an axisymmetrical problem geometry as shown in Fig. 3.1. This formulation will only include such geometries which exhibit cylindrical symmetry in the azimuthal (ϕ) direction. This generally means that the fields and the material properties (σ, ϵ and μ) may only vary in the radial (r) and axial (z) directions but must be independent of ϕ.

Starting with the Maxwell's equations in the frequency domain (where a

sinusoidal field variation in time is assumed), they are written as,

$$\nabla \times \boldsymbol{E} = -j\omega\mu\boldsymbol{H} \tag{3.1}$$

and

$$\nabla \times \boldsymbol{H} = (\sigma + j\omega\varepsilon)\boldsymbol{E} \tag{3.2}$$

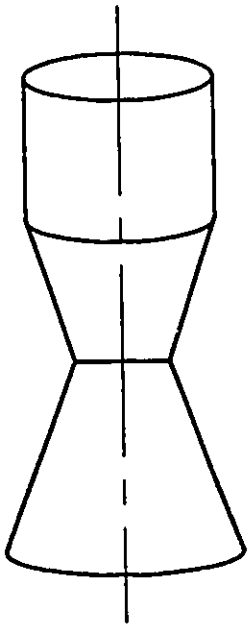

Fig. 3.1 Axisymmetrical problem configuration

When $\boldsymbol{E}$ is eliminated from the above equations the following results,

$$\nabla \times \nabla \times \boldsymbol{H} = (-j\omega\mu\boldsymbol{H})(\sigma + j\omega\varepsilon) \tag{3.3}$$

Due to the nature of the problem configuration as shown in Fig 3.1, there will be no variation of the field with ϕ, (i.e $\partial/\partial\phi=0$), and $H_z = H_r = 0$. This will lead to the simplification of (3.3) to a scalar form as:

$$-\frac{\partial}{\partial z}\left(\frac{\partial H_\phi}{\partial z}\right)-\frac{\partial}{\partial r}\left(\frac{1}{r}\frac{\partial}{\partial r}(rH_\phi)\right)=(-j\omega\mu H_\phi)(\sigma+j\omega\varepsilon) \tag{3.4}$$

Let $Y = (\sigma+j\omega)^{-1}$ and $Z = j\omega\mu$. Then (3.4) becomes,

$$Y\left[-\frac{\partial}{\partial z}\left(\frac{\partial H_\phi}{\partial z}\right)-\frac{\partial}{\partial r}\left(\frac{1}{r}\frac{\partial}{\partial r}(rH_\phi)\right)\right]+ZH_\phi=0 \tag{3.5}$$

Now, equation (3.5) is to be solved for H_ϕ in the problem domain subject to boundary conditions. First, however, the problem domain has to be clearly defined. To illustrate the definition of the problem domain a typical configuration consisting of a cylindrical monopole antenna above a perfect ground plane will be discussed. The configuration is as depicted in Fig. 3.2. As the problem is by nature unbounded, it will only be possible to be solved using the finite element method if a terminating boundary is defined to make it bounded. This boundary is what is known as the radiation boundary and is as shown in Fig. 3.2. Details of the radiation boundary will be provided a little later.

Using the finite element, Galerkin formulation [20] as described in the preceding chapter, equation (3.5) can be discretized by first assuming the trial solution for H_ϕ for the kth element of the domain of the problem as,

$$H_\phi^{(k)} \approx \sum_{j=1}^{n} u_j N_j^{(k)}(r,z) = U^{(k)}(r,z) \tag{3.6}$$

where u_j are unknown complex constants, N_j are real-valued FEM interpolatory functions and n is the number of nodes defining the kth element.

By Galerkin formulation, expansion and testing of equation (3.5) using (3.6) yields,

$$\iint_{(k)} \left\{ -\frac{\partial}{\partial r}\left(\frac{Y}{r}\frac{\partial}{\partial r}(rU^{(k)})\right) - Y\frac{\partial}{\partial z}\left(\frac{\partial U^{(k)}}{\partial z}\right) + ZU^{(k)} \right\} N_i^{(k)}\, dr\, dz = 0 \qquad (3.7)$$

for $i = 1,2,\ldots,n$.

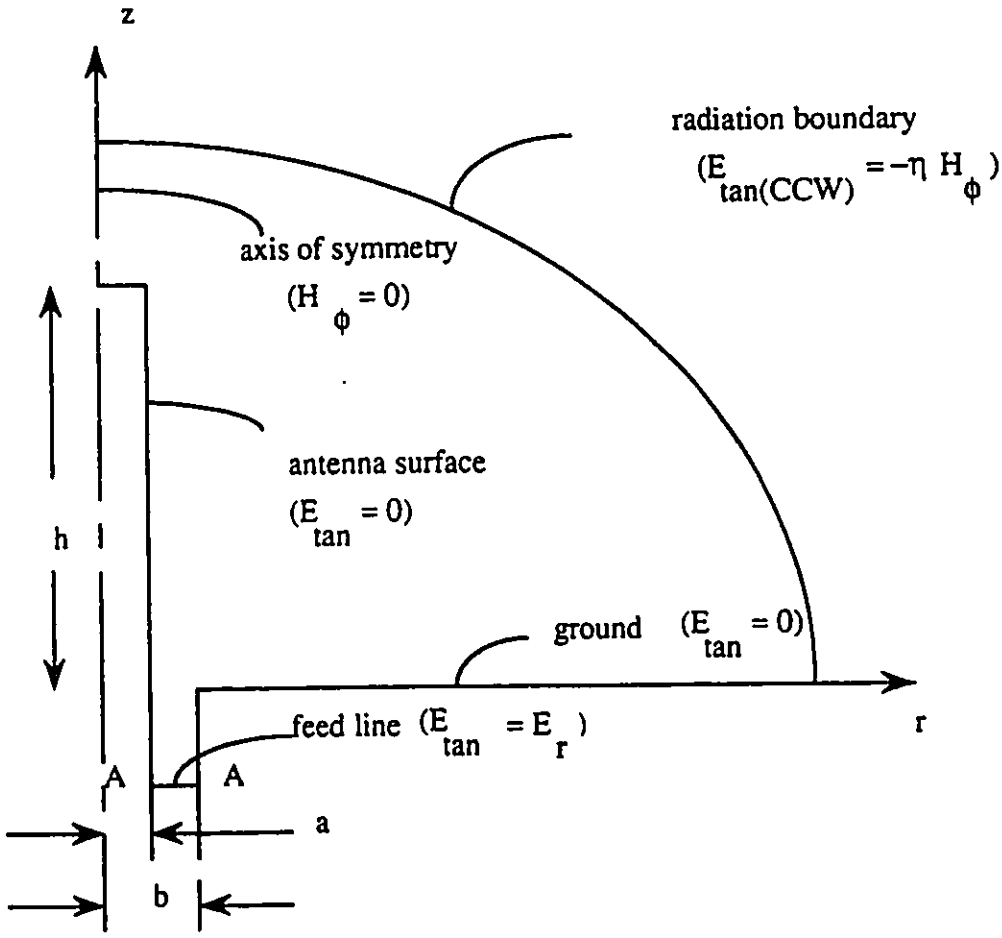

Fig. 3.2 Cylindrical monopole antenna above a perfect ground plane

Using integration by parts, equation (3.7) can be written as,

$$-\iint_{(k)}\left[\frac{\partial}{\partial r}\left(\frac{Y}{r}\frac{\partial}{\partial r}(rU^{(k)})N_i^{(k)}\right)+Y\frac{\partial}{\partial z}\left(\frac{\partial U^{(k)}}{\partial z}N_i^{(k)}\right)\right]dr\,dz$$
$$+\iint_{(k)}\left[\frac{Y}{r}\frac{\partial}{\partial r}(rU^{(k)})\frac{\partial N_i^{(k)}}{\partial r}+Y\frac{\partial U^{(k)}}{\partial z}\frac{\partial N_i^{(k)}}{\partial z}+ZU^{(k)}N_i^{(k)}\right]dr\,dz = 0 \qquad (3.8)$$

Considering the divergence theorem in two dimensions,

$$\iint_S(\nabla.F)\,dA = \oint_C F.n\,dl \qquad (3.9)$$

where F is a vector defined in the surface S, n is an outward unit vector, normal to the boundary, C, enclosing the surface S as shown in Fig. 3.3.

When $F = Pa_x + Qa_y$, (3.9) becomes

$$\iint_S\left(\frac{\partial P}{\partial x}+\frac{\partial Q}{\partial y}\right)dx\,dy = \oint_C(Pa_x.n + Qa_y.n)\,dl \qquad (3.10)$$

But $a_x.n = \cos\alpha$ and $a_y.n = \cos\beta$ are the direction cosines of the outward vector, normal to the boundary.

Thus (3.10) can be written as

$$\iint_S\left(\frac{\partial P}{\partial x}+\frac{\partial Q}{\partial y}\right)dx\,dy = \oint_C(P\cos\alpha + Q\cos\beta)\,dl \qquad (3.11)$$

Equation (3.11) is equivalently the Green's theorem in the x-y plane. Now, upon applying (3.11) to the first double integral of equation (3.8), will transform it to a contour integral along the boundary in a counter clockwise direction, and may be written as:

$$-Y\oint_{(k)}\left[\frac{1}{r}\frac{\partial}{\partial r}(rU^{(k)})N_i^{(k)}\cos\alpha^{(k)}+\frac{\partial U^{(k)}}{\partial z}N_i^{(k)}\cos\beta^{(k)}\right]dl \qquad (3.12)$$

where again, $\cos\alpha^{(k)}$ and $\cos\beta^{(k)}$ are the direction cosines of the outward normal unit vector at a point along the element perimeter as shown in Fig. 3.3.

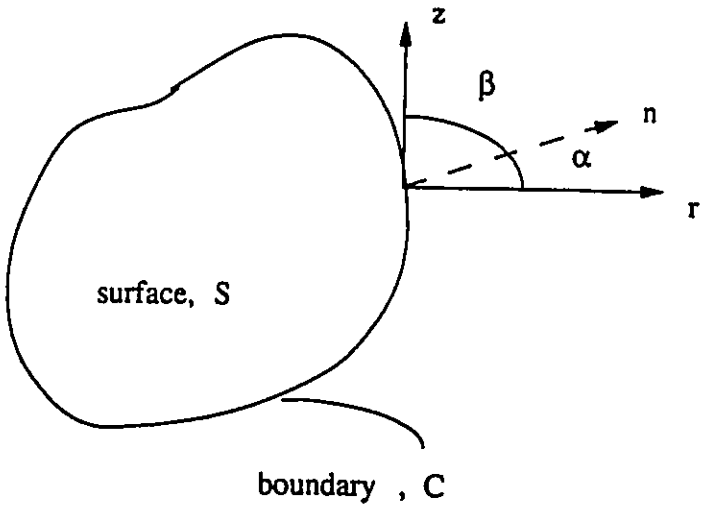

Fig. 3.3 Close look of the element boundary

Equation (3.2) can be re-written as,

$$-\frac{\partial H_\phi}{\partial z}a_r+\frac{1}{r}\frac{\partial}{\partial r}(rH_\phi)a_z=Y^{-1}(E_r a_r+E_z a_z) \tag{3.13}$$

and the following identities can be easily derived:

$$\begin{aligned} E_r &\approx -Y\frac{\partial U_\phi}{\partial z} = \mathscr{E}_r \\ E_z &\approx \frac{Y}{r}\frac{\partial}{\partial r}(rU_\phi) = \mathscr{E}_z \end{aligned} \tag{3.14}$$

Substituting (3.14) in (3.12), the first double integral in (3.8) can now be re-written as,

$$\begin{aligned} &-\oint\left[\mathscr{E}_z^{(k)}N_i^{(k)}\cos\alpha(k)+(-\mathscr{E}_r^{(k)})N_i(k)\cos\beta^{(k)}\right]dl \\ &= -\oint_{(k)}\mathscr{E}_{\tan(CCW)}^{(k)}N_i^{(k)}\,dl \end{aligned} \tag{3.15}$$

since the term in square brackets above is the tangential electric field on a side of element k, considered positive in the counterclockwise direction.
Now , using (3.15), equation (3.8) can be written as,

$$\iint_{(k)}\left[\frac{Y}{r}\frac{\partial}{\partial r}(rU^{(k)})\frac{\partial N_i^{(k)}}{\partial r}+Y\frac{\partial U^{(k)}}{\partial z}\frac{\partial N_i^{(k)}}{\partial z}+ZU^{(k)}N_i^{(k)}\right]dr\,dz = \oint_{(k)}\mathscr{E}^{(k)}_{\tan(CCW)}dl \qquad (3.16)$$

Substituting (3.6) in (3.16) yields,

$$\sum_{j=1}^{n} u_j\iint_{(k)}\left[Y\frac{\partial N_i}{\partial r}\frac{\partial N_j}{\partial r}+Y\frac{\partial N_i}{\partial z}\frac{\partial N_j}{\partial z}+\frac{Y}{r}\frac{\partial N_i}{\partial r}N_j+ZN_iN_j\right]dr\,dz \qquad (3.17)$$
$$= \oint_{(k)}\mathscr{E}^{(k)}_{\tan(CCW)}N_i\,dl, \qquad i=1,2,\ldots,n$$

Equation (3.17) constitutes the discretization of (3.5) for one element within the problem domain. When (3.17) is evaluated, a subsystem of n linear algebraic equations results. This system is to be solved for the undetermined coefficients u_j's, which reflect the values of U (the approximate values of H_ϕ) at the n nodes of the element. It is evident that, because of the third term in the square brackets in (3.17), the element matrix will not be symmetric. This is contrary to the formulation in [22], which seeks to compute rH_ϕ instead of H_ϕ computed in this present formulation. However, as will be discussed below, this formulation has many advantages to be gained.

Individual element subsystems will be assembled for all the elements forming the problem domain, to result into a big system of linear algebraic equations to be solved subject to the boundary conditions. The inclusion of the boundary conditions into the formulation will be discussed in a separate section.

The choice of solving for H_ϕ instead of rH_ϕ suggested in [22], despite the advantages of the latter with regard to resulting in symmetry of the system matrices which is lost in the former, has two main advantages. Firstly, the division by r in many of the contributing integral terms, is avoided. The division by r introduces singularity at $r = 0$ and thus makes the integrals very difficult to evaluate and some of them

impossible to evaluate analytically when r equals zero. Although the nodes falling on $r = 0$ line, which happens to be the axis of symmetry, are on zero Dirichlet boundary condition (as may be seen later), and hence they make no contribution to the system of equations, the problem however, is with the nodes sharing elements with the above-mentioned nodes, which do make contribution to the system of equations. With the rH_ϕ formulation, it has been found out that, it is difficult to obtain analytically some of the contributions from elements with a side on $r = 0$ line. With the H_ϕ formulation, the division by r appears in only one integral and it is in a form which permits evaluation of all the contributions save those from nodes on $r = 0$ line, which do not contribute anything anyway.

The second advantage of the H_ϕ formulation is with regard to the number of generic integrals to be evaluated before implementing them in a program (see Appendix A). While using simplex coordinates, [21], and first order triangular elements, it has been found out that, not only the number of the generic integrals is tremendously reduced, but also even their degree of complexity is substantially reduced. The extent of reduction is overwhelming. The use of the H_ϕ formulation saves much of the processing time even though at the expense of loosing symmetry of the system and all what it implies.

3.2 Boundary Conditions

Consider a cylindrical monopole antenna above a perfect ground plane as shown in Fig. 3.2. This is a typical problem configuration which befits the analysis already given. This problem configuration will be used to illustrate how to include the boundary conditions into the problem formulation.

The boundaries are as depicted in Fig. 3.2. On the boundary along the axis of symmetry, it is known that the magnetic field is zero. Hence this becomes a homogeneous Dirichlet boundary condition. Over the antenna surface and along the

perfectly conducting ground, the continuity of the tangential electric field requires that, the tangential electric field to be zero. This will be taken as a homogeneous Neumann boundary condition since the unknown is the azimuthal magnetic field component which is perpendicular to and directed into the page. At the antenna feed, the tangential electric field component will be non-zero. Only this non-zero tangential electric field will have contributions into the system of equations. In other words, only feed nodes will generally have corresponding rows with non-zero right hand side. The Neumann boundary condition is in-built in the Galerkin formulation, and will be implemented once the tangential component of the electric field, $\mathscr{E}_{tan(CCW)}$, is specified in the equation (3.17).

Treatment of the radiation boundary, along which the tangential component of the electric field is not known in advance, is well explained in [22]. Here below, some information is given again for clarity.

It is known that, in a homogeneous medium, at a far field point,

$$\boldsymbol{H} = \frac{\boldsymbol{n}\times\boldsymbol{E}}{\eta} \tag{3.18}$$

where $\boldsymbol{n}$ is the outward normal unit vector pointing towards the direction of propagation, and η is the intrinsic impedance of the medium which is defined as,

$$\eta = \sqrt{\frac{j\omega\mu}{\sigma+j\omega\varepsilon}} \tag{3.19}$$

Equation (3.18) for the problem geometry specified, reduces to,

$$H_{\phi} = -\frac{E_{tan(CCW)}}{\eta} \tag{3.20}$$

Using the trial solution given by (3.6), equation (3.20) can be written as,

$$g^{(k)}_{tan(CCW)}(r,z) = -\eta^{(k)} \sum_{j=1}^{n} u_j N_j^{(k)}(r,z) \tag{3.21}$$

Thus for elements with a side on the radiation boundary, the system of equations to solve is obtained by substituting (3.21) in (3.17), which yields,

$$\sum_{j=1}^{n} u_j \left\{ \iint_{(k)} \left[Y \left(\frac{\partial N_i^{(k)}}{\partial r} \frac{\partial N_j^{(k)}}{\partial r} + \frac{\partial N_i^{(k)}}{\partial z} \frac{\partial N_j^{(k)}}{\partial z} + \frac{\partial N_i^{(k)}}{\partial r} \frac{N_j^{(k)}}{r} \right) + Z N_i N_j \right] dr\,dz + \eta^{(k)} \oint N_i N_j dl \right\} = 0, \quad i=1,2,\ldots,n \tag{3.22}$$

The radiation boundary condition results into an additional term which is readily taken to the left hand side .

The resulting system obtained after assembling the subsystems is generally a system of linear algebraic equations, to be solved for the unknown values of u_j corresponding to the H_ϕ at the corresponding nodes.

3.3 Modeling of the Monopole Feed

Modeling of the antenna excitation is the most important part in modeling driven antenna radiation. In the past, several approximations to the antenna feed have been suggested to simplify the theoretical and numerical analysis. Here below, some of the most common models for the feed of the monopole, are introduced:

Radial Delta-function Excitation

In this model [23], the antenna is assumed to be excited by a radial electric

field of the form

$$E_r(r,0)=V\delta(r-a) \tag{3.23}$$

where V is the voltage maintained across the infinitely small gap as shown in Fig. 3.4. While assuming this kind of excitation, obviously the higher order modes of the field around the base of the monopole or reflected from the top of the monopole, are neglected. In other words, this model assumes that the voltage generator is directly connected to the monopole driving point. Hence, it is a direct excitation.

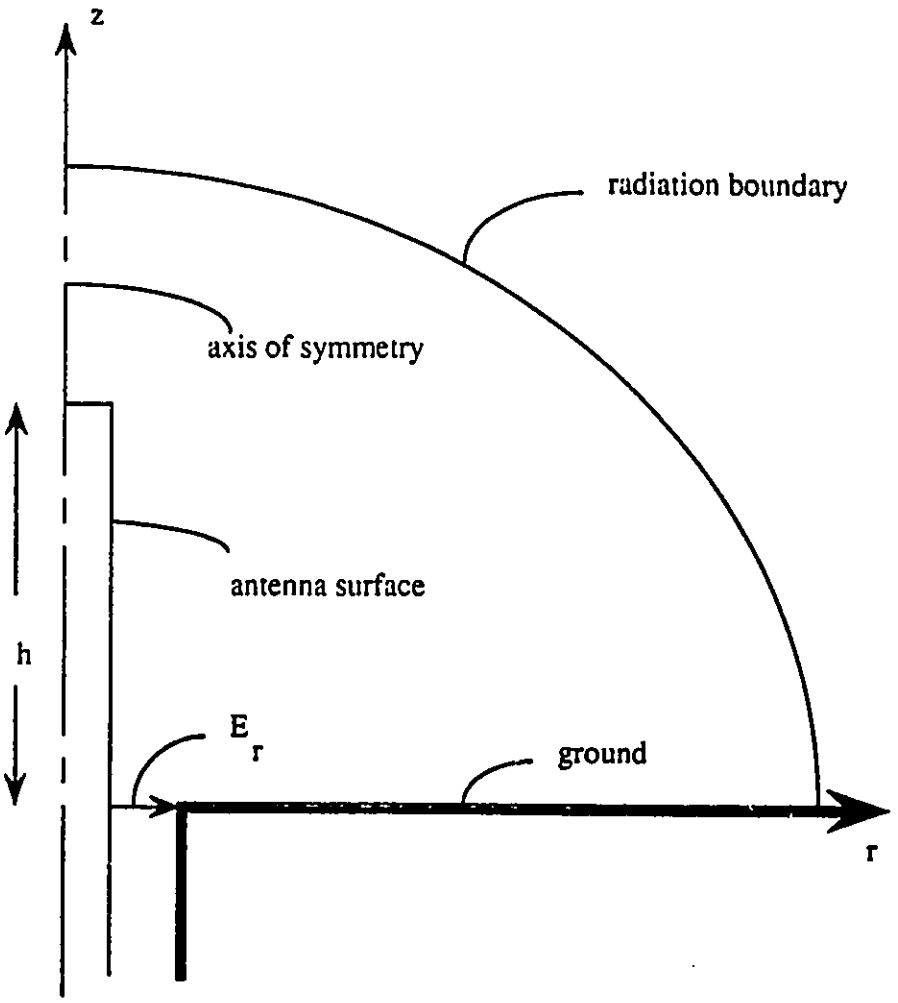

Fig. 3.4 Radial delta gap excitation model

Axial Delta-function Excitation

In this model, an equivalent delta-gap generator is utilized by forcing the normal component of the axial electric field below the monopole to have a fixed value. Assuming an axial voltage V, maintained in a gap of width d, the axial electric field at the gap will be given by,

$$E_z(0,z)=\frac{V}{d}, \qquad (0\le z\le d) \tag{3.24}$$

This model is shown in Fig. 3.5.

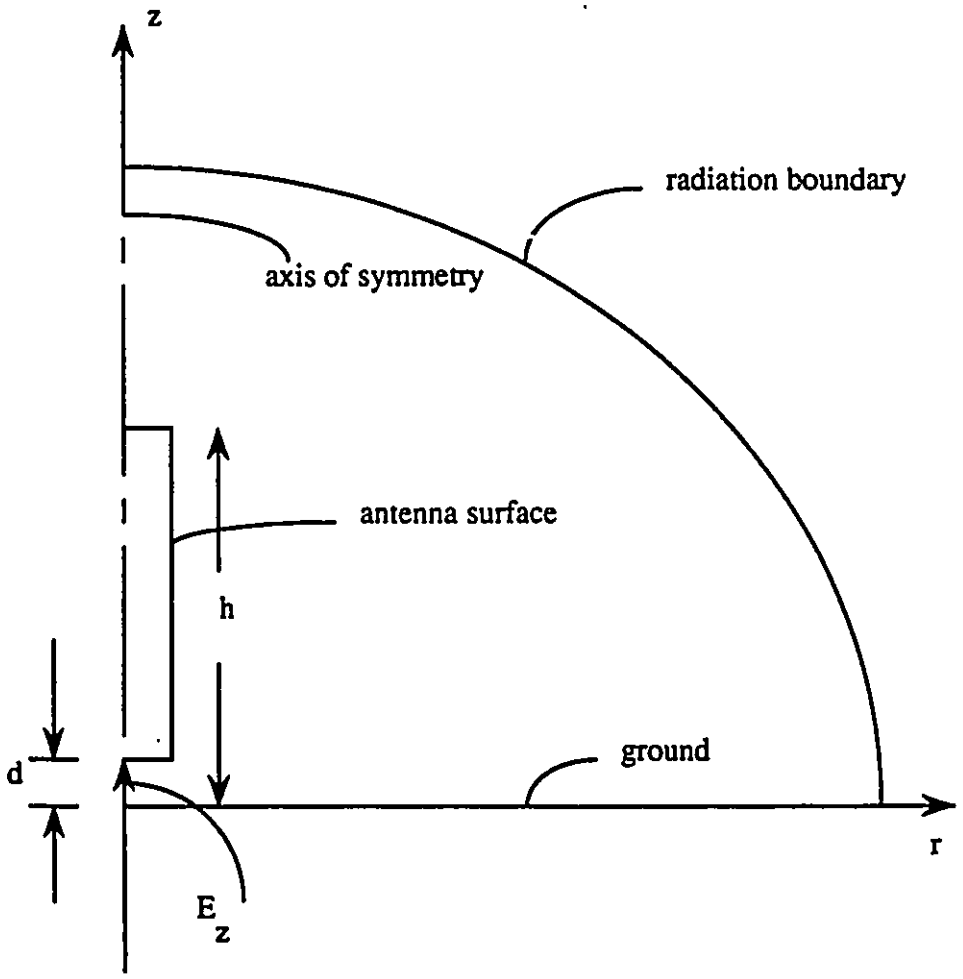

Fig. 3.5 Axial delta gap excitation model

Radial 1/r Excitation

This is the one which is rather more close to modeling a coaxially-driven monopole antenna. It is also known as the magnetic frill generator [24]. The field driving the monopole is that present at the coaxial aperture which is assumed to be purely of the dominant (TEM) mode inside the coaxial line. If the gap is of width *(b-a)* as shown in Fig. 3.4, and the voltage maintained across the gap is of magnitude *V*, then the radial electric field at the gap is given as,

$$E_r(r,0) = \frac{V}{r\ln\left(\frac{b}{a}\right)} \tag{3.25}$$

The corresponding magnetic current distribution is given by,

$$M_\phi = -E_r = -\frac{V}{r\ln\left(\frac{b}{a}\right)} \tag{3.26}$$

Here, *b-a* is assumed to be so small that only TEM mode exists except for the region very close to the end. At the end, evanescent higher order modes exist but to a first approximation they may be neglected.

Chapter 4

4 Finite-Element Time-Domain Problem Formulation

The time-domain formulation used here is similar to its frequency-domain counter-part. The main difference lies in the temporal variation of the fields in the former which requires special handling. It is intended to make this chapter self-dependent and thus the procedure followed in Chapter 3 will be repeated here for the sake of clarity. However, occassional reference to the previous chapter will be made when found necessary.

4.1 General Formulation

The foregoing analysis is applicable to any axisymmetrical radiating structure as the one shown in Fig. 3.1, or equivalently to any two-dimensional electromagnetic wave propagation problem. In this problem configuration, the field does not vary in the azimuthal direction but does so only in the axial and radial directions. Moreover, E, and H are functions of r, z, and time only and are independent of ϕ, the azimuthal coordinate. The material constants σ, μ, and ϵ are independent of frequency and time. The existing electromagnetic field components are E_r, E_z and H_ϕ only.

The time dependent Maxwell's equations can be written as,

$$\nabla \times \boldsymbol{E} = -\mu \frac{\partial \boldsymbol{H}}{\partial t} \tag{4.1}$$

$$\nabla \times \boldsymbol{H} = \sigma \boldsymbol{E} + \varepsilon \frac{\partial \boldsymbol{E}}{\partial t} \tag{4.2}$$

E is eliminated in the above equations by taking curl of (4.2) and then substituting (4.1) to get,

$$\nabla\times\nabla\times H = -\left(\sigma\mu\frac{\partial H}{\partial t} + \varepsilon\mu\frac{\partial^2 H}{\partial t^2}\right) \tag{4.3}$$

Using the information provided above, (4.3) can be reduced to,

$$-\frac{\partial}{\partial r}\left(\frac{1}{r}\frac{\partial}{\partial r}(rH_\phi)\right) - \frac{\partial}{\partial z}\left(\frac{\partial H_\phi}{\partial z}\right) = -\left(\sigma\mu\frac{\partial H_\phi}{\partial t} + \varepsilon\mu\frac{\partial^2 H_\phi}{\partial t^2}\right) \tag{4.4}$$

Equation (4.4) is now to be solved for H_ϕ subject to boundary conditions of the problem. This is to be done using the FEM for setting up the system of differential equations and ultimately solve the equation using differential equation solving techniques.

First, the solution of the unknown, H_ϕ, is assumed in terms of the unknown time-dependent coefficients $u_j(t)$ and N_j, the FEM interpolatory functions [20], which have the property that $N_j = 1$ at node j and $N_j = 0$ at the other nodes (different of j) making up the finite element. Thus, for element k, the approximate value of the H_ϕ is given as,

$$\tilde{H}_\phi^{(k)} = \sum_{j=1}^{n} u_j(t)N_j^{(k)}(r,z) \tag{4.5}$$

By the Galerkin formulation [20], the same FEM interpolatory functions are used for testing equation (4.4) as those used in the trial solution to yield,

$$\iint_{(k)}\left\{-\frac{\partial}{\partial r}\left[\frac{1}{r}\frac{\partial}{\partial r}\left(r\tilde{H}_\phi^{(k)}\right)\right]-\frac{\partial}{\partial z}\left(\frac{\partial\tilde{H}_\phi^{(k)}}{\partial z}\right)+\sigma\mu\frac{\partial\tilde{H}_\phi^{(k)}}{\partial t}+\varepsilon\mu\frac{\partial^2\tilde{H}_\phi^{(k)}}{\partial t^2}\right\}N_i^{(k)}dr\,dz = 0, \quad i=1,2,\ldots,n \tag{4.6}$$

Applying integration by parts to equation (4.6), yields,

$$
\begin{aligned}
&-\int\int_{(k)}\left[\frac{\partial}{\partial r}\left(\frac{1}{r}\frac{\partial}{\partial r}\left(r\tilde{H}_{\phi}^{(k)}\right)N_i^{(k)}\right) + \frac{\partial}{\partial z}\left(\frac{\partial \tilde{H}_{\phi}^{(k)}}{\partial z}N_i^{(k)}\right)\right]dr\,dz \\
&\quad +\int\int_{(k)}\left[\frac{1}{r}\frac{\partial}{\partial r}\left(r\tilde{H}_{\phi}^{(k)}\right)\frac{\partial N_i^{(k)}}{\partial r} + \frac{\partial \tilde{H}_{\phi}^{(k)}}{\partial z}\frac{\partial N_i^{(k)}}{\partial z}\right. \\
&\quad \left. + \left(\sigma\mu\frac{\partial \tilde{H}_{\phi}^{(k)}}{\partial t} + \varepsilon\mu\frac{\partial^2 \tilde{H}_{\phi}^{(k)}}{\partial t^2}\right)N_i^{(k)}\right]dr\,dz = 0
\end{aligned}
\tag{4.7}
$$

Now, upon applying the Green's theorem in the *r-z* plane (see Chapter 3) to the first double integral of equation (4.7), will transform it to a contour integral along the boundary in a counter clockwise direction, as follows:

$$
\begin{aligned}
&-\int\int_{(k)}\left[\frac{\partial}{\partial r}\left(\frac{1}{r}\frac{\partial}{\partial r}\left(r\tilde{H}_{\phi}^{(k)}\right)N_i^{(k)}\right) + \frac{\partial}{\partial z}\left(\frac{\partial \tilde{H}_{\phi}^{(k)}}{\partial z}N_i^{(k)}\right)\right]dr\,dz \\
&\quad = -\oint_{(k)}\left[\frac{1}{r}\frac{\partial}{\partial r}\left(r\tilde{H}_{\phi}^{(k)}\right)N_i^{(k)}\cos\alpha^{(k)} + \frac{\partial \tilde{H}_{\phi}^{(k)}}{\partial z}N_i^{(k)}\cos\beta^{(k)}\right]dl
\end{aligned}
\tag{4.8}
$$

where, $\cos\alpha^{(k)}$, $\cos\beta^{(k)}$ are the direction cosines of the outward normal unit vector at a point along the element perimeter.

Equation (4.3) can, with the assumptions given before, be written as:

$$
-\frac{\partial H_{\phi}}{\partial z}a_r + \frac{1}{r}\frac{\partial}{\partial r}(rH_{\phi})a_z = \left(\sigma E_r + \varepsilon\frac{\partial E_r}{\partial t}\right)a_r + \left(\sigma E_z + \varepsilon\frac{\partial E_z}{\partial t}\right)a_z \tag{4.9}
$$

From (4.9) the following identities can be derived:

$$
\frac{\partial H_{\phi}}{\partial z} = -\left(\sigma E_r + \varepsilon\frac{\partial E_r}{\partial t}\right) \tag{4.10}
$$

and

$$\frac{1}{r}\frac{\partial}{\partial r}(rH_\phi) = \sigma E_z + \varepsilon\frac{\partial E_z}{\partial t} \tag{4.11}$$

Applying (4.10) and (4.11), the right handside of (4.8) which is equal to the first double integral of (4.7), can be written as,

$$-\oint_{(k)}\left\{\left(\sigma\tilde{E}_z^{(k)} + \varepsilon\frac{\partial\tilde{E}_z^{(k)}}{\partial t}\right)N_i^{(k)}\cos\alpha^{(k)} + \left[-\left(\sigma\tilde{E}_r^{(k)} + \varepsilon\frac{\partial\tilde{E}_r^{(k)}}{\partial t}\right)\right]N_i^{(k)}\cos\beta^{(k)}\right\}dl \tag{4.12}$$

This can be further written as,

$$-\oint_{(k)}\left\{\sigma\left[\tilde{E}_z^{(k)}\cos\alpha^{(k)} + \left(-\tilde{E}_r^{(k)}\right)\cos\beta^{(k)}\right] + \varepsilon\frac{\partial}{\partial t}\left[\tilde{E}_z^{(k)}\cos\alpha^{(k)} + \left(-\tilde{E}_r^{(k)}\right)\cos\beta^{(k)}\right]\right\}N_i^{(k)}dl \tag{4.13}$$

The term in square brackets in (4.13) is actually the tangential electric field on a side of element *(k)* which is considered positive in a counterclockwise direction [22].

Thus, using (4.13), equation (4.7) can now be written as,

$$\begin{aligned}\iint_{(k)}\left[\frac{1}{r}\frac{\partial}{\partial r}\left(r\tilde{H}_\phi^{(k)}\right)\frac{\partial N_i^{(k)}}{\partial r} + \frac{\partial\tilde{H}_\phi^{(k)}}{\partial z}\frac{\partial N_i^{(k)}}{\partial z} + \left(\sigma\mu\frac{\partial\tilde{H}_\phi^{(k)}}{\partial t} + \varepsilon\mu\frac{\partial^2\tilde{H}_\phi^{(k)}}{\partial t^2}\right)N_i^{(k)}\right]dr\,dz \\ = \oint_{(k)}\left(\sigma\tilde{E}_{\tan(CCW)}^{(k)} + \varepsilon\frac{\partial}{\partial t}\tilde{E}_{\tan(CCW)}^{(k)}\right)N_i^{(k)}dl \quad , \quad i=1,2,\ldots,n\end{aligned} \tag{4.14}$$

Now substituting the trial solution given by (4.5) into (4.14), yields,

$$\begin{aligned}&\sum_{j=1}^{n}\left\{u_j\iint_{(k)}\left[\frac{\partial N_i^{(k)}}{\partial r}\frac{\partial N_j^{(k)}}{\partial r} + \frac{\partial N_i^{(k)}}{\partial z}\frac{\partial N_j^{(k)}}{\partial z} + \frac{\partial N_i^{(k)}}{\partial r}\frac{N_j^{(k)}}{r}\right]dr\,dz\right. \\ &\left.+\left(\sigma\mu\frac{\partial u_j}{\partial t} + \varepsilon\mu\frac{\partial^2 u_j}{\partial t^2}\right)\iint_{(k)}N_i^{(k)}N_j^{(k)}dr\,dz\right\} = \oint_{(k)}\left(\sigma\tilde{E}_{\tan(CCW)}^{(k)} + \varepsilon\frac{\partial}{\partial t}\tilde{E}_{\tan(CCW)}^{(k)}\right)N_i^{(k)}dl, \\ &\qquad\qquad i=1,2,\ldots,n\end{aligned} \tag{4.15}$$

When equation (4.15) is evaluated, a system of n second order linear differential equations results. It is evident that, because of the third term in the first double integral of (4.15), the matrix associated with the unknown variable u_j, will not be symmetric. However, as discussed earlier, this formulation has many advantages to be gained from.

Individual element subsystems will be assembled for all the elements forming the problem domain, to result into a large system of differential equations to be solved subject to the boundary conditions. The inclusion of the boundary conditions into the formulation will be discussed in the following section.

4.2 Boundary Conditions

Inclusion of the boundary conditions into the problem formulation has been well covered in Chapter 3 for the frequency domain computation. In most cases, the method will be the same except for the temporal variation of the boundary conditions. Unfortunately, due to the variation of the boundary conditions with time, some of the boundary conditions are not easy to implement and very much depend on the computation time, the method of excitation and whether or not the problem domain is lossy. To understand the technique better, the boundary conditions will be discussed against each method of excitation separately.

The boundaries are as depicted in Fig. 3.2. Treatment of all the boundaries other than the radiation boundary and the boundary at the feed, is the same as in the frequency domain, since all these possess zero boundary conditions, and thus independent of time and frequency. The boundary at the feed will from here on be generally referred to as 'the feed line', for simplicity. The discussion on how to fix the boundary conditions at the feed line and at the radiation boundary will be discussed in separate sections.

4.2.1 Implementation of the Radiation Boundary Conditions

The boundary conditions at the outer (radiation) boundary can be fixed in several ways depending on the nature of the problem as will be discussed here below. In most cases the way of specifying the boundary conditions differ a little bit from the way discussed in the frequency domain formulation.

The easiest way of fixing the boundary conditions at the radiation boundary is to let the computation time to be less than the time for the electromagnetic wave to reach the outer boundary, where then, the electric and magnetic field at the boundary will be equal to zero. This, however, will require the outer boundary to be very far if a longer computation time is desired, thus making the problem domain very big. This kind of boundary conditions has been suggested and implemented in [18] for the finite-difference time-domain computation.

The other way is to adapt for time-domain application, the radiation boundary conditions suggested in [22] for frequency domain application.

It is known that, in a homogeneous medium, at a far field point, equation (3.18) holds, where η is the intrinsic impedance of the medium which in frequency domain is defined by (3.19). The reader is reminded here that, the far field position depends on the dimensions of the radiating structure and the highest frequency component of the exciting signal, according to : $r >> 2D^2/\lambda$ and $r >> \lambda$, where r is the distance to a far field point, D is the largest dimension of the radiating structure and λ is the smallest wavelength of the exciting signal.

If the medium is lossless, that is, conductivity, $\sigma = 0$, then η becomes real and can be written as,

$$\eta_{\sigma=0} = \sqrt{\frac{\mu}{\varepsilon}} \tag{4.16}$$

Equation (3.19) with prior and present assumptions can now be written as,

$$H_{\phi} = \frac{-E_{\tan(CCW)}}{\sqrt{\frac{\mu}{\varepsilon}}} \tag{4.17}$$

Using the trial solution given by (4.5), equation (4.17) can be written as,

$$\tilde{E}^{(k)}_{\tan(CCW)}(r,z,t) = -\sqrt{\frac{\mu}{\varepsilon}} \sum_{j=1}^{n} u_j(t) N_j^{(k)}(r,z) \tag{4.18}$$

For elements with a side on the radiation boundary, the right hand side of (4.15) using (4.18) becomes,

$$\varepsilon \oint_{(k)} \frac{\partial}{\partial t} \tilde{E}^{(k)}_{\tan(CCW)} N_i^{(k)} dl = -\sum_{j=1}^{n} \frac{\partial u_j}{\partial t} \sqrt{\mu\varepsilon} \oint_{(k)} N_i^{(k)} N_j^{(k)} dl \quad , \qquad i=1,2,\ldots n \tag{4.19}$$

Substituting (4.19) in (4.15) yields the form of the differential equation subsystem for elements with a side on the radiation boundary given as,

$$\sum_{j=1}^{n} \left\{ u_j \iint_{(k)} \left[\frac{\partial N_i^{(k)}}{\partial r} \frac{\partial N_j^{(k)}}{\partial r} + \frac{\partial N_i^{(k)}}{\partial z} \frac{\partial N_j^{(k)}}{\partial z} + \frac{\partial N_i^{(k)}}{\partial r} \frac{N_j^{(k)}}{r} \right] \right.$$
$$+ \frac{\partial u_j}{\partial t} \left(\sigma\mu \iint_{(k)} N_i^{(k)} N_j^{(k)} dr dz + \sqrt{\mu\varepsilon} \oint_{(k)} N_i^{(k)} N_j^{(k)} dl \right) \tag{4.20}$$
$$\left. + \varepsilon\mu \frac{\partial^2 u_j}{\partial t^2} \iint_{(k)} N_i^{(k)} N_j^{(k)} dr dz \right\} = 0, \qquad i=1,2,\ldots,n$$

The radiation boundary condition results into a first order time derivative term which is readily taken to the left hand side .

4.2.2 Boundary Conditions at the Feed Line

For all the excitation models discussed in Section 3.3, the boundary conditions at the feed line can be specified by substituting into the right-hand side of equation (4.15), the expression for the time-varying tangential electric field corresponding to the excitation function. Theoretically, this function, can be of any time varying form: sinusoidal or non-sinusoidal. It is worth noting here that, the above-mentioned excitation models are all approximate since they are neglecting the higher order modes and the field reflected from different parts of the antenna. In other words, the excitation field at the base of the monopole was considered to retain its original form all through the computation time. This is obviously not the case in reality, unless the generator is connected directly to the base of the monopole. Indeed, the time domain computation would never be complete if the reflected fields were neglected. To have a better model of the feed, a new method of excitation is hereby introduced.

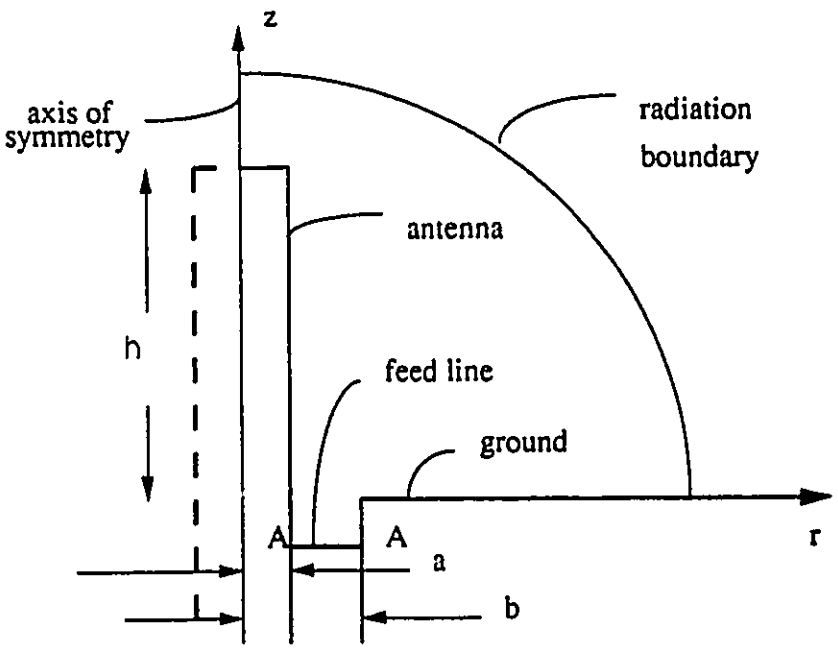

Fig. 4.1 Cylindrical monopole antenna driven by a coaxial line

Consider a problem configuration of Fig. 4.1, which consists of a cylindrical monopole antenna fed by a coaxial line. Boundary conditions have to be defined on the section A-A of the coaxial line. More specifically, appropriate expression for the tangential (r-directed) electric field has to be obtained to be used in equation (4.15). It is known that the incident (TEM) electric field inside a coaxial line is given by,

$$E^i(t) = \frac{V^i(t)}{\ln(b/a)r} a_r \tag{4.21}$$

where $V^i(t)$ is the time-varying excitation voltage, a and b are as shown in Fig. 4.1, and r is the radial distance from the antenna axis. The tangential electric field at the feed line will be as given by equation (4.21) as long as the reflected field from the end of the coaxial line has not reached the feed line. This kind of boundary conditions mentioned so far, has been used for FD-TD computation in [18]. While expressing the electric field at the feed line as above, the computation time has to be less than the time required for the wave to travel twice the distance between the feed line (A-A) and the end of the coaxial line. For longer computation times, the feed line has to be placed very far below the ground level. By doing this, the problem domain is obviously extended and the number of variables is increased. To get an idea of how far below, the feed line has to be placed, consider a case whereby the exciting voltage is sinusoidal with a frequency of 100 MHz. If the steady state condition is achieved after 5 periods counted from the time the wave reaches the base of the monopole, then the feed line has to be placed at a distance greater than or equal to 5 wavelengths (15 meters) below the ground level! This is obtained as follows: Let the feed line be at a distance l_f, below the ground level. For the reflected wave not to reach the feed line the computation time, $t_c \leq 2l_f/c$, where c is the speed of light. At the same time, for the steady state to be achieved, the computation time has to be, $t_c \geq l_f/c + n/f$, where f is the frequency and n is the number of periods required. Solving the two inequations simultaneously, will give the computation time required and the distance of the feed line below the ground level. You can see here that, half of the computation time is wasted in waiting for the wave to reach the base of the antenna.

It is clear by now that, specifying the boundary conditions at the feed line in the manner suggested above, introduces several limitations and complications. In the FD-TD computation a way out is suggested although not implemented in [18]. The technique suggested involves the computation of the boundary field values from the local values by interpolation. It is actually the implementation of the absorbing boundary conditions suggested in [25]. These absorbing boundary conditions are however, specifically tailored for the finite difference algorithm and it is pretty hard to adapt them for the finite element formulation. In the following subsection, absorbing boundary conditions for the reflected field in the coaxial line, are suggested for the first time, to enable the placement of the feed line anywhere below the ground level while still permitting any lengths of the computation time.

4.2.3 Implementation of the Absorbing Boundary Conditions at the Feed Line

Consider a monopole antenna fed by a coaxial line as shown in Fig. 4.1. When a generator is connected to the other end of the coaxial line, the incident TEM electric field at the feed line will be as given by (4.21). When the electromagnetic wave reaches the ground level, because of the discontinuity there, some of the incident field will be reflected and some will proceed to the top of the antenna where the same will happen. At the discontinuities, several higher order modes will be generated. If the dimensions of the coaxial line are small enough, most of the generated higher order modes will not propagate through the line towards the generator, and even those modes whose propagation will be supported by the coaxial line, will be of insignificant amplitudes. This however is much decided by the dimensions of the line and the frequency spectrum of the exciting signal. The TEM mode will certainly propagate towards the generator. If the feed line is far enough below (typically $3(b\text{-}a)$), the reflected wave at the feed line will consist only of the TEM mode.

Now, it is desired to place absorbing boundary conditions for this reflected TEM mode while still giving room for the incident field.

It is known that equation (3.18) holds inside the coaxial transmission line. Or more specifically, for the wave going in the negative z direction in the coaxial line,

$$-H_{\phi}^{R} = \frac{E_{r}^{R}}{\eta} \tag{4.22}$$

where the superscript, R, denotes the reflected field.

Knowing the fact that the field inside the coaxial line at any instant and at any position is the sum of the incident and the reflected field, the right-hand side of equation (4.15), for any point in the coaxial line, can be written as,

$$\oint_{(k)} \left(\sigma \tilde{E}^{R}_{\tan(CCW)} + \varepsilon \frac{\partial}{\partial t} \tilde{E}^{R}_{\tan(CCW)} + \sigma \tilde{E}^{I}_{\tan(CCW)} + \varepsilon \frac{\partial}{\partial t} \tilde{E}^{I}_{\tan(CCW)} \right) N_i^{(k)} dl \tag{4.23}$$

where the superscript, I, denotes the incident field.

If the medium inside the coaxial line is lossless, the first two terms in (4.23) can be handled in the same way as for the case of the radiation boundary conditions in Section 4.2.1, and equation (4.23) will become,

$$-\sum_{j=1}^{n} \left(\frac{\partial u_j^{R}}{\partial t} \sqrt{\mu \varepsilon} \oint_{(k)} N_i^{(k)} N_j^{(k)} dl + \oint_{(k)} \varepsilon \frac{\partial}{\partial t} \tilde{E}^{I}_{\tan(CCW)} N_i^{(k)} dl \right) \tag{4.24}$$

When equation (4.24) is substituted into (4.15), the result is the form of the differential equation subsystem for elements with a side on the feed line, given as,

$$\sum_{j=1}^{n}\left\{u_j\iint_{(k)}\left[\frac{\partial N_i^{(k)}}{\partial r}\frac{\partial N_j^{(k)}}{\partial r}+\frac{\partial N_i^{(k)}}{\partial z}\frac{\partial N_j^{(k)}}{\partial z}+\frac{\partial N_i^{(k)}}{\partial r}\frac{N_j^{(k)}}{r}\right]\right.$$
$$\left.+\frac{\partial u_j^R}{\partial t}\sqrt{\mu\varepsilon}\oint_{(k)}N_i^{(k)}N_j^{(k)}dl+\varepsilon\mu\frac{\partial^2 u_j}{\partial t^2}\iint_{(k)}N_i^{(k)}N_j^{(k)}dr\,dz\right\} \qquad (4.25)$$
$$=\oint_{(k)}\varepsilon\frac{\partial}{\partial t}\vec{E}^I_{tan(CCW)}N_i dl,$$
$$i=1,2,\ldots,n$$

Notice that the absorbing boundary conditions at the feed line have introduced a new variable, u_j^R, thus making the number of unknowns greater than the number of equations. The equations will obvously be difficult to solve. However, recognizing the fact that the u_j's stand for the total ϕ-component of the magnetic field at the corresponding nodes, then simply,

$$u_j = u_j^I + u_j^R \qquad (4.26)$$

Now, using (4.26), all the terms consisting of u_j, $\partial u_j/\partial t$, and $\partial^2 u_j/\partial t^2$, for the feed nodes have to be written in terms of u_j^I and u_j^R. The parts consisting of the u_j^I will readily be taken to the right hand side of (4.25). The incident magnetic field inside the coaxial line can be easily computed from the incident electric field (which is known), through equation (3.18). Thus, for the feed nodes, what will have to be solved for, will be the reflected ϕ-component of the magnetic field. This direct computation of the reflected magnetic field has many advantages, (as will become apparent later), towards the computation of the input admittance of the antenna.

Having placed the absorbing boundary conditions for the generator bound electromagnetic wave, there is no more need to place the feed line far below the ground level. Neither is there a need to approximate the boundary conditions at the feed line by neglecting the higher order modes or the reflected field. Obviously, there is no more limitation in the computation time discussed in subsection 4.2.2, and thus steady state solution is made possible. From here on, the antenna model which

implements an absorbing boundary condition at the feed line will be shortly referred to as 'coaxially-fed antenna model'.

The absorbing boundary conditions at the feed line have provided in addition, one more important advantage. This will become more apparent in Chapter 5, but it is worth mentioning something at this juncture. The solution algorithm chosen for the system of differential equations resulting from the time-domain formulation, requires the specification of the initial conditions for the unknown variable and its first time derivative. It is customary to assume zero field initial conditions at time equal to zero although this may not be true always. In this formulation in particular, the initial field everywhere will not be zero for a non-zero starting excitation. For any form of the excitation field, the corresponding initial conditions with regard to the total magnetic field, for all the nodes in the problem domain can be easily computed. This is because, the initial total magnetic field everywhere in the domain is zero except at the feed line whose value can easily be computed using (3.18). This will be non-zero if a non-zero starting excitation field is applied. It is known however, through the experience of the finite-difference time-domain algorithm, that non-zero initial conditions result in many problems in the solution of the system of differential equations and the solution may be very unreliable. In many cases, non-zero initial conditions are avoided by solving only for the excitation fields which smoothly increase from zero. This is however not necessary if suggested absorbing boundary conditions are implemented at the feed line. The reason to this is the fact that the initial conditions to be specified at the feed nodes are for the reflected field and its first time derivative, which is exactly zero at time equal to zero for what ever form of the excitation field. This fact will allow a unit step response to be computed with apparently no difficulty and thus giving room for the computation of the response of any other known incident field by the use of the convolution integral.

4.2.4 Boundary Conditions for a Lossy Medium

The boundary conditions so far discussed have been derived via the intrinsic impedance of a lossless medium. The concept of impedance is actually a frequency domain one. It has been successfully borrowed to the time domain only for the case of a lossless medium, when the intrinsic impedance is real thus capable of being handled in the time domain. When the medium is lossy, or rather specifically, with non-zero conductivity, σ, the intrinsic impedance as given by (3.19), will be complex. Certainly, as it is, the complex intrinsic impedance will not be accomodated in the time domain.

The simplest, but rather approximate way to include losses in the finite-element problem formulation is to use approximate feed models suggested in Section 3.3 along with zero outer boundary conditions while limiting the computation time to the time required for the wave to reach the outer boundary.

More rigorous methods can be suggested depending on the material properties of the medium, (σ, μ, ϵ), and the bandwidth of the exciting field.

The intrinsic impedance being complex, can be written in the form,

$$\eta = R(\omega)+j\omega L(\omega) \tag{4.27}$$

where $\omega = 2\pi f$, f is the frequency of the excitation field. The form of the intrinsic impedance given in (4.27) can be easily obtained while considering whether the medium is a good or bad dielectric, good or bad conductor, or any other combination of the material properties.

To implement the absorbing boundary conditions in the manner suggested in subsections 4.2.1 and 4.2.3., equation (3.20) is used along with (4.27), to yield,

$$E_{inc(CCW)}(\omega) = -[R(\omega)+j\omega L(\omega)]H_{\phi}(\omega) \tag{4.28}$$

Taking the inverse Fourier transform on (4.28) results in,

$$E_{tan(CCW)}(t) = -[R(t)*H_{\phi}(t)+L(t)*\frac{\partial H_{\phi}(t)}{\partial t}] \tag{4.29}$$

where * denotes convolution.

For a case of a single frequency, $R(\omega)$ and $L(\omega)$ in (4.28) can be made frequency-independent by evaluating them at the given frequency thus making them constants. In that case then, the convolution in (4.29) will just be a normal multiplication. In this particular case, (4.29) can be substituted into the right hand side of (4.15) and the procedure used in subsection 4.2.1 may be followed to yield,

$$\sum_{j=1}^{n}\left\{\mu_j\left[\iint_{(k)}\left(\frac{\partial N_i^{(k)}}{\partial r}\frac{\partial N_j^{(k)}}{\partial r}+\frac{\partial N_i^{(k)}}{\partial z}\frac{\partial N_j^{(k)}}{\partial z}+\frac{\partial N_i^{(k)}}{\partial r}\frac{N_j^{(k)}}{r}\right)dr\,dz+R\sigma\oint_{(k)}N_i^{(k)}N_j^{(k)}\,dl\right]\right.$$
$$+\frac{\partial u_j}{\partial t}\left(\sigma\mu\iint_{(k)}N_i^{(k)}N_j^{(k)}\,dr\,dz+(L\sigma+Re)\oint_{(k)}N_i^{(k)}N_j^{(k)}\,dl\right) \tag{4.30}$$
$$\left.+\frac{\partial^2 u_j}{\partial t^2}\left(\varepsilon\mu\iint_{(k)}N_i^{(k)}N_j^{(k)}\,dr\,dz+L\varepsilon\oint_{(k)}N_i^{(k)}N_j^{(k)}\,dl\right)\right\} = 0,$$
$$i=1,2,\ldots,n$$

Equation (4.30) gives the form of the differential equation subsystem for an element with a side on the radiation boundary, when the medium is lossy but for a monochromatic excitation. The radiation boundary conditions implemented in this way, introduce contributions to every term of the differential equation subsystem of (4.15). Indeed (4.30) can be taken to be the general case, and the case of a lossless medium is only a particular case of (4.30).

When a broadband (multi-frequency) exciting field is used, the time-domain implementation of the radiation boundary conditions becomes exceedingly difficult because of the difficulty in working out the convolution integrals. A method which employs convolution integrals has been introduced in [26], but very discouraging remarks were given on the difficulty in numerically implementing the technique.

Chapter 5

5 Solution of the System of Differential Equations

The system of differential equations obtained from the analysis discussed in Chapter 4 will generally be of the form,

$$M\ddot{u} + C\dot{u} + Ku - f = 0 \tag{5.1}$$

The coefficient matrices M, C and K, are obtained after working out analytically or otherwise, a couple of surface and line integrals as shown in Chapter 4 and after assembling the element differential equation subsystems. Several analytical expressions for the generic integrals are provided in Appendix A, for all the cases encountered in the time domain formulation. The emphasis was put in the time domain formulation, however, majority of these generic integrals may be found useful in the frequency domain formulation.

A general algorithm for solving such a system of differential equations has been given in [27]. The algorithm, apart from being easy to implement, provides flexibility in changing the time step to suit the manner in which the variable changes. This feature is particularly useful in dealing with transients which may be fast changing in the beginning and slow varying at their falling edges. All this flexibility of the algorithm, is achieved with a very reasonable level of accuracy and is generally time saving. Here below the algorithm is discussed briefly in general and in particular to the way it has been implemented in this work.

In a single time interval Δt, shown in Fig. 5.1, the unknown function u is approximated by a polynomial of degree p in time t, taken as zero at point n. Thus u may be written as:

$$u = u_n + \dot{u}_n t + \ddot{u}_n \frac{1}{2}t^2 + \ldots \alpha_n^{(p)} t^p \frac{1}{p!} \tag{5.2}$$

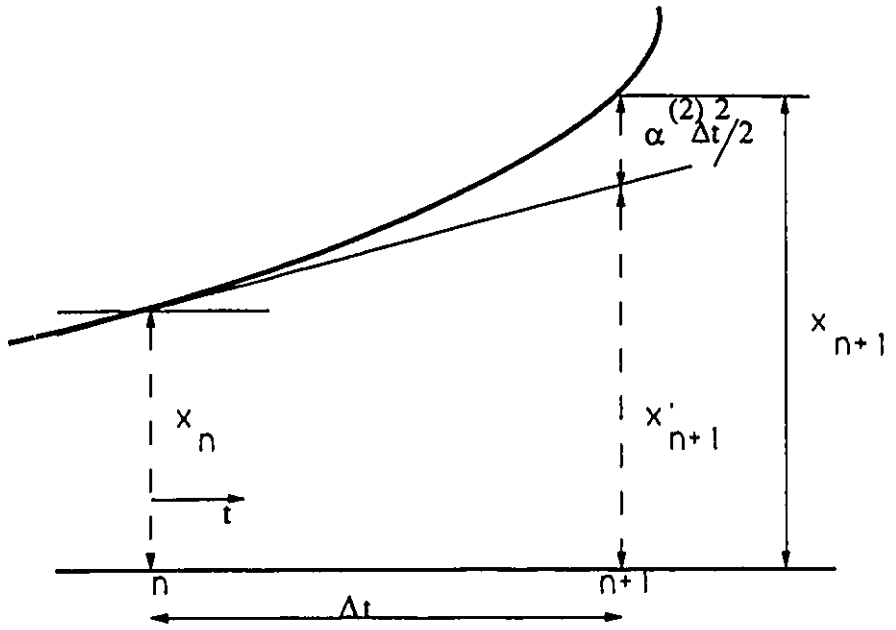

Fig. 5.1 A second order time step approximation

Equation (5.2) can also be written as

$$u = \sum_{q=0}^{p-1} u_n^q \frac{t^q}{q!} + \alpha_n^{(p)} t^p \frac{1}{p!} \tag{5.3}$$

where the following notation has been used:

$$u_n^q = \left(\frac{d^q}{dt^q} u_n \right) , \qquad 0<t<\Delta t \tag{5.4}$$

It is generally assumed that, at the start of the time interval, u_n and its time derivatives up to order (p-1) are known. The unknown vector $\alpha_n^{(p)}$, remains to be determined which will in turn lead to the determination of u_{n+1} and its time derivatives as follows:

$$u_{n+1} = \sum_{q=0}^{p-1} u_n^q \frac{\Delta t^p}{q!} + \alpha_n^{(p)} \frac{\Delta t^p}{p!} = u'_{n+1} + \alpha_n^{(p)} \frac{\Delta t^p}{p!}$$
$$\dot{u}_{n+1} = \sum_{q=1}^{p-1} u_n^q \frac{\Delta t^{q-1}}{(q-1)!} + \alpha_n^{(p)} \frac{\Delta t^{p-1}}{(p-1)!} = \dot{u}'_{n+1} + \alpha_n^{(p)} \frac{\Delta t^{p-1}}{(p-1)!} \qquad (5.5)$$

etc.

For the determination of the unknown parameter α_n^p, a weighted residual method is applied which will demand that,

$$\int_0^{\Delta t} W(M\ddot{u} + C\dot{u} + Ku - f)\, dt = 0 \qquad (5.6)$$

If the following is defined,

$$\frac{\int_0^{\Delta t} W t^q dt}{\int_0^{\Delta t} W dt} = \theta_q \Delta t^q \qquad q=1 \text{ to } p \quad \theta_0 \equiv 1 \quad 0 \le \theta_q \le 1 \qquad (5.7)$$

then, using equation (5.3),

$$\frac{\int_0^{\Delta t} W u\, dt}{\int_0^{\Delta t} W dt} = \sum_{q=0}^{p-1} u_n^q \frac{\Delta t^q}{q!} \theta_q + \alpha_n^{(p)} \frac{\Delta t^p}{p!} \theta_p$$
$$\frac{\int_0^{\Delta t} W \dot{u}\, dt}{\int_0^{\Delta t} W dt} = \sum_{q=1}^{p-1} u_n^q \frac{\Delta t^{q-1}}{(q-1)!} \theta_{q-1} + \alpha_n^{(p)} \frac{\Delta t^{p-1}}{(p-1)!} \theta_{p-1}$$
$$\frac{\int_0^{\Delta t} W \ddot{u}\, dt}{\int_0^{\Delta t} W dt} = \sum_{q=2}^{p-1} u_n^q \frac{\Delta t^{q-2}}{(q-2)!} \theta_{q-2} + \alpha_n^{(p)} \frac{\Delta t^{p-2}}{(p-2)!} \theta_{p-2} \qquad (5.8)$$
$$\frac{\int_0^{\Delta t} W f\, dt}{\int_0^{\Delta t} W dt} = \bar{f}$$

When equation (5.6) is divided by the denominator of the left-hand side of (5.7), the following can be written:

$$\begin{aligned} M\left(\sum_{q=2}^{p-1} u_n^q \frac{\Delta t^{q-2}}{(q-2)!}\theta_{q-2} + \alpha_n^{(p)} \frac{\Delta t^{p-2}}{(p-2)!}\theta_{p-2}\right) \\ +C\left(\sum_{q=1}^{p-1} u_n^q \frac{\Delta t^{q-1}}{(q-1)!}\theta_{q-1} + \alpha_n^{(p)} \frac{\Delta t^{p-1}}{(p-1)!}\theta_{p-1}\right) \\ +K\left(\sum_{q=0}^{p-1} u_n^q \frac{\Delta t^{q}}{q!}\theta_{q} + \alpha_n^{(p)} \frac{\Delta t^{p}}{p!}\theta_{p}\right) - \bar{f} = 0 \end{aligned} \tag{5.9}$$

From equation (5.9), $\alpha_n^{(p)}$ can be determined as,

$$\alpha_n^{(p)} = \left(\frac{\Delta t^{p-2}}{(p-2)!}\theta_{p-2}M + \frac{\Delta t^{p-1}}{(p-1)!}\theta_{p-1}C + \frac{\Delta t^{p}}{p!}\theta_{p}K\right)^{-1} (\bar{f} - M\ddot{u}_{n+1}^{//} - C\dot{u}_{n+1}^{//} - Ku_{n+1}^{//}) \tag{5.10}$$

where the following parameters have been used,

$$\begin{aligned} u_{n+1}^{//} &= \sum_{q=0}^{p-1} u_n^q \frac{\Delta t^q}{q!}\theta_q \\ \dot{u}_{n+1}^{//} &= \sum_{q=1}^{p-1} u_n^q \frac{\Delta t^{q-1}}{(q-1)!}\theta_{q-1} \\ \ddot{u}_{n+1}^{//} &= \sum_{q=2}^{p-1} u_n^q \frac{\Delta t^{q-2}}{(q-2)!}\theta_{q-2} \end{aligned} \tag{5.11}$$

Equation (5.11) completes the definition of the pth-order algorithm. The only requirement for the algorithm to work, is the specification of the initial values of the variable u and all its time derivatives up to the order p-1.

For the second order algorithm (p=2), (the one used in this work), the procedure required can be stated briefly as follows:

(i) Choose parameters θ_1 and θ_2

(ii) Compute $u''_{n+1}=u_n+\dot{u}_n\Delta t\theta_1$, $\ddot{u}''_{n+1}=\ddot{u}_n$

(iii) Compute $\alpha_n^{(2)}=\left(M+\Delta t\theta_1 C+\frac{\Delta t^2}{2}\theta_2 K\right)^{-1}(\bar{f}-C\dot{u}''_{n+1}-Ku''_{n+1})$ (5.12)

(iv) Compute $u_{n+1}=u_n+\Delta t\dot{u}_n+\alpha_n^{(2)}\Delta t^2/2$, $\dot{u}_{n+1}=\dot{u}_n+\alpha_n^{(2)}\Delta t$

The load vector is computed as,

$$\bar{f}=\theta_1 f_{n+1}+(1-\theta_1)f_n \tag{5.13}$$

The requirement for an unconditional stability of the algorithm [27], is

$$\begin{aligned}\theta_1 &\geq 0.5\\ \theta_2 &\geq \theta_1\end{aligned} \tag{5.14}$$

Even though the unconditional stability is guaranteed when (5.14) is satisfied, big time steps may still give rise to undesirable oscillations. And even if the oscillations are not observed, too big time steps may degrade the accuracy. It has been found better to adhere to the Courant stability condition and at the same time ensure minimum dispersion [28] by satisfying the following conditions respectively,

$$\begin{aligned}c(\Delta t) &\leq h\\ \lambda_{min} &> 8h\end{aligned} \tag{5.15}$$

where c is the velocity of wave propagation, h is the length of the shortest element side, and λ_{min} is the minimum wavelength in the spectrum of the exciting pulse. For some forms of the excitation voltage, especially those having high slopes of a voltage increase, (e.g double exponential pulse), adherence to the Courant stability condition is still not a guarantee for a stable solution. It is characteristic of marching-on-in-time algorithms to surfer from late-time oscillations despite having satisfied the Courant

condition. This phenomenon has also been observed to happen in integral methods [29]. The causes given so far are such as insufficient samples (spacial and temporal), possibilities of internal resonances and/or errors caused while evaluating various intermediate quantities. Several techniques have been suggested to overcome this problem, which include averaging of the computed values [29]. The process of averaging, of course, extends the computation time and adds an additional burden to the memory requirement as it requires storage of the solution of the previous two steps. For this reason this method was not implemented in this work. In the method used in this work, whenever such a problem was observed to happen, it was overcome by simply changing the time step well before the time the oscillations were observed. This would be done in such a way that the ratio $h/\Delta t$ (length of element side/time step), is approximately maintained in the same order all through the domain of the problem. For instance, the step size can be changed, say increased, during the time the wave reaches the elements close to the outer boundary, which are normally made very coarse. In this respect, to be on a safe side, the element sizes should not differ much and most of the time there will be no need for adjusting the time step.

This algorithm, as explained in [27], provides a way of automatically changing the time step to suit a certain specified error criterion. For a pth order algorithm the estimate of the error is given as,

$$\frac{\Delta t^p}{(p+1)!}(\alpha_n^{(p)}-\alpha_{n-1}^{(p)}) \tag{5.16}$$

The criterion for changing the time step is based on the norm of the error given in (5.16). The procedure involves reduction of the time step if the norm of this error

$$\left|\frac{\Delta t^p}{(p+1)!}(\alpha_n^{(p)}-\alpha_{n-1}^{(p)})\right| > E_{\max} \tag{5.17}$$

and increasing the time step when

$$\left| \frac{\Delta t^p}{(p+1)!} (\alpha_n^{(p)} - \alpha_{n-1}^{(p)}) \right| < \gamma E_{max} \tag{5.18}$$

typical value of γ and the one used in this work is 0.5.

The maximum permissible error, E_{max}, is specified to be a certain fraction of the maximum norm of u, recorded in the process of computation. This fraction, which can be called the relative error, can be chosen as small as desired to improve the accuracy. However too small a value of the relative error may unnecessarily prolong the computation time. In this process, the upper and the lower limit of the time step needs to be specified. All the two limits should satisfy the stability condition mentioned above.

This algorithm as used in this work, is provided as a FORTRAN computer program DSDIF, written in the course of this work and presented in Appendix B. More details are provided in the program itself.

Chapter 6

6 Computational Results and Discussion

6.1 Validation

To test the validity of the formulation, some common antenna configurations were analyzed. But before the results are presented, there are some few issues which need to be made clear of, for a deserving evaluation of this new method of computation.

It should have to be understood that, results obtained out of this formulation as well as any other numerical methods, very much depend on the problem set-up. Unlike in the frequency domain formulations for which a particular suitable set-up can be fixed for a particular frequency under consideration, in the time domain normally a big range of frequencies are dealt with at the same time thus making it a little difficult to come up with an optimum set-up. The set-up mentioned here is with regard to element sizes at different locations of the problem domain, number of nodes and elements, position of the radiation boundary and even the choice of the time step. Although this fact was given a due concern, optimum set-ups are in no way claimed to have been achieved while analyzing the above-mentioned antenna configurations.

Attention is also drawn to the fact that, the analysis provided, only sets out to compute the magnetic field in the vicinity of the radiating structure, which in turn enables the computation of the current distribution on the surface of the radiating structure. The near field itself is a very useful information with regard to the problems this method is intended to work on, i.e EMI in PCB configurations. The solution values at the outer boundary of the problem domain can only serve as an approximation to the far field, since the outer boundary is only assumed to be in the far field but in reality that is not precisely the case. The far field values however, may easily be more accurately determined by using the computed surface current

distribution using well known techniques. This was, however, not done in this work (as the prime purpose was to demonstrate the validity of the method), and only approximate far field values are provided.

6.1.1 Application to a Cylindrical Monopole Antenna

The first test to the method was to model a problem configuration consisting of a cylindrical monopole antenna above a perfect ground plane. Different forms of excitation mentioned in Chapters 3 and 4, are studied in separate occassions. In all the cases the region surrounding the antenna was a free space and a 1 V voltage excitation was used.

In one occassion, antenna dimensions similar to those given in [22], were chosen. That is, $b/a = 1.189$, $h/\lambda_0 = 0.375$, $a/\lambda_0 = 0.0254$. To be able to make comparison with the published frequency domain data, the voltage excitation was taken to be sinusoidal with a frequency of 114 MHz, and described as,

$$V(t) = V_o \sin\omega t \tag{6.1}$$

The domain of the problem was bounded as shown in Fig. 6.1, (for both radial and axial delta gap excitations), where a quarter-circular radiation boundary was placed 3.5 meters from the base of the monopole. A total of 667 triangular elements discretized the problem domain with 370 nodes. The computation was made with an average time step of 25 pico seconds.

Using the matrix assembling program and the differential equation solving program written in the course of this work, the distribution of current on the antenna surface and the far field were computed as functions of time. The current distribution on the surface of the antenna was calculated via the relation, $\boldsymbol{n} \times \boldsymbol{H} = \boldsymbol{J}_s$, where $\boldsymbol{J}_s$ is the surface current density on the antenna and $\boldsymbol{n}$ is the unit vector normal to the surface. The current is obtained by multiplying the current density with the

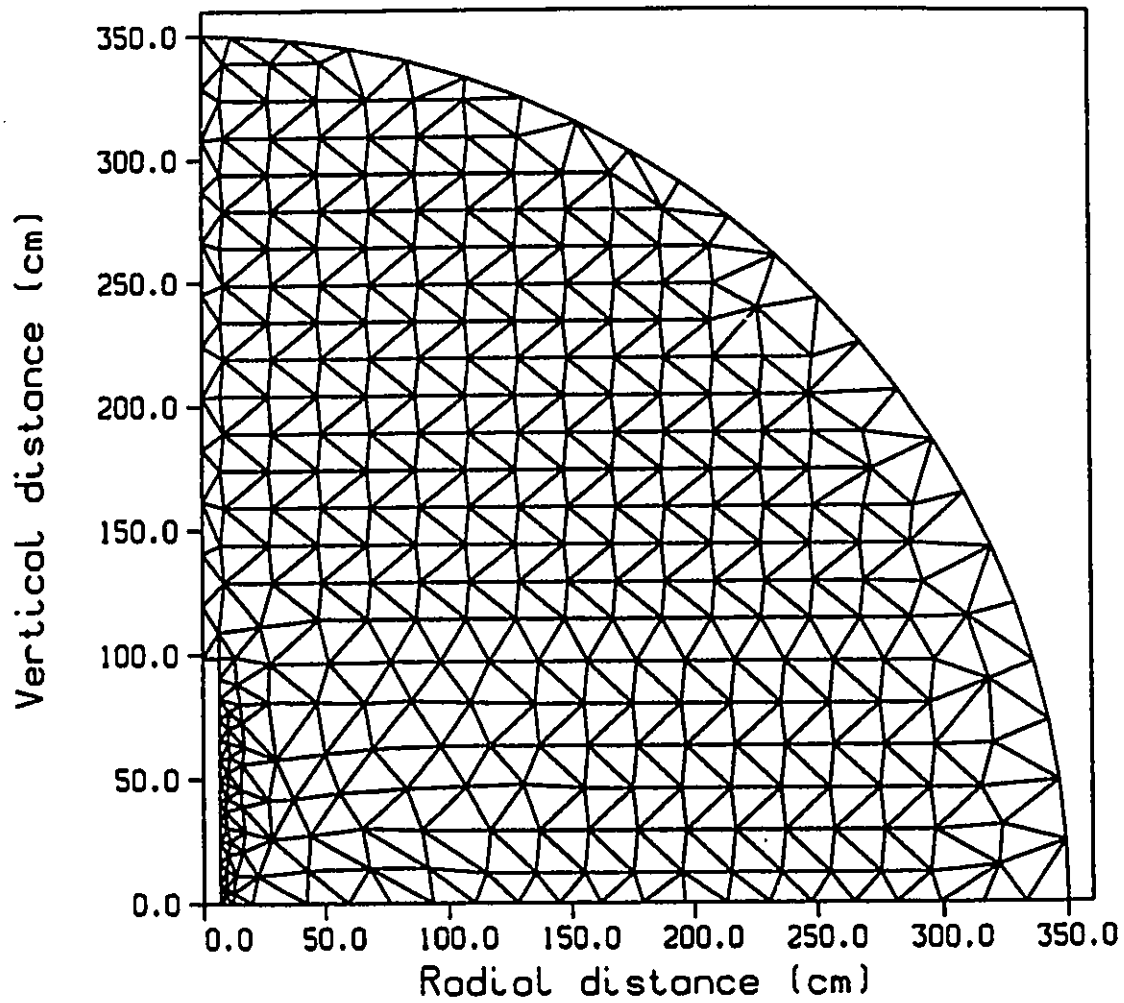

Fig. 6.1 Finite element mesh for a radial delta gap excitation of a cylindrical monopole antenna above a perfect ground plane

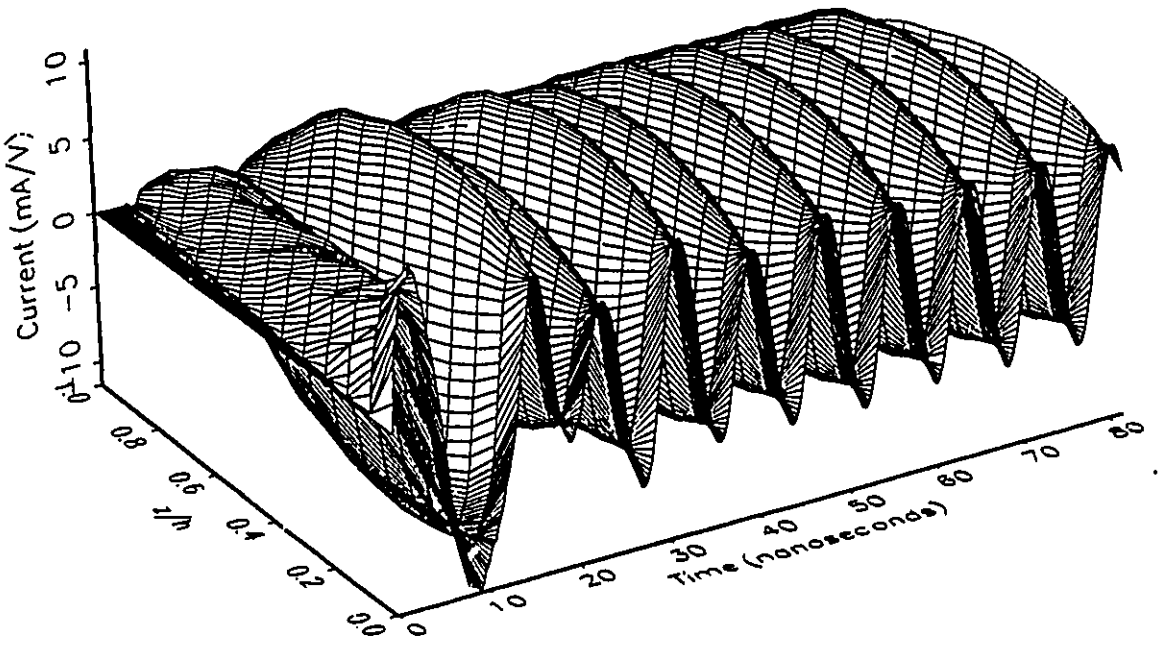

Fig. 6.2 Distribution of current on a cylindrical monopole antenna excited by a 1-V sinusoidal voltage through a radial delta gap

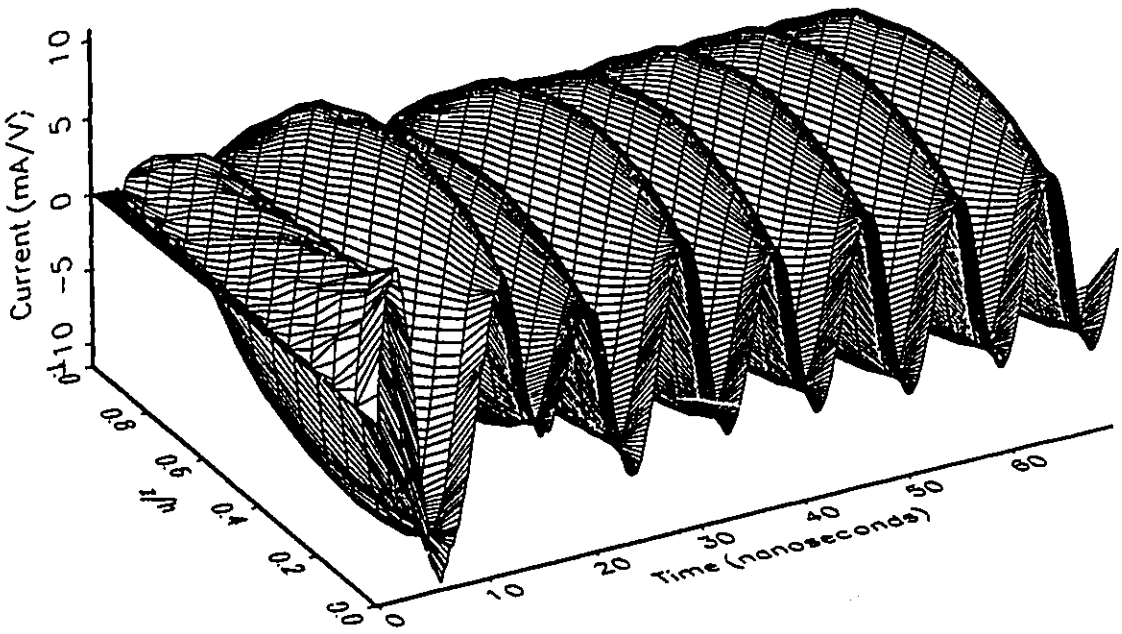

Fig. 6.3 Distribution of current on a cylindrical monopole antenna excited by a 1-V sinusoidal voltage through an axial delta gap

circumference of the antenna cross-section.

It is observed that in most cases, a steady state condition is achieved after about seven periods. The antenna current distribution for a radial delta gap excitation is plotted in Fig. 6.2. Fig. 6.3 gives the current distribution for an axial delta gap excitation.

The coaxially-fed model of the above-mentioned antenna was formulated as in Fig. 6.4. The problem domain was discretized into 676 triangles made up by 379 nodes and the radiation boundary was placed as above. The feed line was placed only 16 cm below the ground level. The results are plotted in Fig. 6.5. The driving point currents for the different modes of excitation are compared in Fig. 6.6. Observe the difference between the early time peaks and the steady state peaks. The first peaks are nearly twice larger than the steady state peaks. Indeed the frequency domain solutions miss up a very important information which is quite easily captured by the time domain formulation. This is the beauty of the time domain formulation.

Fig. 6.7 shows the FEM results along with the theoretical data published by King [30]. As can be seen from Fig. 6.7, the results obtained, are in good agreement with the theoretical data published by King. This can be said so especially when considering the degree of coarseness of the used finite element mesh. The big difference observed with regard to the case of the coaxially-fed antenna model discussed in Chapter 4, should not be misinterpreted as to be representing a poor model. It should be remembered that, the theoretical model used in [30] was only an approximation where higher order modes at different locations, were neglected. The coaxially-fed antenna model discussed, closely resembles the typical situation encountered in practice. Indeed, the model consisting of an antenna fed by a coaxial line, generally does not make the above-mentioned approximation and in view of this, the model is superior to the others. In fact, it is suggested that the results obtained via this model, have to be taken as a reference for comparing other models for reasons which will be more apparent a little later. The superiority of the coaxially-fed antenna model, will be demonstrated more clearly while comparing the model results with the measured data. While adopting the suggested reference, the King's model

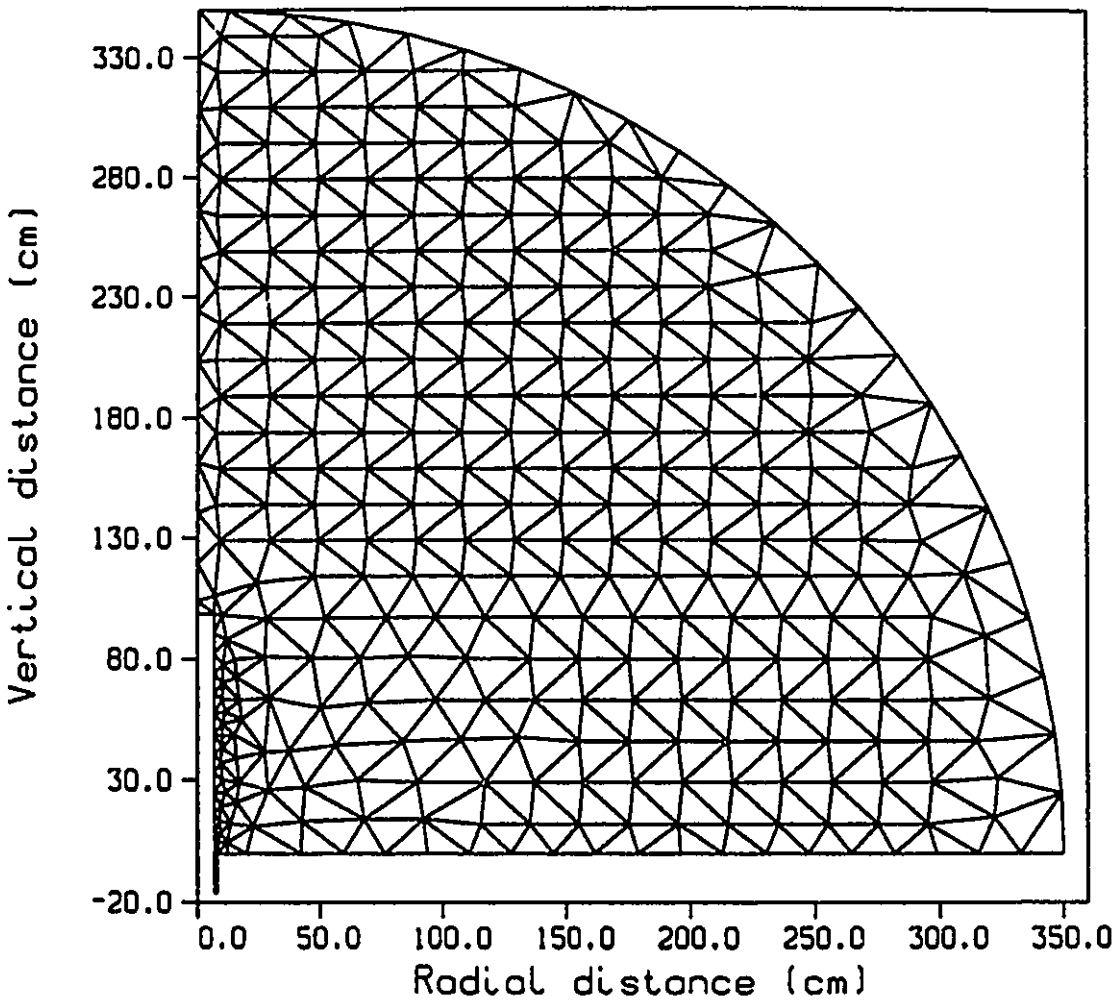

Fig. 6.4 Finite element mesh for a coaxially-fed cylindrical monopole antenna model

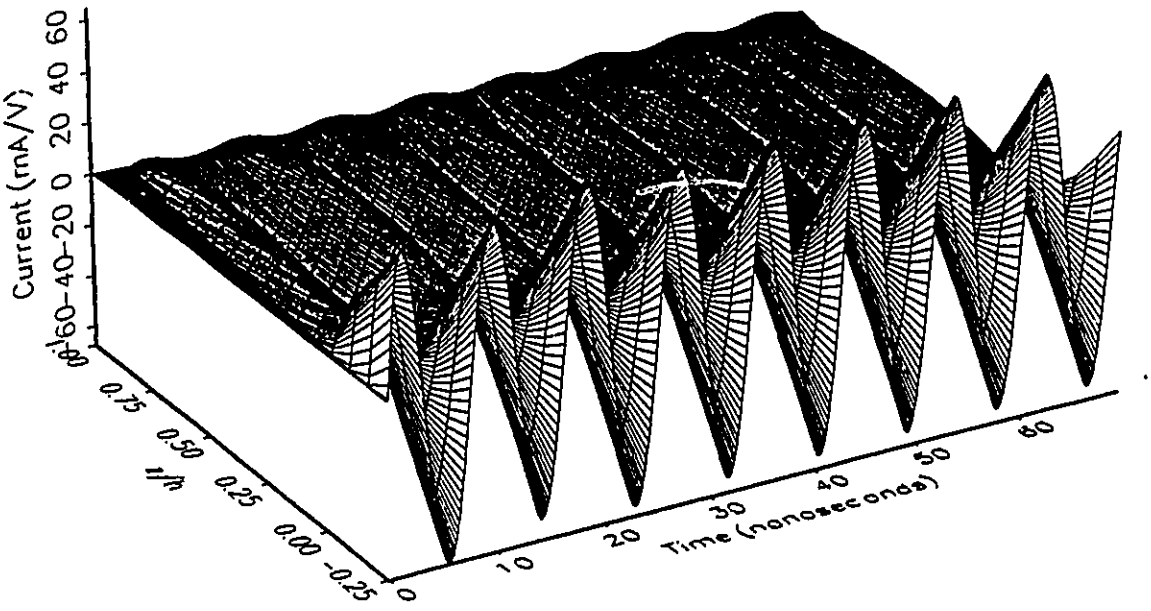

Fig. 6.5 Distribution of current on a section of the inner conductor of a coaxial line and on the surface of a cylindrical monopole antenna (The antenna stretches from $z/h = 0$ to 1.0)

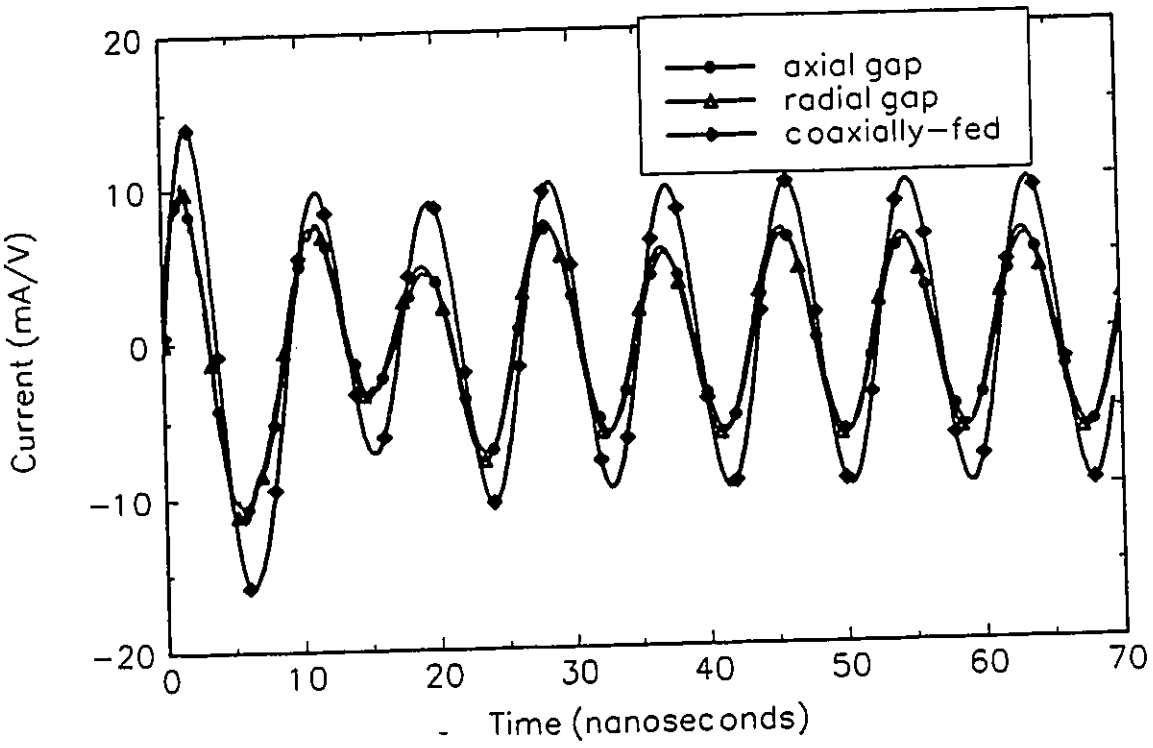

Fig. 6.6 Driving point current on a cylindrical monopole antenna above a perfect ground plane for different axcitation models

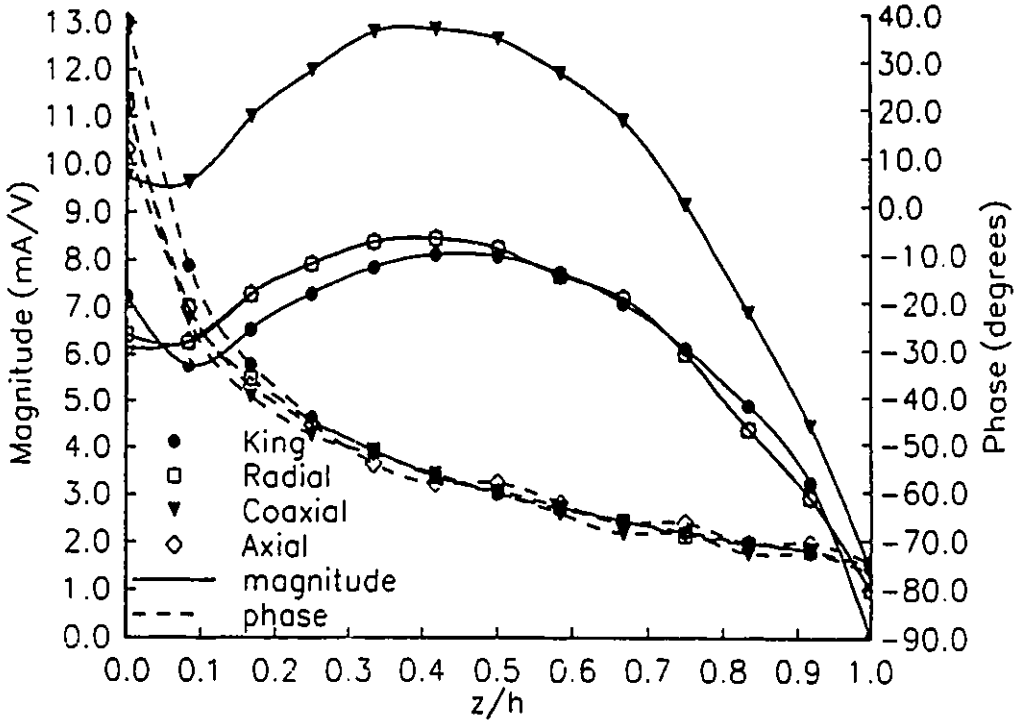

Fig. 6.7 The numerical (FEM) and theoretical results for the current distribution on a cylindrical monopole antenna above a perfect ground plane driven by a sinusoidal voltage

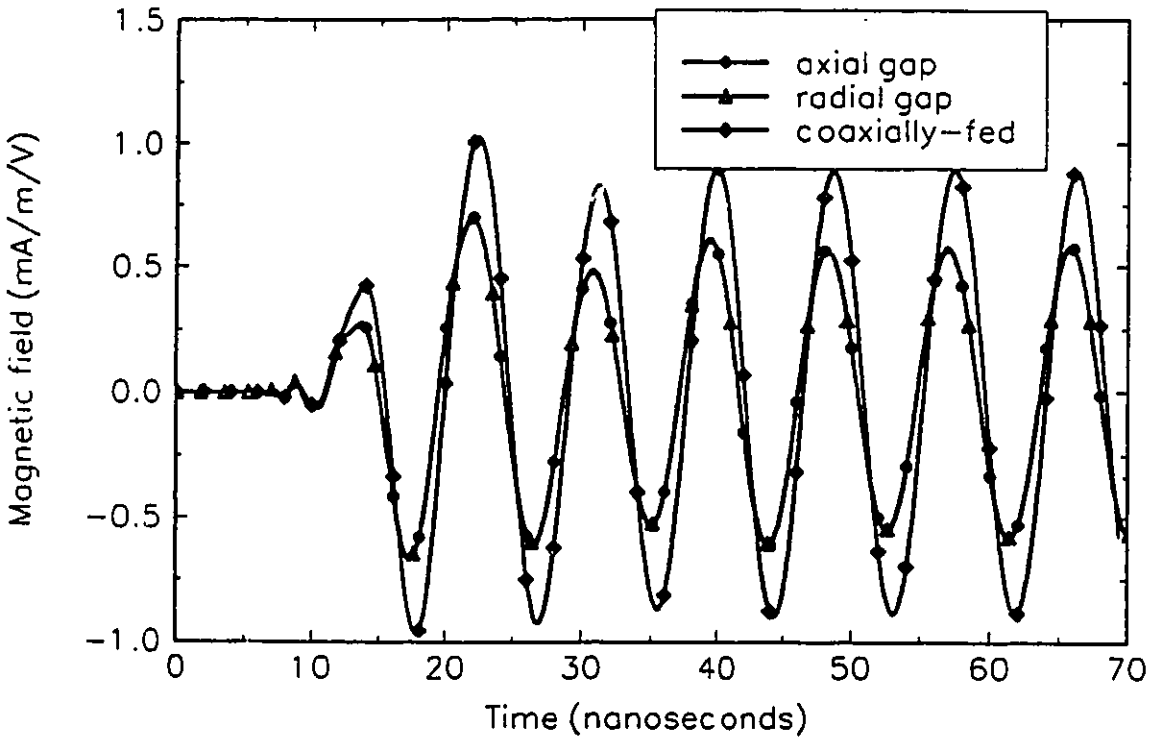

Fig. 6.8 The azimuthal component of the magnetic far field at the broadside of a cylindrical monopole antenna excited by a 1 V sinusoidal voltage

is seen to be closer followed by the radial delta gap model and finally the axial delta gap model. The latter two give almost same results.

The far-field time variation of the ϕ-component of the magnetic field at the broadside of the antenna is depicted in Fig. 6.8. Table 6.1 lists the computed input admittance for different models. The input admittance is computed through dividing

Method of computation	Input Admittance (mS)	
	Real Part	Imaginary Part
Axial delta gap	6.01	1.23
Radial delta gap	6.01	2.31
Coaxially-fed	9.05	3.61
Theoretical (King)	5.68	4.47

Table 6.1 Input admittance of a cylindrical monopole antenna computed using different methods.

the driving point current with the gap voltage for all models except the coaxial line driven model. In this, the reflected magnetic field at the feed line is simply divided by the incident magnetic field at the same position to yield the reflection coefficient. The reflection coefficient, is used, in turn, to compute the input admittance at the position of the feed line looking towards the antenna using,

$$Y_{in} = Y_c \frac{1+\Gamma}{1-\Gamma} \tag{6.2}$$

where Y_c is the characteristic admittance of the coaxial line, and Γ is the reflection coefficient at the specified position of the coaxial line. The antenna input admittance, Y_a, is then computed using the relation,

$$Y_{in} = \frac{Y_a + jY_c \tan\beta l}{Y_c + jY_a \tan\beta l} \tag{6.3}$$

where l is the distance of the feed line from the antenna base and $\beta = 2\pi/\lambda$.

Yet another proof of the validity of the formulation was achieved by investigating the response to a nonsinusoidal voltage excitation. A cylindrical monopole antenna excited by a 1 V Gaussian pulse through a coaxial line, was investigated. The Gaussian pulse is described as follows:

$$V(t) = V_0 \exp(-t^2/2\tau_p^2) \tag{6.4}$$

The antenna is characterized by the time τ_a = h/c; this being the time for the electromagnetic wave to traverse its length. τ_p is the characteristic time of the Gaussian pulse. To be able to make a proper comparison with the measured and numerical results published in [18], a similar problem configuration was used. The parameters used were as follows: b/a = 2.30, h/a = 32.8, and $\tau_p/\tau_a = 1.61 \times 10^{-1}$. The Gaussian pulse was delayed by four times its characteristic time in order to achieve a smooth increase of the excitation field. The problem set up was as shown in Fig. 6.9. The feed line, was placed only 28 cm below the ground level. This can be contrasted with the distance from the feed line used in [18] which is more than twice the antenna height! This can easily be observed in Fig. 8 of [18].

The reflected voltage in the coaxial line can be computed directly from the values of the reflected ϕ-component of the magnetic field via the relation,

$$V^R = -\eta H_\phi^R \ln(b/a) r \tag{6.5}$$

where r is the r-coordinate of the point where the voltage is computed and η is the intrinsic impedance of the medium.

The comparison between the results obtained using this present formulation implementing a coaxially-fed antenna model, and the measured data provided in [18] with regard to the reflected voltage in the coaxial line, is shown in Fig. 6.10. No

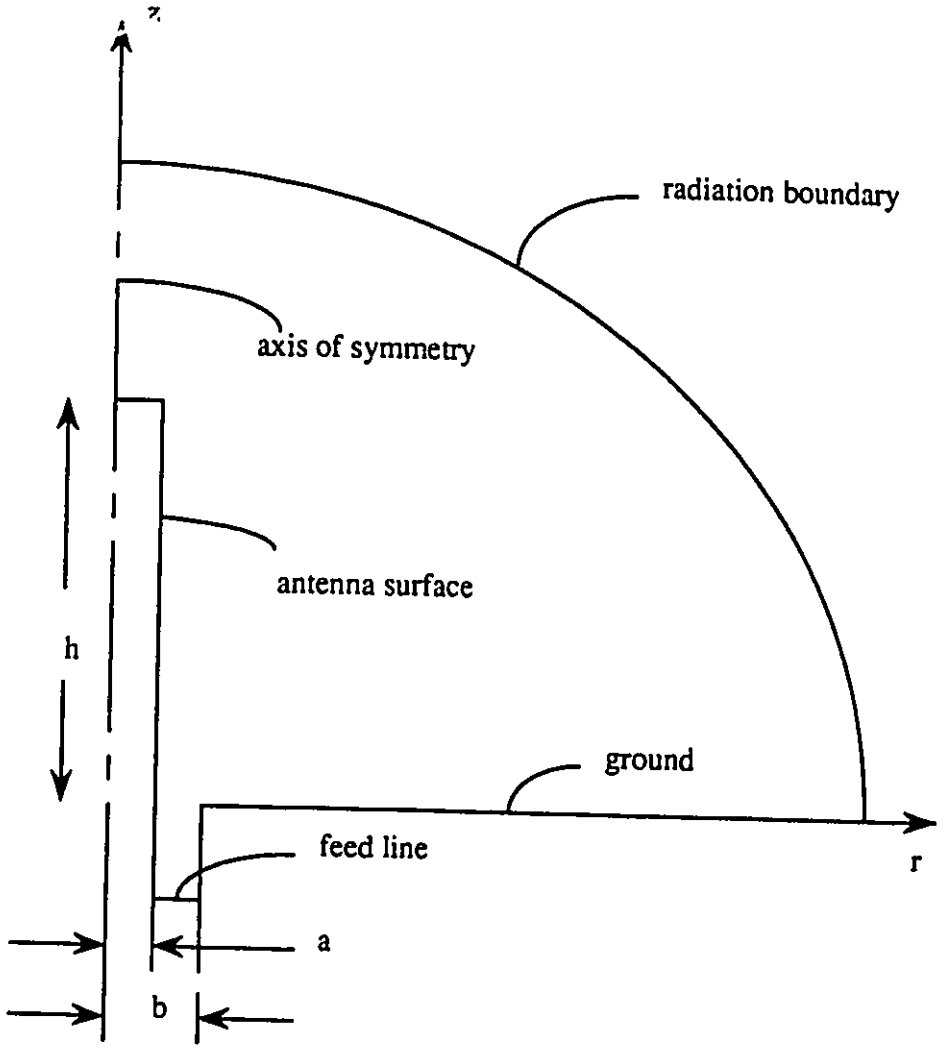

Fig. 6.9 Problem set up for the coaxially-fed cylindrical monopole antenna above a perfect ground plane

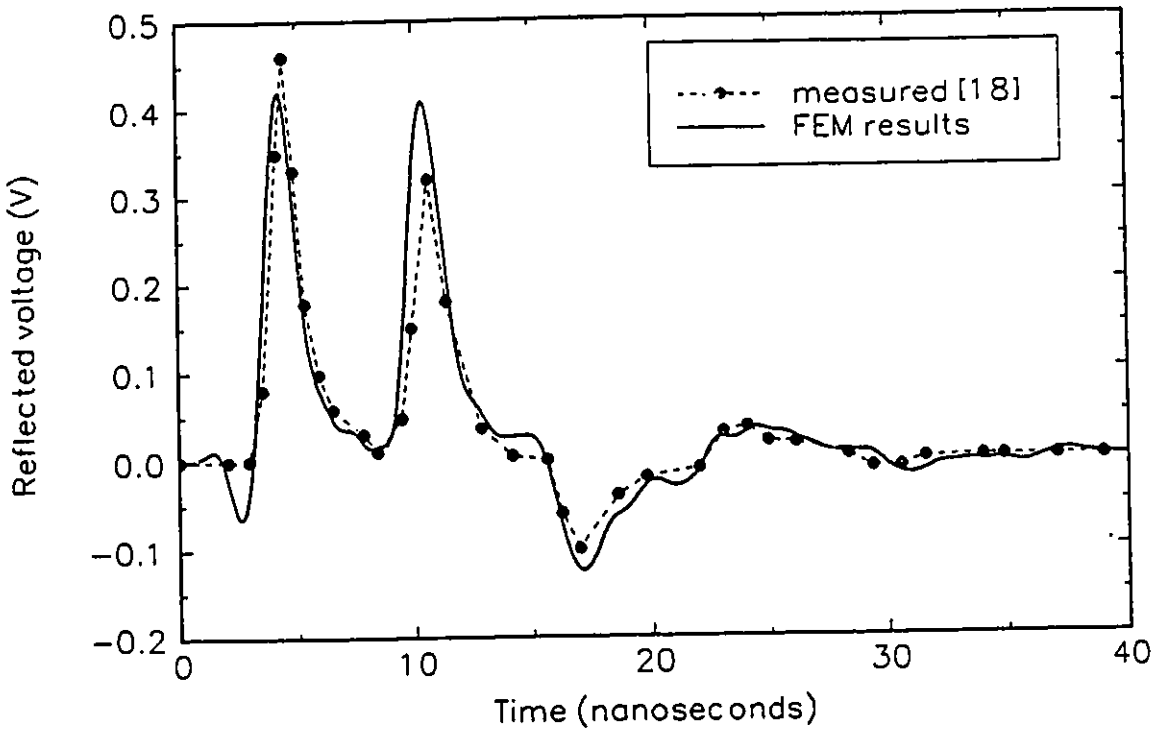

Fig. 6.10 Reflected voltage in a coaxial line feeding a cylindrical monopole antenna with a 1 V Gaussian pulse

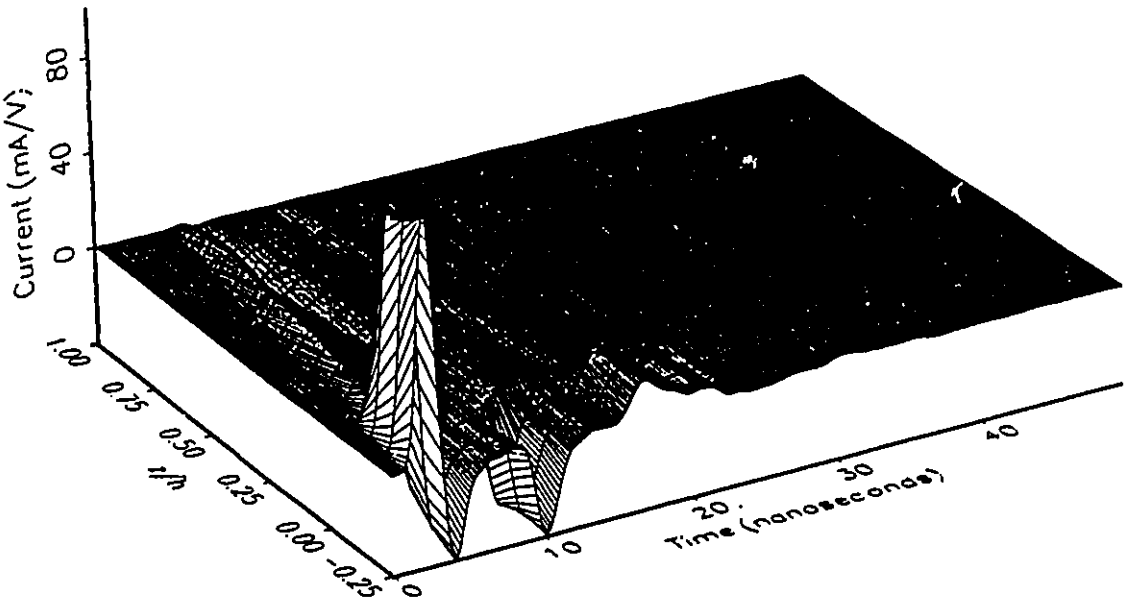

Fig. 6.11 Distribution of current over part of the inner conductor of a coaxial line and on the surface of a cylindrical monopole antenna driven by a 1 V Gaussian pulse

doubt, the agreement is quite good. Minor variations observed, apart from being due to different methods used, may be attributed to the differences in the problem dimensions used such as absolute values of b, a and h. These values were not explicitly specified in [18]. Different values of h will result in different intervals in the voltage peaks observed in Fig. 6.10. Another obvious reason for the variation in the two results is the fact that the measured data was only approximately read from the plot of Fig. 8 in [18]. The other reason would be due to the fact that the reflected voltage was computed at a position different from that measured in [18]. However, there is a very good agreement in the form and magnitude of the peaks. The larger peaks correspond to the reflections from the coaxial line end and from the top end of the monopole. The interval between the two peaks is approximately equal to twice the time required for the electromagnetic wave to travel the antenna length.

The three-dimensional plot given in Fig. 6.11, shows the distribution of current over part of the inner conductor of the coaxial line and on the surface of the cylindrical monopole antenna. While following closely the peaks and the troughs, the propagation of the incident and the reflected waves can be easily seen. Part of the wave incident on the antenna base is reflected and part of it continues to propagate towards the end of the monopole. A difference in the magnitude of the peaks between the wave incident at the antenna base and the transmitted wave is quite clearly shown in Fig. 6.11. Observe that only small part of the wave proceeds towards the top of the antenna. This in turn means that, only small part of the wave is radiated in this particular case. The wave reflected back into the coaxial line is reversed in phase as expected, which could be interpreted as the current directed toward the generator. This wave is not seen to be re-reflected back to the antenna, thus proving the suitability of the absorbing boundary conditions placed at the feed line. When the transmitted wave reaches the top end of the antenna, again some of it is reflected. This can be seen also in Fig. 6.11, by observing the wave trough that starts from the antenna top end and proceeds towards the coaxial line. When the reflected wave reaches the base of the monopole it is reflected again, and this process continues until

all the wave vanishes. The formulation has successfully demonstrated the actual wave propagation phenomenon taking place in the problem in question. This is quite impressive!

6.1.2 Application to a Conical Monopole Antenna

A conical monopole antenna above a perfect ground plane, presented another problem configuration suitable for testing the validity of this finite-element time domain formulation. To be able to make comparison with the published data a problem geometry similar to the one chosen in [18], was investigated. The problem geometry is as shown in Fig. 6.12 with its corresponding finite element mesh shown in Fig. 6.13. The problem dimensions were as follows: b/a = 2.3 (50 Ω characteristic impedance), h/a = 23.1, h'/h = 8.63 x 10^{-1}, α = 30°, and τ_p/τ_a = 2.29 x 10^{-1}. The Gaussian pulse was delayed by four times its characteristic time for a smooth increase of the excitation voltage. The finite element mesh comprised of 398 nodes making up a total of 711 triangles. The feed line was placed only 30 cm from the ground level while implementing the suggested absorbing boundary conditions at the feed line. The radiation boundary was placed 350 cm away from the vertex of the monopole. The time step was made to vary between 2.5 x 10^{-10} and 3.5 x 10^{-10} seconds.

The most easy parameter to compare with that given in [18] is the reflected voltage inside the coaxial line. Observe that same remarks as provided in subsection 6.1.1 applies in this case with regard to the preciseness of comparison without the specification of the absolute geometry dimensions. However, the best has been done to make available the data provided in [18] for comparison with this present formulation.

The reflected voltage computed using equation (6.4) is compared with that obtained in [18] and is shown in Fig. 6.14. As can be seen, except for variations due to reasons mentioned in the preceding section, the two results compare well. The current distribution on the part of the inner conductor of the coaxial line and over the

surface of the conical monopole is as depicted in Fig. 6.15. Again in this figure the wave propagation can be seen very clearly. Unlike the case of a cylindrical monopole antenna, very small part of the Gaussian pulse is reflected back to the coaxial line and a greater part of it proceeds towards the antenna top. Even at the antenna top very small part of the pulse is reflected back as can be clearly seen in Fig. 6.15. This can be simply thought of being due to the capability of the conical monopole antenna to accomodate a broad range of frequencies making up the Gaussian pulse. In other words, a conical monopole antenna is a broadband antenna capable of radiating a broad spectrum of frequencies. This is a good indication that a conical monopole is a better radiator than a cylindrical one for a wide range of frequencies.

A response of the conical monopole antenna described above, to a 1 V sinusoidal voltage is also provided in Fig. 6.16 for the current distribution. The far-field time variation of the ϕ-component of the magnetic field at the ground level is presented in Fig. 6.17, and the reflected voltage in the coaxial line is shown in Fig. 6.18. Comparing the far field presented in Fig. 6.17 for a conical monopole antenna case and that shown in Fig. 6.8 for the case of a cylindrical monopole antenna, the superiority of the former becomes evident with regard to radiation effectiveness. This may be a good design clue for an EMI engineer who may wish to lower radiated emissions from the components of the equipment he wishes to design. By investigating the radiated field for different component shapes, the optimum shape can be determined especially when nonsinusoidal exciting voltages are involved.

Generally speaking, the conical monopole antenna configuration was seen to be rather more sensitive to the discretization of the problem domain, particularly with the size of triangles and the density of nodes around the discontinuities. These discontinuities include the junction between the conical monopole and the center conductor of the coaxial line, the junction between the ground and the outer conductor of the coaxial line, and the top edge of the cone. Insufficient discretization would normally give rise to instability, despite having satisfied the Courant stability condition. For best results, the triangle sizes should not differ much and obviously a reasonably small time steps have to be used.

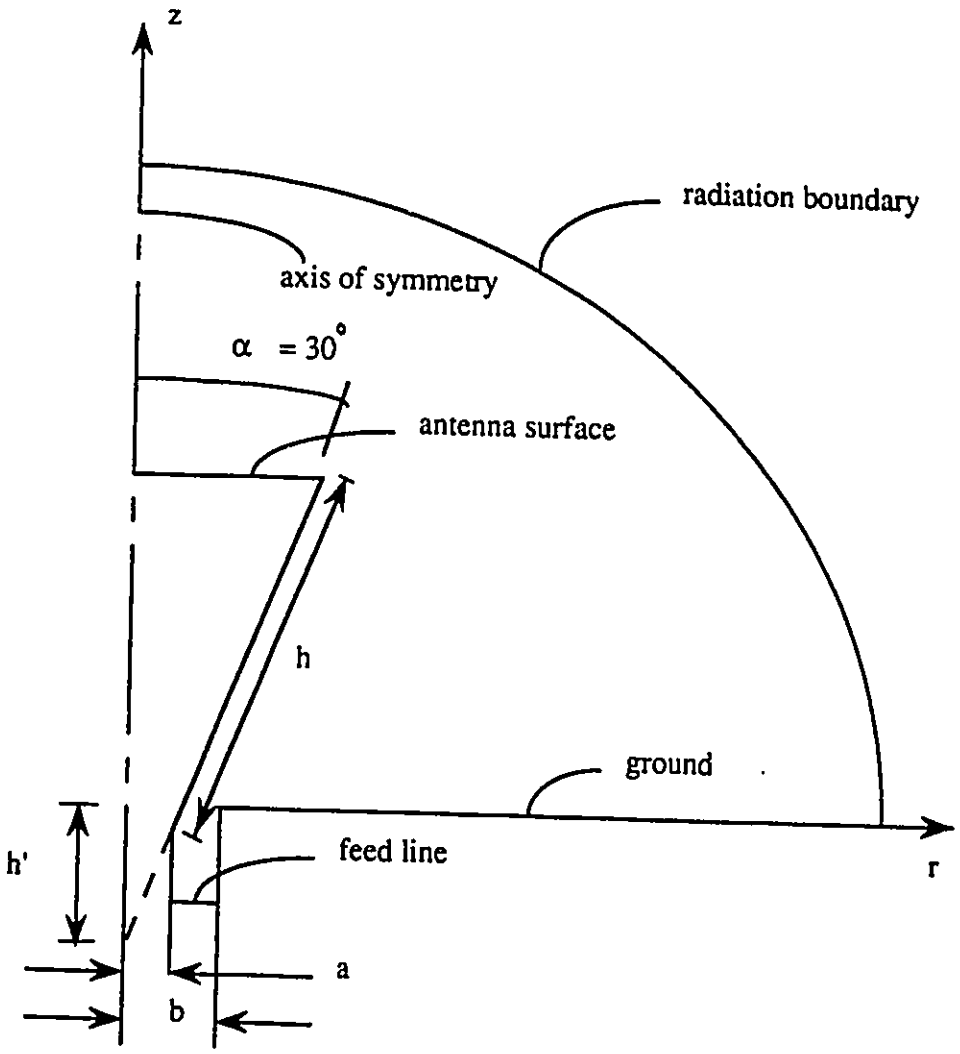

Fig. 6.12 Problem configuration consisting of a conical monopole antenna above a perfect ground plane, driven by a coaxial line

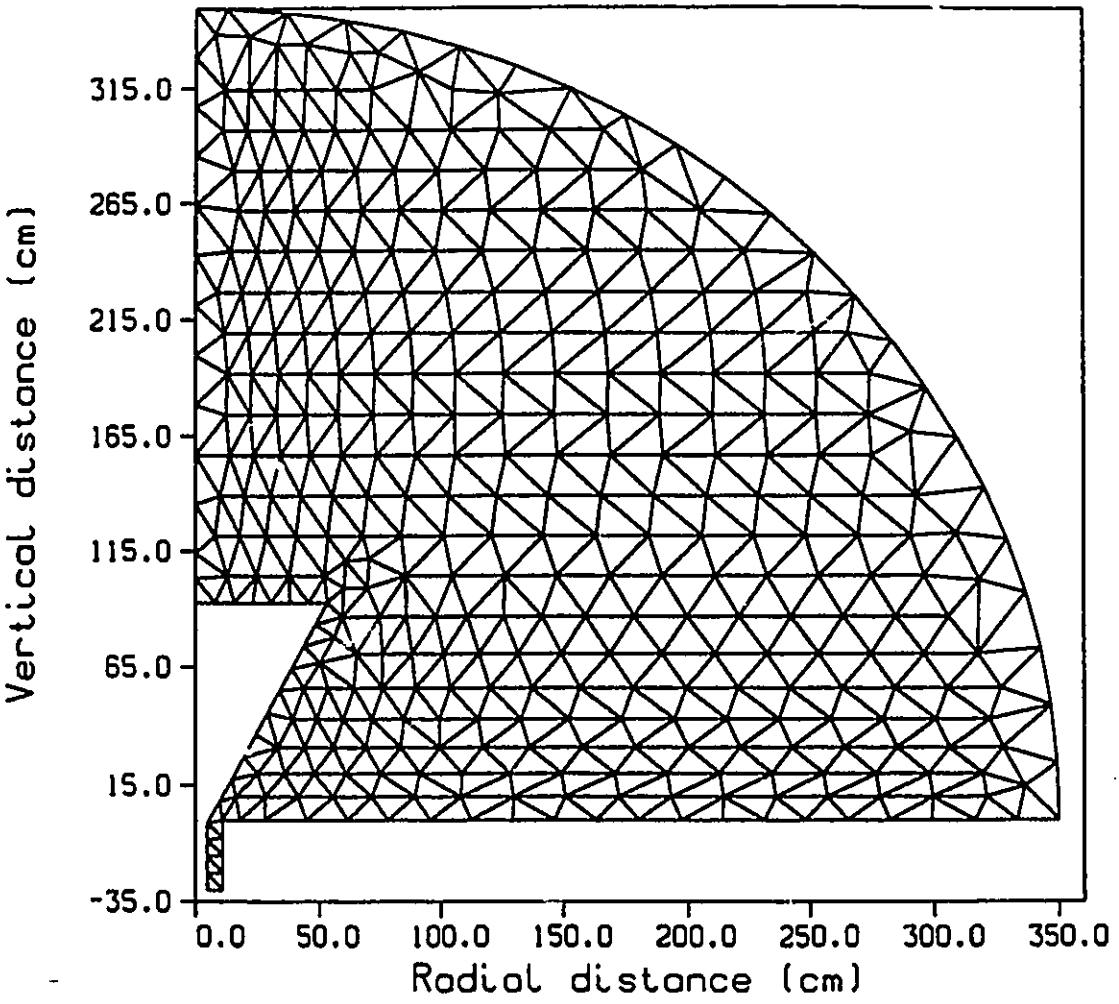

Fig. 6.13 Finite element mesh for a conical monopole antenna configuration.

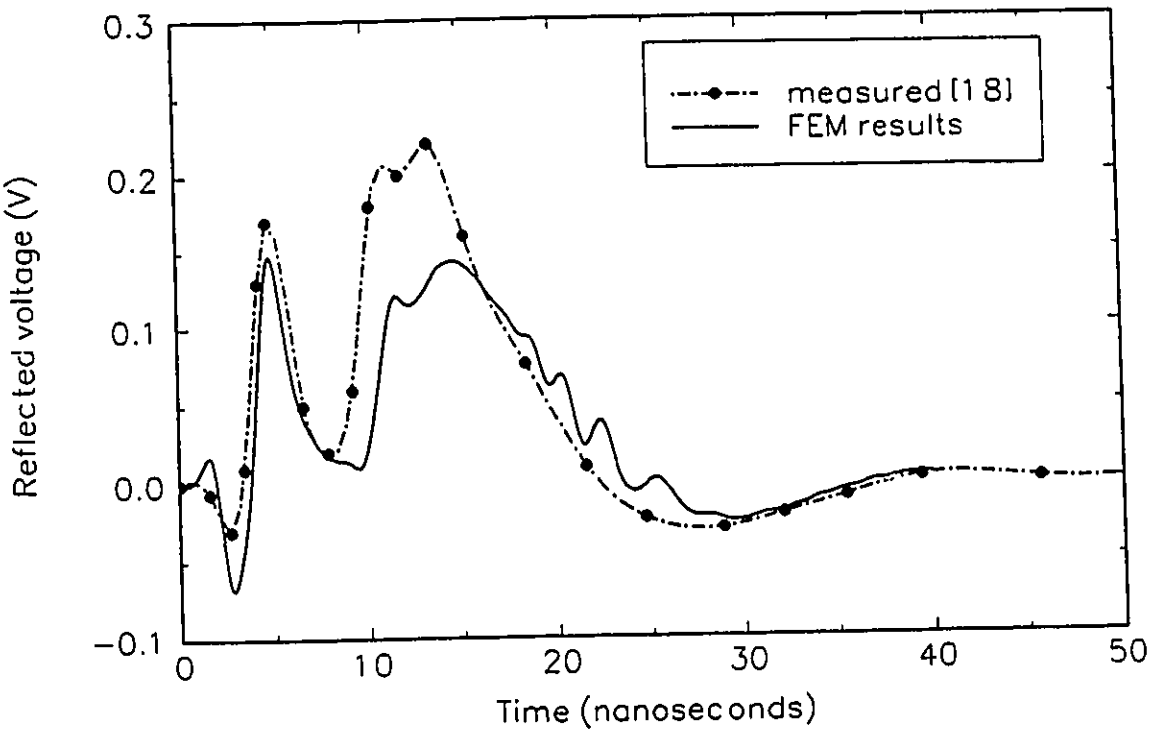

Fig. 6.14 Reflected voltage in a coaxial line feeding a conical monopole antenna with a 1 V Gaussian pulse

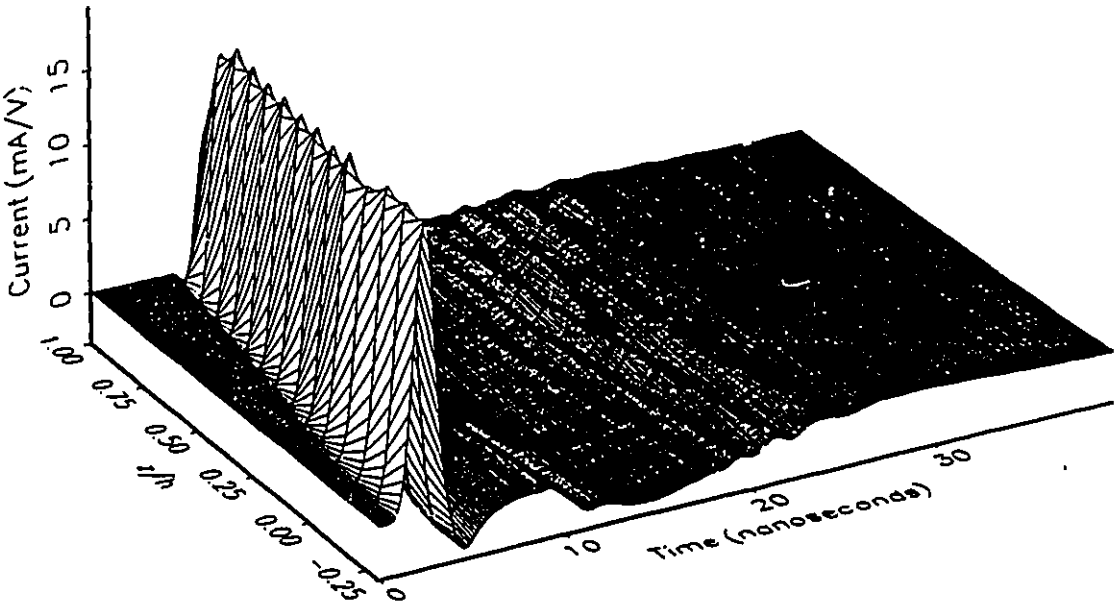

Fig. 6.15 Distribution of current over part of the inner conductor of a coaxial line and over the surface of a conical monopole driven by a 1 V Gaussian pulse

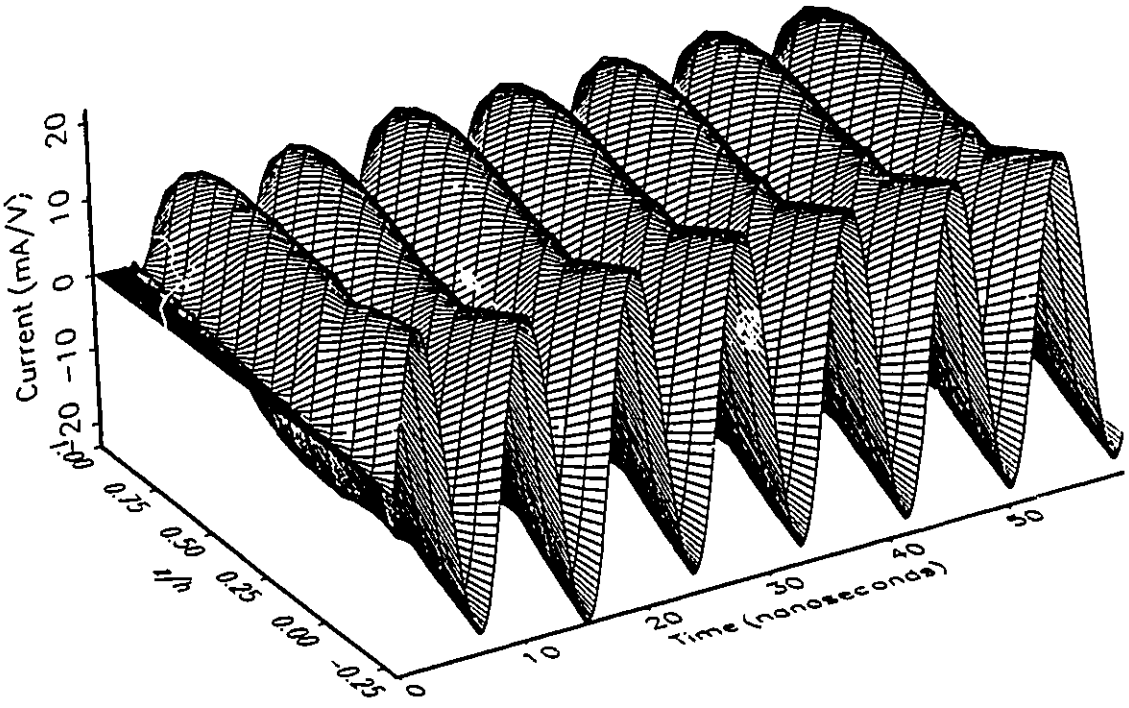

Fig. 6.16 Distribution of current over part of the inner conductor of a coaxial line and over the surface of a conical monopole driven by a 1 V sinusoidal voltage.

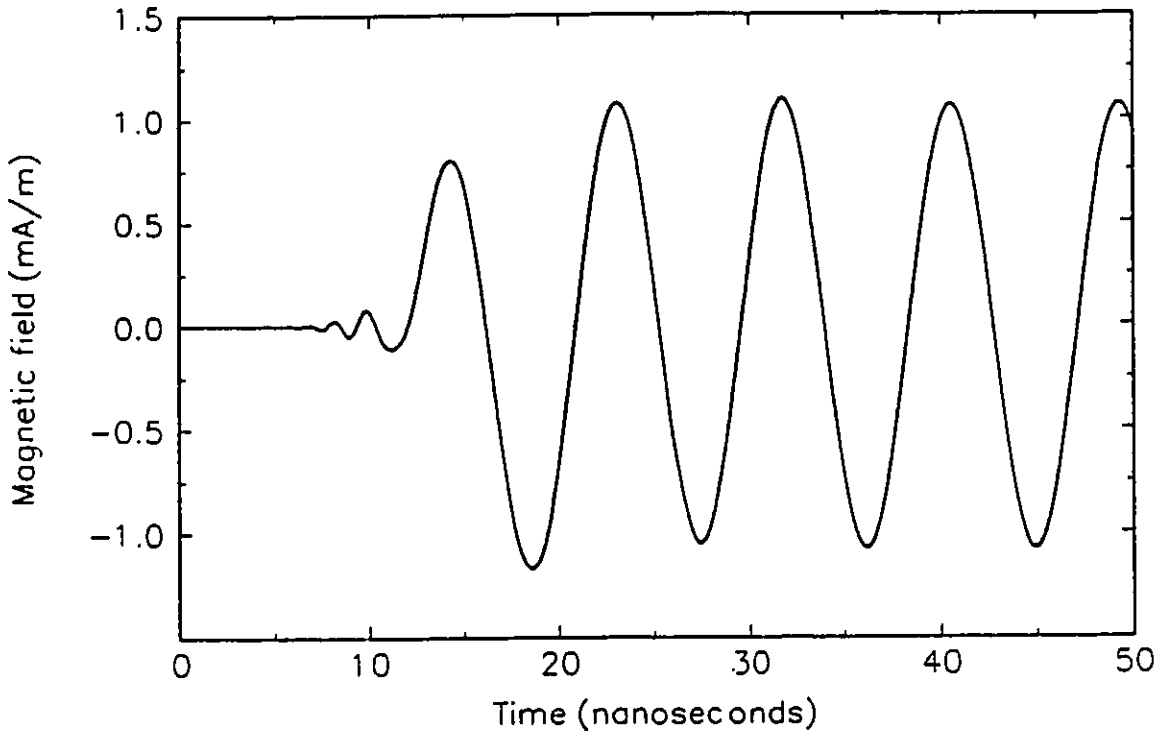

Fig. 6.17 The ϕ-component of the magnetic far field at the broadside of a conical monopole antenna excited by a 1 V sinusoidal voltage.

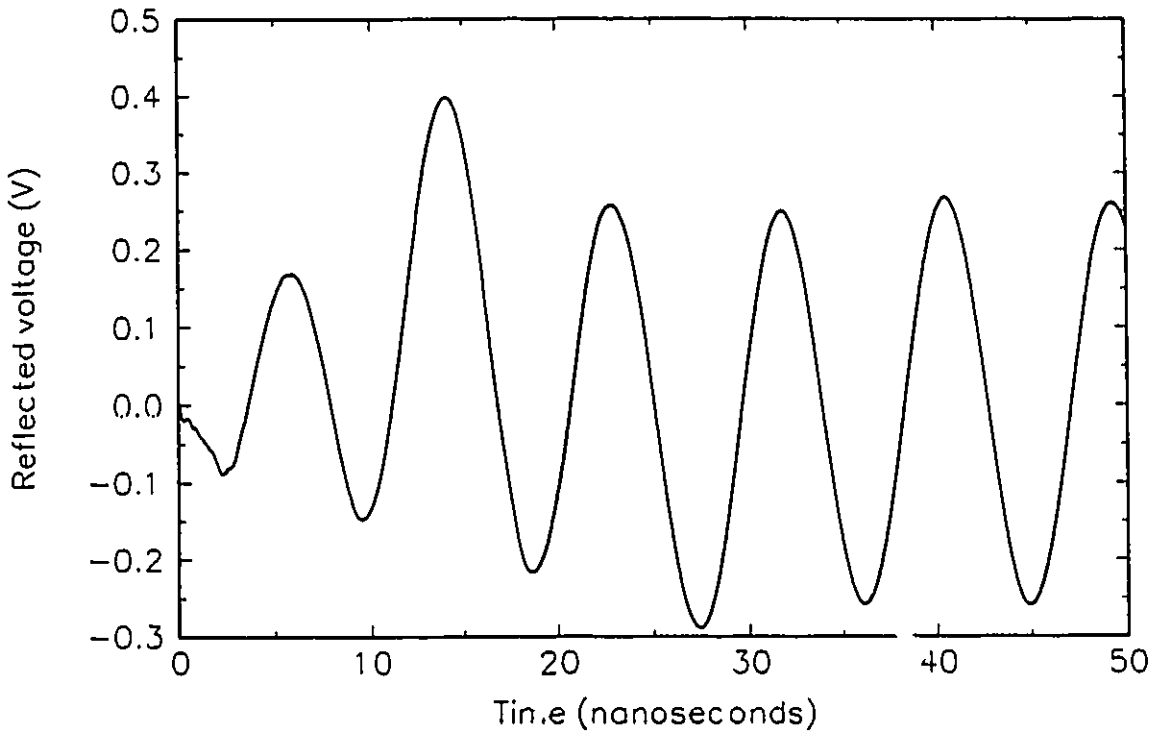

Fig. 6.18 The reflected voltage in a coaxial line feeding a conical monopole antenna with a 1 V sinusoidal voltage

6.1.3 Response to Other Transient Excitations

After proving the validity of the formulation, a further test was given for a double exponential excitation. This would typically represent an EMP (Electromagnetic Pulse as a result of a nuclear explosion) or ESD (Electrostatic Discharge) or a lightning signal. The double exponential excitation may be written as,

$$V(t) = e^{-\alpha t} - e^{-\beta t} \tag{6.6}$$

where typically, $\alpha = 4.0 \times 10^6$ s^{-1}, $\beta = 4.76 \times 10^8$ s^{-1}. The results for a cylindrical monopole antenna configuration of Fig. 6.4, are shown in Fig. 6.19 for the current distribution and Fig. 6.20 for the radiated ϕ-component of the magnetic field at a broadside far field point. The reflected voltage in the coaxial line in this case is shown in Fig. 6.21.

The more complicated excitation used next was a unit step voltage defined as,

$$\begin{aligned} V(t) &= 0 \quad , \quad t<0 \\ &= 1 \quad , \quad t\geq 0 \end{aligned} \tag{6.7}$$

The configuration of Fig. 6.4 was again used and the results are as shown in Fig. 6.22, Fig. 6.23 and Fig. 6.24. Observe the faithful reproduction of the 1 V reflected voltage shown in Fig. 6.24 when the antenna ceases to radiate at the steady state due to purely dc voltage applied at its base! This is very impressive! The driving point current and the far field results are seen to surfer from some numerical noise which is quite understandable for the cases involving a step voltage. Unfortunately, even after a thorough search in literature, published results relating the double exponential and the unit step excitations, were not found for comparison especially for a coaxially fed monopole configuration. But, the results presented here, are considered accurate especially after the formulation has passed several tests discussed in the preceding sections.

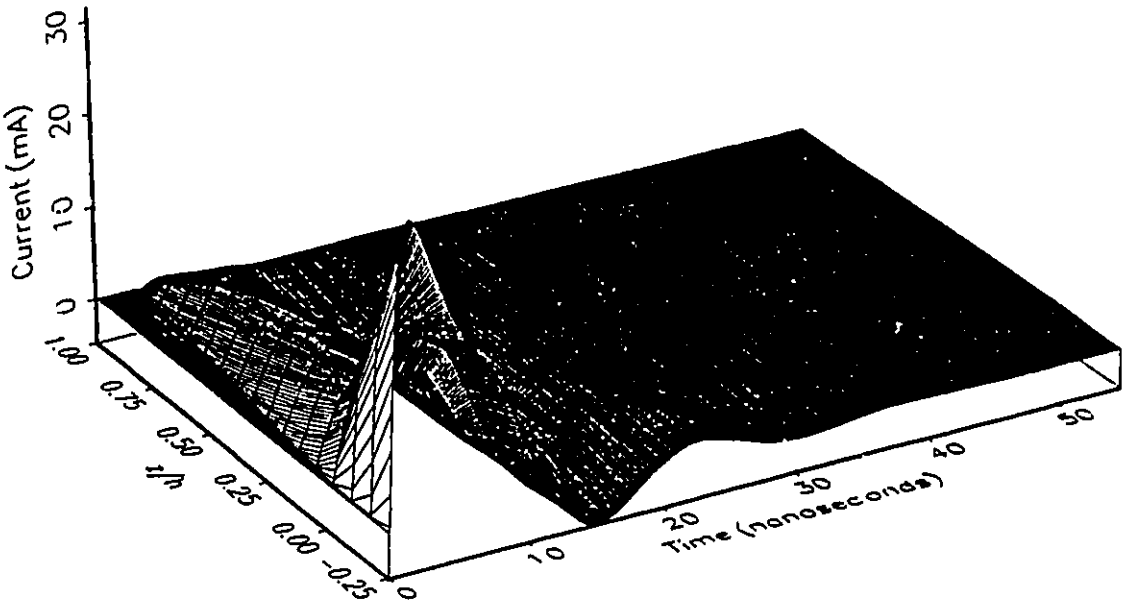

Fig. 6.19 Distribution of current over part of the inner conductor of a coaxial line and over the surface of a cylindrical monopole driven by a double-exponential pulse

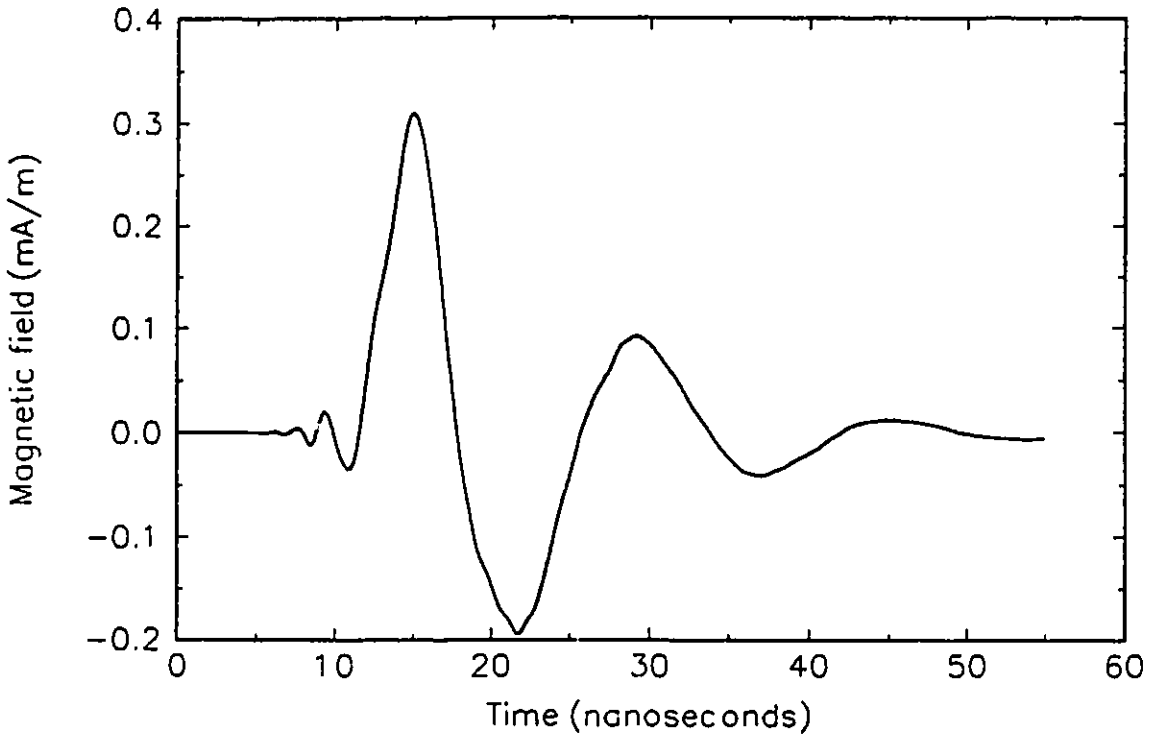

Fig. 6.20 The ϕ-component of the magnetic far field at the broadside of a cylindrical monopole antenna excite . . . ouble exponential pulse.

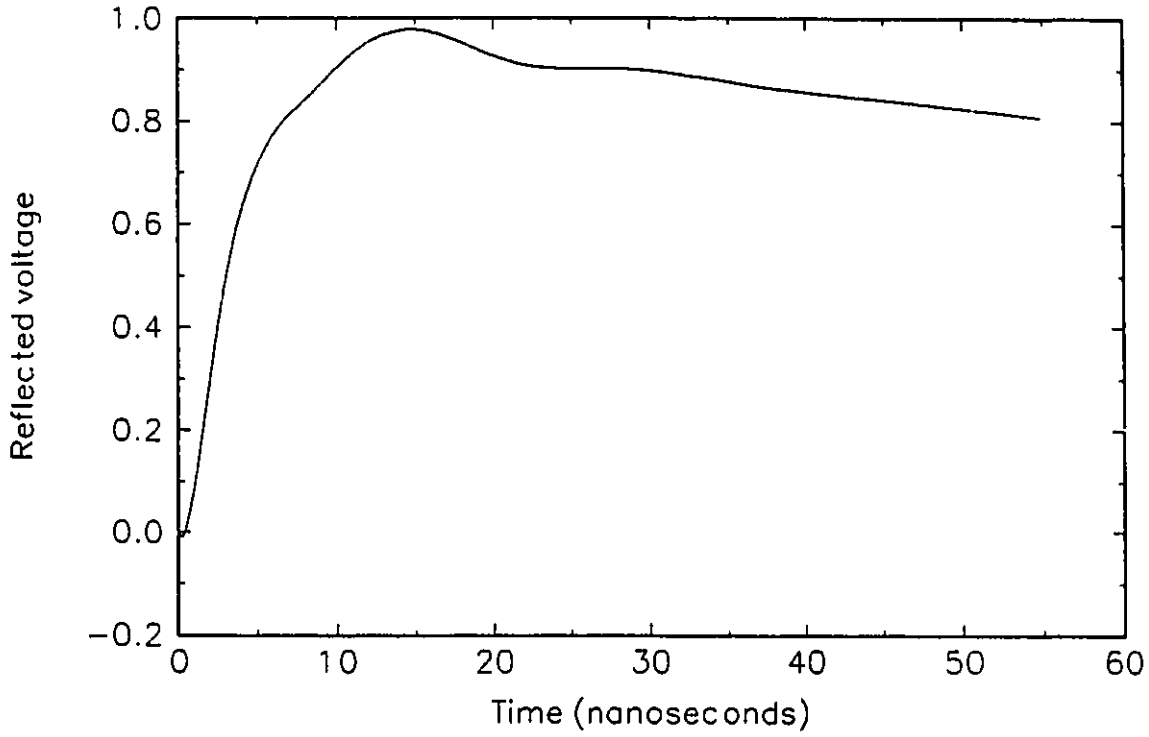

Fig. 6.21 The reflected voltage in a coaxial line feeding a cylindrical monopole antenna with a double exponential pulse

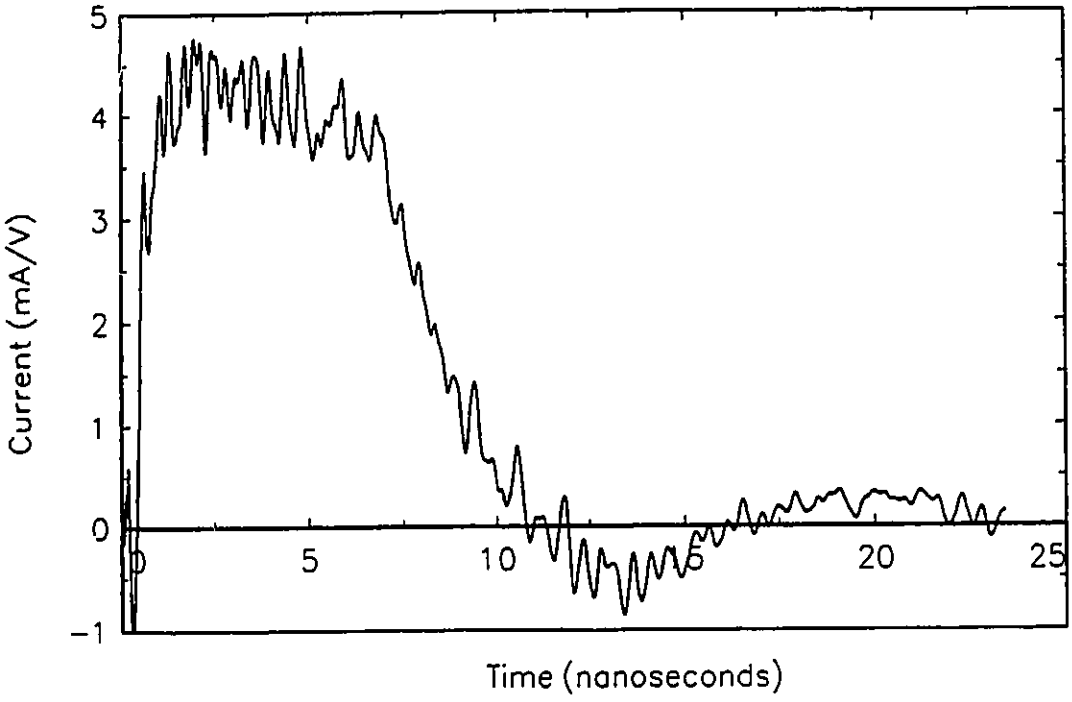

Fig. 6.22 Driving point current for a cylindrical monopole antenna coaxially driven by a 1 V step voltage

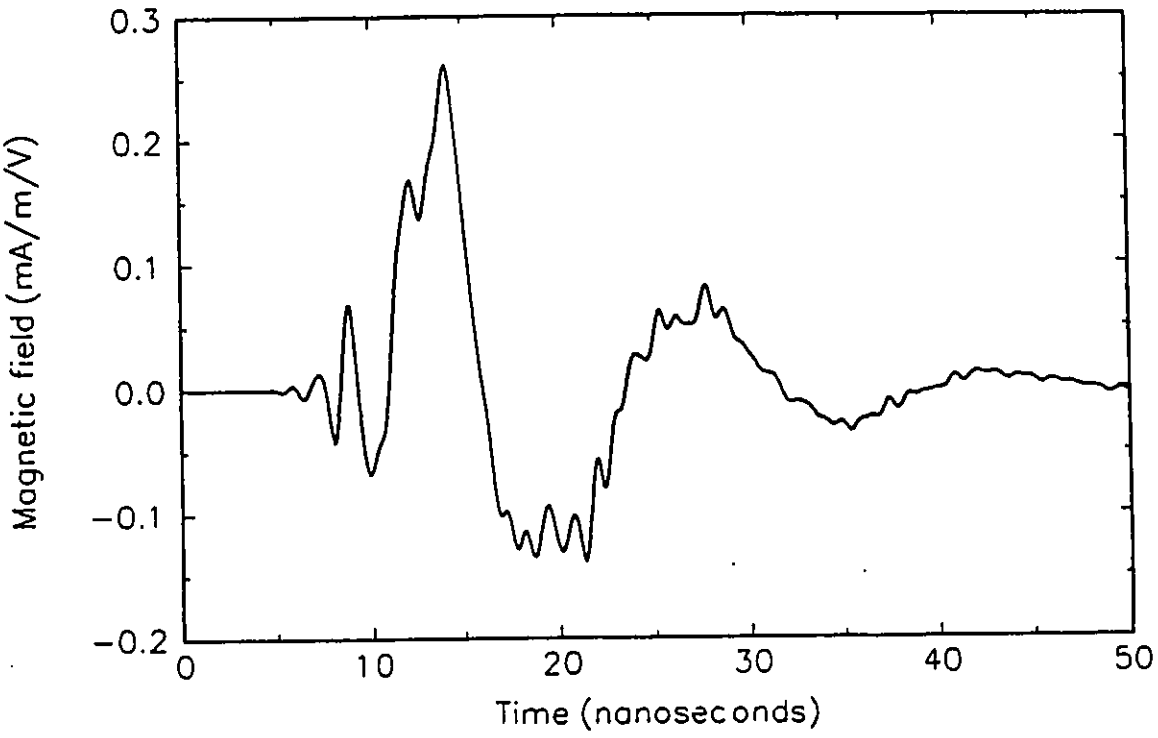

Fig. 6.23 The ϕ-component of the magnetic far field at the broadside of a cylindrical monopole antenna excited by a 1 V step voltage.

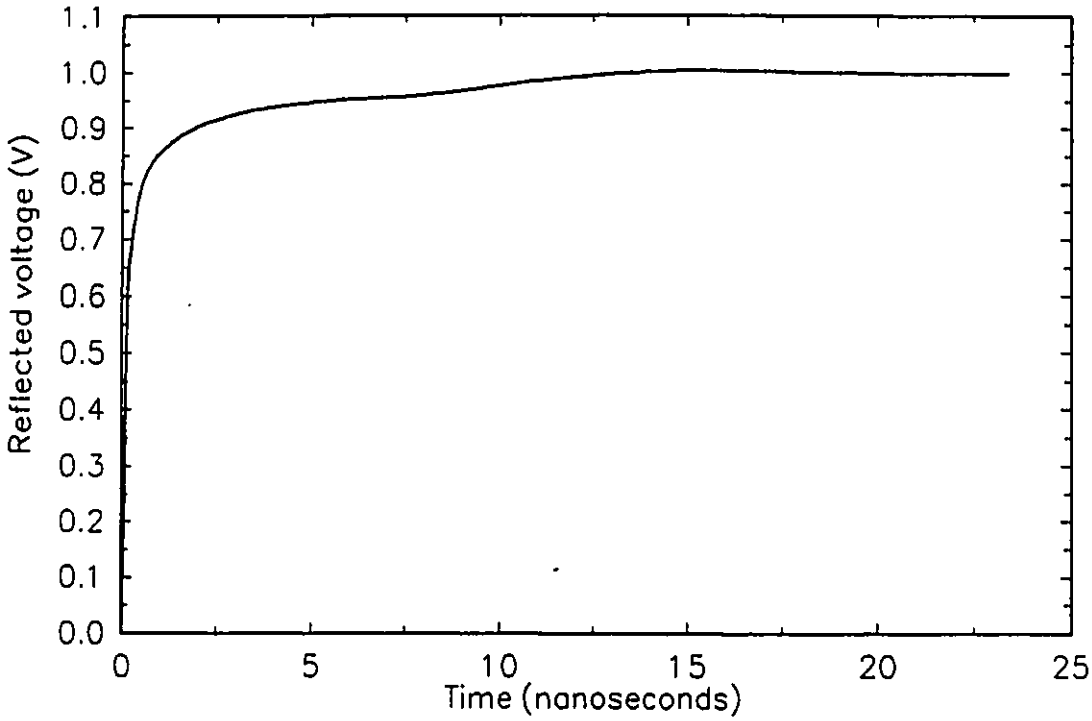

Fig. 6.24 The reflected voltage in a coaxial line feeding a cylindrical monopole antenna with a 1 V step voltage

Chapter 7

7 Conclusions

This thesis has presented a direct time-domain method of analysis of axisymmetrical electromagnetic wave propagation problems. The problems are directly formulated in the time domain using the finite element method which is used to discretize the problem domain. As a result of the discretization, a system of second order differential equations is realized. This system of differential equations is then solved for the unknown magnetic field component using an appropriate differential equation solving algorithm. In the course of this work, an efficient and yet accurate differential equation solving algorithm has been realised in a form of a FORTRAN computer program. This algorithm together with the FORTRAN program which formulates the system of differential equations, (both written by the author), have been successfully used to analyze simple driven axisymmetrical monopole antennas. Cylindrical and conical monopole antennas located in free space, have been investigated for sinusoidal, Gaussian, double exponential and unit step types of excitations. Different excitation models have been used and compared. Accurately computed are the near field values of the magnetic field which in turn were used to accurately compute current distribution on the surface of the radiating structure. From the computed current distribution, a far field can be computed. Experimentally realizable model consisting of a coaxially-driven axisymmetrical monopole antenna, has been successfully studied. This particular formulation enables accurate computation of the input admittance of the monopole antenna calculated from the reflected field. Approximate far field is also computed directly.

Generally speaking, the results have shown good agreement with the theoretical and experimental data already published. In addition the results make possible a clear visualization of the wave propagation phenomenon in the situation involving transmission line feeding a monopole antenna. This may be quite

appreciated by those who are not very familiar with the wave propagation phenomenon.

As was one of the objectives of this thesis, the method used in this work, may be successfully used to study radiated emissions from components in printed circuit board configurations. These configurations comprise of inhomogeneities and variation of material properties which can be well modeled by the finite element method. With this method, more accurate estimation of the radiated emissions can be done especially when transient exciting fields are involved. As has been apparent in all the results presented, the steady state value of the field is far less than the maximum instantaneous value of the field. Thus frequency domain solutions may sometimes be deceiving as to the expected level of the radiated field thus making transient analysis vital especially in such sensitive configurations.

Future research is recommended in this area to accomplissh the following:

- application of the method to the study of radiated emissions from components on printed circuit board configurations: integrated circuits, heatsinks, connecting tracks etc. and to the study of any other interesting axisymmetrical problem configuration.

- extension of the axisymmetrical wave propagation method of analysis to cover problem situations involving antennas located in dispersive media and driven by broadband exciting fields.

- extension of the method for direct time-domain analysis of wave propagation for full three-dimensional problem configurations in dispersive and inhomogeneous media using the finite element method.

Appendix A: Finite Element Generic Integrals

In the finite element analysis, the equations to solve, are obtained after working out a number of surface and line integrals. In this appendix, analytical expressions of all the required generic integrals are provided using simplex (area) coordinates [21]. When the integrals are worked out in simplex coordinates the expressions for the integrals are the same regardless of the position of the element.

The global cylindrical coordinates of any point in a triangular element are related to the simplex coordinates of the nodes describing the element by,

$$\begin{aligned} r &= \sum_{k=1}^{3} r_k \zeta_k \\ z &= \sum_{k=1}^{3} z_k \zeta_k \end{aligned} \qquad \text{(A-1)}$$

where r_k, z_k are the coordinates of the triangle nodes and ζ_k are the corresponding simplex coordinates with values ranging from 0 (at node other than k) to 1 (at node k). For first order approximation, the simplex coordinates are the same as the finite element interpolatory functions, N_j, whose expressions are given in equation (2.6). The integrals with respect to the global cylindrical coordinates can be easily expressed as integrals with respect to the simplex coordinates via the relation,

$$\begin{aligned} \int_\Omega dr\,dz &= 2A \int_\Omega d\zeta_1 d\zeta_2 \\ \int_\Gamma dl &= L \int_\Gamma d\zeta_k \end{aligned} \qquad \text{(A-2)}$$

where A is the area of the triangle and L is the length of the element side. The surface integral with respect to only two simplex coordinates is made possible because of the possibility of expressing the third simplex coordinate in terms of the other two through,

$$\zeta_1+\zeta_2+\zeta_3 = 1 \tag{A-3}$$

The derivatives of the simplex coordinates with respect to the global cylindrical coordinates are given as follows

$$\begin{aligned} \frac{\partial \zeta_i}{\partial r} &= \frac{b_i}{2A} \\ \frac{\partial \zeta_i}{\partial z} &= \frac{c_i}{2A} \end{aligned} \tag{A-4}$$

where

$$\begin{aligned} b_i &= z_{i+1}-z_{i-1} \\ c_i &= r_{i-1}-r_{i+1} \end{aligned} \tag{A-5}$$

the subsript i is understood to progress cyclically around the triangle vertices or rather it can be said, it progresses modulo 3.

Expressions for several integrals with respect to the simplex coordinates are given here below:

$$\begin{aligned} \int_0^1\int_0^{1-\zeta_1}\zeta_1\zeta_2 d\zeta_1 d\zeta_2 &= 1/24 \\ \int_0^1\int_0^{1-\zeta_1}\zeta_1^2 d\zeta_1 d\zeta_2 &= 1/12 \\ \int_0^1\int_0^{1-\zeta_1}\zeta_2^2 d\zeta_1 d\zeta_2 &= 1/12 \end{aligned} \tag{A-6}$$

$$\begin{aligned} \int_0^1\zeta_1\zeta_2 d\zeta_2 &= 1/6 \\ \int_0^1\zeta_1^2 d\zeta_2 &= 1/3 \\ \int_0^1\zeta_2^2 d\zeta_2 &= 1/3 \end{aligned} \tag{A-7}$$

In the following expressions the following symbols have been used:

r_1, r_2, r_3 are the cylindrical r-coordinates of the triangle vertices.

$k_1 = r_1 - r_3$, $k_2 = r_2 - r_1$, $k_3 = r_3 - r_2$

$l_1 = \ln(r_1) - \ln(r_3)$, $l_2 = \ln(r_2) - \ln(r_1)$, $l_3 = \ln(r_3) - \ln(r_2)$

$m_1 = r_3/k_1$, $m_2 = r_2/k_2$, $m_3 = r_1/k_2$, $m_4 = r_3/k_3$

Due to singularities involved for different values of the r-coordinates of the triangle vertices, different situations are tackled differently. For every generic integral presented below the expressions are given in the following order of conditions:

(i) $r_1 = r_2$; $r_1 = 0$

(ii) $r_1 = r_2$; $r_3 = 0$

(iii) $r_1 = r_2$; $r_1 \neq 0$; $r_3 \neq 0$

(iv) $r_1 = r_3$; $r_1 = 0$

(v) $r_1 = r_3$; $r_2 = 0$

(vi) $r_1 = r_3$; $r_1 \neq 0$; $r_2 \neq 0$

(vii) $r_2 = r_3$; $r_2 = 0$

(viii) $r_2 = r_3$; $r_1 = 0$

(ix) $r_2 = r_3$; $r_2 \neq 0$; $r_1 \neq 0$

(x) $r_1 = 0$; $r_2 \neq r_3$

(xi) $r_2 = 0$; $r_1 \neq r_3$

(xii) $r_3 = 0$; $r_1 \neq r_2$

(xiii) $r_1 \neq r_2 \neq r_3$

When the analytical expression for the integral for a particular condition is not available, the respective line will be marked with *N/A*.

The following are the expressions for the surface integral

$$\int_0^1 \int_0^{1-\zeta_1} \frac{\zeta_1}{r} d\zeta_1 d\zeta_2 \qquad \textbf{(A-8)}$$

(i) N/A
(ii) $1/4r_1$
(iii) $(m_1^2 l_1 + 0.5 - m_1)/2k_1$
(iv) N/A
(v) $1/4r_1$
(vi) $(m_2^2 l_2 - 0.5 - m_2)/2k_2$
(vii) $1/2r_1$ (A-9)
(viii) $1/2r_2$
(ix) $(m_2 - 0.5 + m_2 l_2(1 - m_2))/k_2$
(x) $l_3/2k_3$
(xi) $(m_1 - m_1^2 l_1)/2r_3$
(xii) $(m_2^2 l_2 - m_2)/2r_2$
(xiii) $(m_1 + m_2 - m_1^2 l_1 - m_2^2 l_2)/2k_3$

The following are the expressions for the surface integral,

$$\int_0^1 \int_0^{1-\zeta_1} \frac{\zeta_2}{r} d\zeta_1 d\zeta_2 \qquad \text{(A-10)}$$

(i) N/A
(ii) $1/4r_1$
(iii) $(m_1^2 l_1 + 0.5 - m_1)/2k_1$
(iv) $1/2r_2$
(v) $1/2r_1$
(vi) $(0.5 - m_2 m_3 l_2 + m_3)/k_2$
(vii) N/A (A-11)
(viii) $1/4r_2$
(ix) $(1.5 - (m_2 + m_3) l_2 - m_2 + m_2^2 l_2)/2k_2$
(x) $(m_4 l_3 - 1)/2k_3$
(xi) $l_1/2k_1$
(xii) $(1/r_2 - (m_3 l_2 + r_1/r_2)/k_2)/2$
(xiii) $-(0.5 + 0.5k_1(m_2^2 l_2 + m_1^2 l_1 - m_2 - m_1)/k_3 + m_4(m_2 l_2 - m_1 l_1))/k_3$

The following are the expressions for the line integral,

$$\int_0^1 \frac{\zeta_1}{r} d\zeta_2 \tag{A-12}$$

along the line $\zeta_3 = 0$. If r_1 is replaced with r_2 and vice versa in the expressions provided, the expressions will correspond to those for the line integral,

$$\int_0^1 \frac{\zeta_2}{r} d\zeta_2 \tag{A-13}$$

along the line $\zeta_3 = 0$, etc.

(i) *N/A*
(ii) $1/2r_1$
(iii) $1/2r_1$
(iv) *N/A*
(v) $1/r_1$
(vi) $(l_2(1+m_3)-1)/k_2$
(vii) $1/r_1$ (A-14)
(viii) *N/A*
(ix) $(l_2(1+m_3)-1)/k_2$
(x) *N/A*
(xi) $1/r_1$
(xii) $(l_2(1+m_3)-1)/k_2$
(xiii) $(l_2(1+m_3)-1)/k_2$

Another useful generic integral is,

$$\int_0^1 \int_0^{1-\zeta_i} \zeta_i \zeta_j d\zeta_i d\zeta_j \tag{A-15}$$

The value of the above surface integral is 1/12 when $i = j$ and is 1/24 otherwise. The following line integral will also be encountered in the finite element analysis provided,

$$\int_0^1 \zeta_i \zeta_j d\zeta_j$$

where i and j proceed cyclically. When $i = j$ then the value of the above integral is 1/3, otherwise the value is 1/6.

Appendix B: Computer Programs

```
CCCCCCCCCCCCCCCCCCCCCCCCCCCCCCCCCCCCCCCCCCCCCCCCCCCCCCCCCCCCCCC
      PROGRAM RADTIDS
C
C 'RADIATION PROBLEM, TIME DOMAIN SOLUTION'
C
      IMPLICIT NONE
C
C This program computes the time-domain solution of the
C H-field phi component in a  region radiated by
C an axisymmetrical monopole antenna above a perfect ground plane.
C The antenna is excited  by a coaxial line connected to a generator.
C The coaxial line stretches from the ground level vertically downwards,
C while the monopole streches vertically upwards.
C The distribution of current on the surface of the antenna is easily
C computed through the corresponding computed magnetic field.
C The prog:am needs the specification of the following which can be
C easily changed in the program:
C   NN= Total number of nodes
C   NOTR=Total number of triangles
C   NSN=Number of nodes on the antenna whose currents are
C           to be computed (Number of Solution Nodes)
C   ND=Number of nodes on the Dirichlet boundary(axis of the antenna)
C   ITN=Number of iterations, and hence number of output values, for
C          each solution node
C   NNB=Number of the node at the antenna base (first out of NSN)
C   NNT=Number of the node at the top of the antenna (last out of NSN)
C   Note: It is assumed that the antenna surface nodes are sequentially
C            numbered, from the base to the top.
C   NNFF= Number of the first node on the feed line
C   NNFL= Number of the last node on the feed line.
C   e.g. if nodes 19,20,21 are on the feed line, then, NNFF=19,NNFL=21
C   The input files and their formats are given below:
C   FILE:  'coaxnod.dat'
C   FORMAT:
C   Seven comment lines followed by,
C   [node number]  [x-coordinate (cm)]  [y-coordinate (cm)]
C   FILE:  'coaxtri.dat'
C   FORMAT:
C   Seven comment lines followed by,
C   [triangle no.] [1st node no.] [2nd node no.] [3rd node no]
C   Note: The numbering of the triangles should be counter clockwise.
C   FILE:  'coaxbou.dat'
C   FORMAT:
C    [triangle no.]  [node ID] [triangle ID] [mu] [epsilon] [sigma]
C   Note: Each node and each triangle is given an identification number (ID).
C   While giving the ID's the following has been assumed:
C   1)  The radiation boundary, intersect the antenna axis (Dirichlet
```

```
C       boundary) above and the perfect ground(homogeneous Neumann
C       boundary) below.
C  2)  The feed line (inhomogeneous Neumann boundary) intersects
C       the ground on one side and the antenna surface on the other,
C       which are both homogegeous neumann boundaries.
C  3)  The Dirichlet boundary touches the antenna surface from above.
C
C  The node ID's are as follows:
C
C  1 -  for nodes on radiation boundary only.
C  2 -  for nodes on Dirichlet boundary only.
C  3 -  for nodes on inhomogeneous Neumann boundary only.
C  4 -  for nodes on intersection of inhomogeneous Neumann and
C         homogeneous Neumann boundaries.
C  5 -  for nodes on intersection of radiation and Dirichlet boundaries.
C  6 -  for nodes on intersection of homogeneous Neumann and
C         Dirichlet boundaries.
C  7 -  for nodes on intersection of radiation and homogeneous
C         Neumann boundaries.
C  0 -  for any other.
C
C  The triangle ID's are as follows:
C
C  1 -  for triangles with a side on the radiation boundary.
C  2 -  for triangles with a side on the feed line
C
C At the end of this program there are four sets of functions: DER,F1,F2.
C Each of these sets corresponds to a particular type of the excitation
C function specified at the beginning of each function. The included sets
C are for Double exponential pulse, Gaussian pulse, sinusoidal and unit
C step function. Other functions can easily be included following the example
C of those provided. The characteristics of the exciting function are to be
C specified in these functions before running the program. One has to choose
C the set he wants and the other sets can be easily excluded by
C commenting them out ,(by typing 'C' at the beginning of each line).
C
C Start time has to be specified through variable PRMT(1). Time step for
C  each iteration is specified through PRMT(3). Variable STEP specifies
C the time interval for the results to be recorded. Two sets of time steps
C are used, one for normal time steps and the other for special time steps
C during time intervals specified in the subroutine DSDIF through variables
C LIM1 and LIM2.
C
      PARAMETER NOTR=676
      PARAMETER NN=379
      PARAMETER ITN=512 ! power of 2 if Fourier trans. is to be done
      INTEGER  ND
      INTEGER  I,J,K,L,N(3)
      INTEGER  LC,NL(3)
      INTEGER  NI(NOTR,3)
      INTEGER  ITR,NSN,NNB,NNT
      INTEGER  NDIR,NEXT,NNFL,NNFF
```

```
      INTEGER  TRID(NOTR)
      INTEGER  NP(NN)
      INTEGER  NOID(NOTR)
      REAL*8   F(NN)
      REAL*8   X(NN)
      REAL*8   Y(NN)
      REAL*8   R,B(3),C(3),S(3,3),T(3,3),W(3,3),Z(3,3)
      REAL*8  X1,X2,X3,Y1,Y2,Y3
      REAL*8  FH(30)
      REAL*8  DATA1(ITN)
      REAL*8  DATA(2*ITN)
      REAL*8  WM(NN,NN)
      REAL*8  TM(NN,NN)
      REAL*8  SM(NN,NN)
      REAL*8  DET,PI,DER
      REAL*8  MUO,EPSO
      REAL*8  MU(NOTR)
      REAL*8  EPS(NOTR)
      REAL*8  SIGMA(NOTR)
      REAL*8  TIME,DET1
      REAL*8  DERIV,F1,F2
      REAL*8  ZETA1BYRS,ZETA2BYRS
C
C Declarations pertaining to the differential equation solver
C
      REAL*8 FY(NN)
      REAL*8 DY(NN)
      REAL*8  PRMT(7),THETA(2)
      REAL*8  WORKR(NN)
      REAL*8  TRALPHA(NN)
      REAL*8   STEP
      REAL*8   START,RCOND
      INTEGER  WORKI(NN)
      INTEGER  INDEX,DONE
C
      OPEN(UNIT=1,FILE='coaxnod.dat',STATUS='UNKNOWN')   !node coordinates
      OPEN(UNIT=2,FILE='coaxtri.dat',STATUS='UNKNOWN')   !triangle nodes
      OPEN(UNIT=3,FILE='coaxbou.dat',STATUS='UNKNOWN' ) !boundary info.
      OPEN(UNIT=4,FILE='output.res',STATUS='UNKNOWN' )    !output file
      OPEN(UNIT=5,FILE='fourier.res',STATUS='UNKNOWN' ) !fourier output
C
      NNFF=374
      NNFL=375
      NNB=22
      NNT=34
      ND=14
      NSN=13
      PI=DACOS(-1.0D0)
      EPSO=1.0D-9/(PI*3.6D1)
      MUO=4.0D-7*PI
C
C   Initialize system matrices
```

```
C
      DO I=1,NN
         F(I)=0.0D0
         DO J=1,NN
            WM(J,I)=0.0D0
         ENDDO
      ENDDO
      DO I=1,NN
         DO J=1,NN
            TM(J,I)=0.0D0
         ENDDO
      ENDDO
      DO I=1,NN
         DO J=1,NN
            SM(J,I)=0.0D0
         ENDDO
      ENDDO
C
C  Get node, triangle, boundary and material information
C
C   skip the upper text lines
C
      DO I=1,7
         READ(1,*)
      ENDDO
C
      DO 30 I=1,NN
         READ(1,*) TRID(I),X(I),Y(I)
30    CONTINUE
C
C  Change coordinates to meters
C
      DO I=1,NN
      X(I)=1.0D-2*X(I)
      Y(I)=1.0D-2*Y(I)
      ENDDO
C
C   skip the upper text lines
C
      DO I=1,7
         READ(2,*)
      ENDDO
C
      DO 40 I=1,NOTR
      READ(2,*) TRID(I),NI(I,1),NI(I,2),NI(I,3)
40    CONTINUE
C
      DO 50 I=1,NOTR
      READ(3,*) TRID(I),NOID(I),TRID(I),MU(I),EPS(I),SIGMA(I)
50    CONTINUE
C
```

```
C  Find new adjusted node positions after removing Dirichlet nodes
C
      NDIR=0
      DO I=1,NN
            IF((NOID(I).EQ.2).OR.(NOID(I).EQ.5)
     &      .OR.(NOID(I).EQ.5)) THEN
            NP(I)=NN-NDIR
                  NDIR=NDIR+1
           ELSE
            NP(I)=I-NDIR
                 END IF
      ENDDO
C
      TIME=0.0D0                ! start time
C
C Compute and assemble element contributions
C
      DO 60 ITR=1,NOTR
C
C  General preparation
C
        X1=X(NI(ITR,1))
        X2=X(NI(ITR,2))
        X3=X(NI(ITR,3))
        Y1=Y(NI(ITR,1))
        Y2=Y(NI(ITR,2))
        Y3=Y(NI(ITR,3))
        B(1)=Y2-Y3
        B(2)=Y3-Y1
        B(3)=Y1-Y2
        C(1)=X3-X2
        C(2)=X1-X3
        C(3)=X2-X1
        DET1=X1*Y2-X2*Y1+X2*Y3
     $          -X3*Y2+X3*Y1-X1*Y3
        DET=DABS(DET1)  ! Area of triangle
        DO I=1,3
          N(I)=NI(ITR,I)     ! triangle node numbers
        ENDDO
C
C  Start computing WM matrix contribution
C
      W(1,1)= MU(ITR)*MUO*EPS(ITR)*EPSO*DET/1.2D1
      W(1,2)= MU(ITR)*MUO*EPS(ITR)*EPSO*DET/2.4D1
      W(1,3)= MU(ITR)*MUO*EPS(ITR)*EPSO*DET/2.4D1
      W(2,2)= MU(ITR)*MUO*EPS(ITR)*EPSO*DET/1.2D1
      W(2,3)= MU(ITR)*MUO*EPS(ITR)*EPSO*DET/2.4D1
      W(3,3)= MU(ITR)*MUO*EPS(ITR)*EPSO*DET/1.2D1
      DO I=1,3
            DO J=1,I
           W(I,J)=W(J,I)
            ENDDO
```

```
      ENDDO
      DO I=1,3
            L=N(I)
              DO J=1,3
                  LC=N(J)
                  WM(NP(L),NP(LC))=WM(NP(L),NP(LC))+W(I,J)
               ENDDO
       ENDDO
      Z(1,1)= MU(ITR)*MUO*SIGMA(ITR)*DET/1.2D1
      Z(1,2)= MU(ITR)*MUO*SIGMA(ITR)*DET/2.4D1
      Z(1,3)= MU(ITR)*MUO*SIGMA(ITR)*DET/2.4D1
      Z(2,2)= MU(ITR)*MUO*SIGMA(ITR)*DET/1.2D1
      Z(2,3)= MU(ITR)*MUO*SIGMA(ITR)*DET/2.4D1
      Z(3,3)= MU(ITR)*MUO*SIGMA(ITR)*DET/1.2D1
      DO I=1,3
              DO J=1,I
            Z(I,J)=Z(J,I)
              ENDDO
      ENDDO
      DO I=1,3
             L=N(I)
               DO J=1,3
                   LC=N(J)
                   TM(NP(L),NP(LC))=TM(NP(L),NP(LC))+Z(I,J)
                ENDDO
       ENDDO
C  End computing WM matrix contribution
C
C  Special handling of triangles with side on radiation boundary
C  leading to computation of TM matrix contribution
C
      IF(TRID(ITR).EQ.1) THEN
      IF ((NOID(NI(ITR,1)).EQ.1.OR.NOID(NI(ITR,1)).EQ.5.OR.
     * NOID(NI(ITR,1)).EQ.7).AND.(NOID(NI(ITR,2)).EQ.1.OR.
     * NOID(NI(ITR,2)).EQ.5.OR.NOID(NI(ITR,2)).EQ.7)) THEN
           I=1
      ELSE IF ((NOID(NI(ITR,2)).EQ.1.OR.NOID(NI(ITR,2)).EQ.5.OR.
     * NOID(NI(ITR,2)).EQ.7).AND.(NOID(NI(ITR,3)).EQ.1.OR.
     * NOID(NI(ITR,3)).EQ.5.OR.NOID(NI(ITR,3)).EQ.7)) THEN
           I=2
      ELSE
           I=3
      END IF
        CALL MODULO3(I,NEXT)
        NL(1)=NI(ITR,I)
        NL(2)=NI(ITR,NEXT)
        CALL MODULO3(NEXT,NEXT)
        NL(3)=NI(ITR,NEXT)
        R=DSQRT((X(NL(1))-X(NL(2)))**2+(Y(NL(1))-Y(NL(2)))**2)
             TM(NP(NL(1)),NP(NL(1)))=TM(NP(NL(1)),NP(NL(1)))
     &            +DSQRT(MU(ITR)*MUO*EPS(ITR)*EPSO)*R/3.0D0
             TM(NP(NL(1)),NP(NL(2)))=TM(NP(NL(1)),NP(NL(2)))
```

```
     &            +DSQRT(MU(ITR)*MUO*EPS(ITR)*EPSO)*R/6.0D0
           TM(NP(NL(2)),NP(NL(2)))=TM(NP(NL(2)),NP(NL(2)))
     &            +DSQRT(MU(ITR)*MUO*EPS(ITR)*EPSO)*R/3.0D0
          TM(NP(NL(2)),NP(NL(1)))=TM(NP(NL(2)),NP(NL(1)))
     &            +DSQRT(MU(ITR)*MUO*EPS(ITR)*EPSO)*R/6.0D0
      END IF
C
C  Introduce an ABC at feed line hence modify TM matrix
C
      IF(TRID(ITR).EQ.2) THEN
        IF(((NOID(NI(ITR,1)).EQ.3).OR.(NOID(NI(ITR,1)).EQ.4)).AND.
     *  ((NOID(NI(ITR,2)).EQ.3)
     *  .OR.(NOID(NI(ITR,2)).EQ.4))) THEN
          I=1
        ELSE IF(((NOID(NI(ITR,2)).EQ.3).OR.(NOID(NI(ITR,2)).EQ.4)).AND.
     *  ((NOID(NI(ITR,3)).EQ.3)
     *  .OR.(NOID(NI(ITR,3)).EQ.4))) THEN
          I=2
        ELSE
          I=3
      END IF
        CALL MODULO3(I,NEXT)
        NL(1)=NI(ITR,I)
        NL(2)=NI(ITR,NEXT)
        CALL MODULO3(NEXT,NEXT)
        NL(3)=NI(ITR,NEXT)
       R=DSQRT((X(NL(1))-X(NL(2)))**2+(Y(NL(1))-Y(NL(2)))**2)
            TM(NP(NL(1)),NP(NL(1)))=TM(NP(NL(1)),NP(NL(1)))
     &            +DSQRT(MU(ITR)*MUO*EPS(ITR)*EPSO)*R/3.0D0
           TM(NP(NL(1)),NP(NL(2)))=TM(NP(NL(1)),NP(NL(2)))
     &            +DSQRT(MU(ITR)*MUO*EPS(ITR)*EPSO)*R/6.0D0
          TM(NP(NL(2)),NP(NL(2)))=TM(NP(NL(2)),NP(NL(2)))
     &            +DSQRT(MU(ITR)*MUO*EPS(ITR)*EPSO)*R/3.0D0
         TM(NP(NL(2)),NP(NL(1)))=TM(NP(NL(2)),NP(NL(1)))
     &            +DSQRT(MU(ITR)*MUO*EPS(ITR)*EPSO)*R/6.0D0
      END IF
C
C  End of computation of TM matrix contribution
C
C  Start computing SM matrix contribution
C
      DO I=1,3
      DO J=1,3
      S(I,J)=0.5D0*(B(I)*B(J)+C(I)*C(J))/DET
      ENDDO
      ENDDO
      DO I=1,3
      T(I,1)=B(I)*ZETA1BYRS(X1,X2,X3)
      T(I,2)=B(I)*ZETA2BYRS(X1,X2,X3)
      T(I,3)=B(I)*ZETA2BYRS(X1,X3,X2)
      ENDDO
      DO I=1,3
```

```
          L=N(I)
            DO J=1,3
                LC=N(J)
                SM(NP(L),NP(LC))=SM(NP(L),NP(LC))+S(I,J)+T(I,J)
            ENDDO
      ENDDO
C
C  End of computation of SM matrix contribution
C
C  Start computing the RHS contribution
C
      DERIV=DER(TIME,SIGMA(ITR),EPS(ITR))
      CALL F_ON_BOUNDARY(NN,NOTR,ITR,DERIV,F,NI,TRID,NOID,X,Y,NP)
C
C End of computation of the RHS contribution
C
60    CONTINUE
C
C Change the variable at the feed line to be reflected H-field
C hence subtract out the contribution of the incident H-field
C and send it to the RHS
C
          DO I=1,NN
      IF(NOID(I).EQ.3.OR.NOID(I).EQ.4) THEN
          DO J=1,NN
      F(NP(J))=F(NP(J))-SM(NP(J),NP(I))*F1(TIME,X(I))
     &                 -WM(NP(J),NP(I))*F2(TIME,X(I))
          ENDDO
      END IF
        ENDDO
C
C  Solving the system of differential equations
C
C Initial values
      DO I=1,NN-ND
          FY(I)=0.0D0 ! node H-field
          DY(I)=0.0D0 ! first derivative of the node H-field
      ENDDO
C
C Define parameters for the differential equation solver
C
      THETA(1)=0.6D0 ! used with the differential eqn. solver
      THETA(2)=1.0D0! used with the differential eqn. solver
              START=0.0D0 ! start time
C
      PRMT(1)=START ! start time (used with dif. eqn. solver)
              PRMT(6)=1.0D-13 !relative error (used with dif. eqn. solver)
              PRMT(7)=5.0D-1 ! gamma (used with dif. eqn. solver)
C
C Array FH takes the values of current for the solution nodes
C
              DO I=NNB,NNT
```

```
            FH(I-NNB+1)=FY(I)*2.0D0*PI*X(I) !antenna surface current
           ENDDO
    DATA1(1)=0.0D0 !reflected field (for FFT)
C
    WRITE(4,992) PRMT(1),FY(362),FY(363),FY(364),FY(365),
   &                (FH(I),I=1,NSN),FY(1)
C
           INDEX=1
           DONE=0
C
      DO I=1,ITN-1
       IF (INDEX.EQ.10) GO TO 999
       WRITE(*,*)'STEP ',I
        IF (DONE.EQ.0) THEN ! first special step or steps
          PRMT(3)=2.5D-11 !Time step in each iteration
          PRMT(4)= 2.5D-11!Min. time step in each iteration
          PRMT(5)=3.0D-11 !Max. time step in each iteration
          STEP=1.0D-10 !Time step satisfying Nyquist criterion
        ELSE ! normal steps
          PRMT(3)=2.5D-11 !Time step in each iteration
          PRMT(4)=2.5D-11 !Min. time step in each iteration
          PRMT(5)=3.0D-11!Max. time step in each iteration
          STEP=1.0D-10 !Time step satisfying Nyquist criterion
        END IF
        PRMT(2)= PRMT(1)+STEP ! Current time
C
C  Now solve the system of of differential equations
C
        CALL DSDIF(NOTR,NN,NN-ND,THETA,PRMT,SM,TM,WM,F,FY,DY,INDEX,EPS,
     $  SIGMA,MU,WORKR,WORKI,TRALPHA,NI,TRID,NOID,X,Y,NP,DONE)
        DO J=NNB,NNT
         FH(J-NNB+1)=FY(J)*2.0D0*PI*X(J) !antenna surface current
        ENDDO
        DO J=363,365
         FY(J)=FY(J)*2.0D0*PI*X(NNB) !coaxial line surface current
        ENDDO
        DATA1(I+1)=FY(NP(NNFL)) !reflected field (for FFT)
        WRITE(4,992) PRMT(1),FY(362),FY(363),FY(364),FY(365),
     &              (FH(J),J=1,NSN),FY(1)
         ENDDO
992   FORMAT(E11.4,3X,4E13.4,<NSN>E13.4,E13.4)
C
C Get frequency spectrum using the Fast Fourier Transform
C
              DO J=1,ITN
               DATA(2*J-1)=DATA1(J)
               DATA(2*J)=0.0D0
              ENDDO
              CALL FOUR1(DATA,ITN,1)
               DO J=1,ITN
            WRITE(5,993) DATA(2*J-1),DATA(2*J)
               ENDDO
```

```
993     FORMAT(PE16.9,1X,PE16.9)
C
      CLOSE (UNIT=1)
      CLOSE (UNIT=2)
      CLOSE (UNIT=3)
      CLOSE (UNIT=4)
      CLOSE (UNIT=5)
999             STOP
      END
C
CCCCCCCCCCCCCCCCCCCCCCCCCCCCCCCCCCCCCCCCCCCCCCCCCCCCCCCCCCCCCCCCCCCCCCC
C
      REAL*8  FUNCTION  ZETA1BYRS(R1,R2,R3)
C
      IMPLICIT NONE
C
C  This function computes the surface integral (in simplex coordinates)
C  of zeta1/R, where R is the r-coordinate (cylindrical) of an arbitrary
C  point in a triangle with R1,R2,R3 as r-coordinates of the vertices.
C
      REAL*8 R1,R2,R3,ZE,K1,K2,K3,L1,L2,L3,M1,M2
      ZE=0.0D0
      K1=R1-R3
      K2=R2-R1
      K3=R3-R2
      IF(K1.NE.ZE)M1=R3/K1
      IF(K2.NE.ZE)M2=R2/K2
      IF((R1.NE.ZE).AND.(R3.NE.ZE))L1=DLOG(R1)-DLOG(R3)
      IF((R1.NE.ZE).AND.(R2.NE.ZE))    L2=DLOG(R2)-DLOG(R1)
      IF((R2.NE.ZE).AND.(R3.NE.ZE))    L3=DLOG(R3)-DLOG(R2)
      IF(R1.EQ.R2) THEN
        IF(R1.EQ.ZE) THEN
          ZETA1BYRS=ZE
        ELSE IF(R3.EQ.ZE) THEN
          ZETA1BYRS=1.0D0/(4.0D0*R1)
        ELSE
          ZETA1BYRS =(M1**2*L1+0.5D0-M1)/(2.0D0*K1)
        END IF
      ELSE IF(R1.EQ.R3) THEN
         IF(R1.EQ.ZE) THEN
          ZETA1BYRS =ZE
        ELSE IF(R2.EQ.ZE) THEN
          ZETA1BYRS =1.0D0/(4.0D0*R1)
        ELSE
          ZETA1BYRS =(M2**2*L2-0.5D0-M2)/(2.0D0*K2)
        END IF
      ELSE IF(R2.EQ.R3) THEN
         IF(R2.EQ.ZE) THEN
          ZETA1BYRS =1.0/(2.0D0*R1)
        ELSE IF(R1.EQ.ZE) THEN
          ZETA1BYRS =1.0D0/(2.0D0*R2)
        ELSE
```

```
        ZETA1BYRS = (M2-0.5D0+M2*L2*(1-M2))/K2
      END IF
    ELSE IF((R1.EQ.ZE).AND.(R2.NE.R3)) THEN
          ZETA1BYRS =(0.5D0*L3)/K3
    ELSE IF((R2.EQ.ZE).AND.(R1.NE.R3)) THEN
          ZETA1BYRS =(M1-M1**2*L1)/(2.0D0*R3)
    ELSE IF((R3.EQ.ZE).AND.(R1.NE.R2)) THEN
          ZETA1BYRS =(M2**2*L2-M2)/(2.0D0*R2)
    ELSE
          ZETA1BYRS=(M1+M2-M1**2*L1-M2**2*L2)/(2.0D0*K3)
    END IF
    RETURN
    END
C
CCCCCCCCCCCCCCCCCCCCCCCCCCCCCCCCCCCCCCCCCCCCCCCCCCCCCCCCCCCCCCCCCCC
C
    REAL*8 FUNCTION ZETA2BYRS(R1,R2,R3)
C
    IMPLICIT NONE
C
C This function computes the surface integral (in simplex coordinates)
C of zeta2/R, where R is the r-coordinate (cylindrical) of an arbitrary
C point in a triangle with R1,R2,R3 as r-coordinates of the vertices.
C
    REAL*8 R1,R2,R3,ZE,K1,K2,K3,L1,L2,L3,M1,M2,M3,M4
    ZE=0.0D0
    K1=R1-R3
    K2=R2-R1
    K3=R3-R2
    IF(K1.NE.ZE)M1=R3/K1
    IF(K2.NE.ZE)M2=R2/K2
    IF(K2.NE.ZE)M3=R1/K2
    IF(K3.NE.ZE)M4=R3/K3
    IF((R1.NE.ZE).AND.(R3.NE.ZE))L1=DLOG(R1)-DLOG(R3)
    IF((R1.NE.ZE).AND.(R2.NE.ZE))   L2=DLOG(R2)-DLOG(R1)
    IF((R2.NE.ZE).AND.(R3.NE.ZE))   L3=DLOG(R3)-DLOG(R2)
    IF(R1.EQ.R2) THEN
      IF(R1.EQ.ZE) THEN
        ZETA2BYRS=ZE
      ELSE IF(R3.EQ.ZE) THEN
        ZETA2BYRS=1.0D0/(4.0D0*R1)
      ELSE
        ZETA2BYRS =(M1**2*L1+0.5D0-M1)/(2.0D0*K1)
      END IF
    ELSE IF(R1.EQ.R3) THEN
      IF(R1.EQ.ZE) THEN
        ZETA2BYRS =1.0/(2.0D0*R2)
      ELSE IF(R2.EQ.ZE) THEN
        ZETA2BYRS =1.0/(2.0D0*R1)
      ELSE
        ZETA2BYRS =(0.5D0-M2*M3*L2+M3)/K2
      END IF
```

```
      ELSE IF(R2.EQ.R3) THEN
         IF(R2.EQ.ZE) THEN
           ZETA2BYRS =ZE
         ELSE IF(R1.EQ.ZE) THEN
           ZETA2BYRS =1.0D0/(4.0D0*R2)
         ELSE
           ZETA2BYRS = (1.5D0-(M2+M3)*L2-M2+M2**2*L2)/(2.0D0*K2)
         END IF
      ELSE IF((R1.EQ.ZE).AND.(R2.NE.R3)) THEN
            ZETA2BYRS =(M4*L3-1.0D0)/(2.0D0*K3)
      ELSE IF((R2.EQ.ZE).AND.(R1.NE.R3)) THEN
            ZETA2BYRS =L1/(2.0D0*K1)
      ELSE IF((R3.EQ.ZE).AND.(R1.NE.R2)) THEN
            ZETA2BYRS =0.5D0*(1.0D0/R2-(M3*L2+R1/R2)/K2)
      ELSE
            ZETA2BYRS=-(0.5D0+0.5D0*K1*(M2**2*L2+M1**2*L1-M2-M1)/K3
     &                          +M4*(M2*L2-M1*L1))/K3
      END IF
      RETURN
      END
C
CCCCCCCCCCCCCCCCCCCCCCCCCCCCCCCCCCCCCCCCCCCCCCCCCCCCCCCCCCCCCCCCCCC
C
      REAL*8  FUNCTION  ZETA1BYRL(R1,R2,R3)
C
      IMPLICIT NONE
C
C  This function computes the line integral (in simplex coordinates)
C  of zeta1/R, along line zeta3=0,
C  where R is the r-coordinate (cylindrical) of an arbitrary
C  point in a triangle with R1,R2,R3 as r-coordinates of the vertices.
C  Calling ZETA1BYRL(R2,R1,R3) will effectively compute the line integral
C of zeta2/R along line zeta3=0, etc.
C
      REAL*8 R1,R2,R3,ZE,K2,L2,M1
      ZE=0.0D0
      K2=R2-R1
      IF (K2.NE.ZE) M1=R1/K2
      IF((R1.NE.ZE).AND.(R2.NE.ZE))    L2=DLOG(R2)-DLOG(R1)
      IF(R1.EQ.R2) THEN
        IF(R1.EQ.ZE) THEN
          ZETA1BYRL=ZE
        ELSE IF(R3.EQ.ZE) THEN
          ZETA1BYRL=  1.0D0/(2.0D0*R1)
        ELSE
          ZETA1BYRL= 1.0D0/(2.0D0*R1)
        END IF
      ELSE IF(R1.EQ.R3) THEN
         IF(R1.EQ.ZE) THEN
           ZETA1BYRL=ZE
        ELSE IF(R2.EQ.ZE) THEN
           ZETA1BYRL=1.0D0/R1
```

```
      ELSE
        ZETA1BYRL= ((1.0D0+M1)*L2-1.0D0)/K2
      END IF
    ELSE IF(R2.EQ.R3) THEN
      IF(R2.EQ.ZE) THEN
        ZETA1BYRL=1.0D0/R1
      ELSE IF(R1.EQ.ZE) THEN
        ZETA1BYRL= ZE
      ELSE
        ZETA1BYRL= ((1.0D0+M1)*L2-1.0D0)/K2
      END IF
    ELSE IF((R1.EQ.ZE).AND.(R2.NE.R3)) THEN
          ZETA1BYRL= ZE
    ELSE IF((R2.EQ.ZE).AND.(R1.NE.R3)) THEN
          ZETA1BYRL= 1.0D0/R1
    ELSE IF((R3.EQ.ZE).AND.(R1.NE.R2)) THEN
          ZETA1BYRL =((1.0D0+M1)*L2-1.0D0)/K2
    ELSE
    ZETA1BYRL = ((1.0D0+M1)*L2-1.0D0)/K2
    END IF
    RETURN
    END
C
CCCCCCCCCCCCCCCCCCCCCCCCCCCCCCCCCCCCCCCCCCCCCCCCCCCCCCCCCCCCCCC
C
    SUBROUTINE MODULO3(I,NEXT)
C
    IMPLICIT NONE
C
C Computes the next value of I where I follows MODULO 3
C
    INTEGER  I,NEXT
    IF(I.LT.3) THEN
      NEXT=I+1
    ELSE
      NEXT=1
    END IF
    RETURN
    END
C
CCCCCCCCCCCCCCCCCCCCCCCCCCCCCCCCCCCCCCCCCCCCCCCCCCCCCCCCCCCCCCC
C
     SUBROUTINE F_ON_BOUNDARY(NN,NOTR,ITR,DERIV,F,NI,TRID,NOID,
    *X,Y,NP)
C
    IMPLICIT NONE
C
C  Assembles contributions to F, (the RHS term of the system of diff. eqns.)
C
    INTEGER NN,NOTR
    INTEGER I,NI(NOTR,3),NL(3),NP(NN)
    INTEGER ITR,NEXT,TRID(NOTR),NOID(NOTR)
```

```
      REAL*8 X(NN),Y(NN)
      REAL*8  F(NN),R
      REAL*8 DERIV,ZETA1BYRL
      IF(TRID(ITR).EQ.2) THEN
        IF(((NOID(NI(ITR,1)).EQ.3).OR.(NOID(NI(ITR,1)).EQ.4)).AND.
     *  ((NOID(NI(ITR,2)).EQ.3)
     *  .OR.(NOID(NI(ITR,2)).EQ.4))) THEN
          I=1
        ELSE IF(((NOID(NI(ITR,2)).EQ.3).OR.(NOID(NI(ITR,2)).EQ.4)).AND.
     *  ((NOID(NI(ITR,3)).EQ.3)
     *  .OR.(NOID(NI(ITR,3)).EQ.4))) THEN
          I=2
        ELSE
          I=3
        END IF
        CALL MODULO3(I,NEXT)
        NL(1)=NI(ITR,I)
        NL(2)=NI(ITR,NEXT)
        CALL MODULO3(NEXT,NEXT)
        NL(3)=NI(ITR,NEXT)
        R=DSQRT((X(NL(1))-X(NL(2)))**2+(Y(NL(1))-Y(NL(2)))**2)
        F(NP(NL(1)))=F(NP(NL(1)))+R*DERIV
     &              *ZETA1BYRL(X(NL(1)),X(NL(2)),X(NL(3)))
        F(NP(NL(2)))=F(NP(NL(2)))+R*DERIV
     &              *ZETA1BYRL(X(NL(2)),X(NL(1)),X(NL(3)))
      END IF
      RETURN
      END
C
CCCCCCCCCCCCCCCCCCCCCCCCCCCCCCCCCCCCCCCCCCCCCCCCCCCCCCCCCCCCCCCCCCCCCCC
C
c     REAL*8 FUNCTION DER(TIME,SIGMA,EPS)
cC
cC Double exponential pulse response
cC
c     IMPLICIT NONE
cC
cC  Computes contributions to the RHS of the subsytem of diff. eqns.
c     REAL*8 TIME,ALPHA,BETA,E_ZERO,T1,T2,A,B
c     REAL*8 SIGMA,EPS,EPSO,PI,B_OVER_A
c     ALPHA=4.0D6
c     BETA=4.76D8
c     B_OVER_A=1.189D0
c     E_ZERO=1.0D0/DLOG(B_OVER_A)
c     PI=DACOS(-1.0D0)
c     EPSO=1.0D-9/(PI*3.6D1)
c     T1=ALPHA*TIME
c     T2=BETA*TIME
c     IF(T1.LT.2.0D2) THEN
c     A=DEXP(-T1)
c     ELSE
c     A=0.0D0
```

```
c     END IF
c     IF(T2.LT.2.0D2) THEN
c     B=DEXP(-T2)
c     ELSE
c     B=0.0D0
c     END IF
c     DER=E_ZERO*(SIGMA*(A-B)
c     &              +EPS*EPSO*(-ALPHA*A+BETA*B))
c     RETURN
c     END
cC
cC**********************************************************************
cC
c     REAL*8 FUNCTION F1(TIME,R)
cC
cC Double exponential pulse response
cC
c     IMPLICIT NONE
cC
cC  Computes contributions to the RHS of the subsytem of diff. eqns.
c     REAL*8 TIME,ALPHA,BETA,H_ZERO,T1,T2,R,A,B
c     REAL*8 ETA,EPS,EPSO,MUO,PI,B_OVER_A
c     ALPHA=4.0D6
c     BETA=4.76D8
c     B_OVER_A=1.189D0
c     PI=DACOS(-1.0D0)
c     EPSO=1.0D-9/(PI*3.6D1)
c     MUO=4.0D-7*PI
c     ETA=DSQRT(MUO/EPSO)
c     H_ZERO=1.0D0/(ETA*R*DLOG(B_OVER_A))
c     T1=ALPHA*TIME
c     T2=BETA*TIME
c     IF(T1.LT.2.0D2) THEN
c     A=DEXP(-T1)
c     ELSE
c     A=0.0D0
c     END IF
c     IF(T2.LT.2.0D2) THEN
c     B=DEXP(-T2)
c     ELSE
c     B=0.0D0
c     END IF
c     F1=H_ZERO*(A-B)
c     RETURN
c     END
cC
cC**********************************************************************
cC
c     REAL*8 FUNCTION F2(TIME,R)
cC
cC Double exponential pulse response
cC
```

```
c    IMPLICIT NONE
cC
cC  Computes contributions to the RHS of the subsytem of diff. eqns.
c    REAL*8 TIME,ALPHA,BETA,H_ZERO,T1,T2,R,A,B
c    REAL*8 ETA,EPS,EPSO,MUO,PI,B_OVER_A
c    ALPHA=4.0D6
c    BETA=4.76D8
c    B_OVER_A=1.189D0
c    PI=DACOS(-1.0D0)
c    EPSO=1.0D-9/(PI*3.6D1)
c    MUO=4.0D-7*PI
c    ETA=DSQRT(MUO/EPSO)
c    H_ZERO=1.0D0/(ETA*R*DLOG(B_OVER_A))
c    T1=ALPHA*TIME
c    T2=BETA*TIME
c    IF(T1.LT.2.0D2) THEN
c    A=DEXP(-T1)
c    ELSE
c    A=0.0D0
c    END IF
c    IF(T2.LT.2.0D2) THEN
c    B=DEXP(-T2)
c    ELSE
c    B=0.0D0
c    END IF
c    F2=H_ZERO*(ALPHA**2*A-BETA**2*B)
c    RETURN
c    END
cC
cCCCCCCCCCCCCCCCCCCCCCCCCCCCCCCCCCCCCCCCCCCCCCCCCCCCCCCCCCCCCCCCCC
cC
c    REAL*8 FUNCTION DER(TIME,SIGMA,EPS)
cC
cC Gaussian pulse response
cC
c    IMPLICIT NONE
cC
cC  Computes contributions to the RHS of the subsytem of diff. eqns.
cC
c    REAL*8 TIME,HEIGHT,TAUA,TAUP,E_ZERO,T,A
c    REAL*8 SIGMA,EPS,EPSO,PI,C,T0,B_OVER_A
c    C=3.0D8
c    HEIGHT=3.75D-1*C/1.14D8
c    TAUA=HEIGHT/C
c    TAUP=1.61D-1*TAUA
c    T0=TIME-4.0D0*TAUP
c    B_OVER_A=2.301D0
c    E_ZERO=1.0D0/DLOG(B_OVER_A)
c    PI=DACOS(-1.0D0)
c    EPSO=1.0D-9/(PI*3.6D1)
c    T=(T0/TAUP)**2
c    IF(T.LT.4.0D2) THEN
```

```
C     A=DEXP(-T/2.0D0)
C     ELSE
C     A=0.0D0
C     END IF
c     DER=E_ZERO*(SIGMA*A
c     &           +EPS*EPSO*(-T/T0*A))
c     RETURN
c     END
cC
cC**********************************************************************
cC
c     REAL*8 FUNCTION F1(TIME,R)
cC
cC  Gaussian pulse response
cC
c     IMPLICIT NONE
cC
cC  Computes the incident (TEM)  H-field at feed nodes, given time and
cC  r-coordinate of the feed node.
cC
c     REAL*8 TIME,HEIGHT,TAUA,TAUP,H_ZERO
c     REAL*8 R,C,T0,B_OVER_A,MUO,EPSO,PI,ETA,T,A
c     C=3.0D8
c     HEIGHT=3.75D-1*C/1.14D8
c     TAUA=HEIGHT/C
c     TAUP=1.61D-1*TAUA
c     T0=TIME-4.0D0*TAUP
c     PI=DACOS(-1.0D0)
c     EPSO=1.0D-9/(PI*3.6D1)
c     MUO=4.0D-7*PI
c     ETA=DSQRT(MUO/EPSO)
c     B_OVER_A=2.301D0
c     H_ZERO=1.0D0/(ETA*R*DLOG(B_OVER_A))
c     T=(T0/TAUP)**2
c     IF(T.LT.4.0D2) THEN
C     A=DEXP(-T/2.0D0)
C     ELSE
C     A=0.0D0
C     END IF
c     F1=H_ZERO*A
c     RETURN
c     END
cC
cC**********  **********************************************************
cC
c     REAL*8 FUNCTION F2(TIME,R)
cC
cC  Gaussian pulse response
cC
c     IMPLICIT NONE
cC
cC Computes the 2nd. derivative of the incident (TEM)  H-field at feed nodes,
```

```
cC given time and r-coordinate of the feed node.
cC
c     REAL*8 TIME,HEIGHT,TAUA,TAUP,H_ZERO,T,A
c     REAL*8 R,C,T0,B_OVER_A,MUO,EPSO,PI,ETA
c     C=3.0D8
c     HEIGHT=3.75D-1*C/1.14D8
c     TAUA=HEIGHT/C
c     TAUP=1.61D-1*TAUA
c     T0=TIME-4.0D0*TAUP
c     PI=DACOS(-1.0D0)
c     EPSO=1.0D-9/(PI*3.6D1)
c     MUO=4.0D-7*PI
c     ETA=DSQRT(MUO/EPSO)
c     B_OVER_A=2.301D0
c     H_ZERO=1.0D0/(ETA*R*DLOG(B_OVER_A))
c     T=(T0/TAUP)**2
c     IF(T.LT.4.0D2) THEN
C      A=DEXP(-T/2.0D0)
C      ELSE
C      A=0.0D0
C      END IF
c     F2=H_ZERO*A*(T-1.0D0)/TAUP**2
c     RETURN
c     END
cC
cCCCCCCCCCCCCCCCCCCCCCCCCCCCCCCCCCCCCCCCCCCCCCCCCCCCCCCCCCCCCCCCCCCCC
cC
c     REAL*8 FUNCTION DER(TIME,SIGMA,EPS)
cC
cC Sinusoidal response
cC
c     IMPLICIT NONE
cC
cC Computes contributions to the RHS of the subsytem of diff. eqns.
cC
c     REAL*8 TIME,E_ZERO,FREQ,OMEGA
c     REAL*8 SIGMA,EPS,EPSO,PI,B_OVER_A
c     FREQ=1.14D8  !1.216835D8
c     PI=DACOS(-1.0D0)
c     OMEGA=2.0D0*PI*FREQ
c     B_OVER_A=1.189D0  !2.301D0
c     E_ZERO=1.0D0/DLOG(B_OVER_A)
c     EPSO=1.0D-9/(PI*3.6D1)
c     DER=E_ZERO*(SIGMA*DSIN(OMEGA*TIME)
c     &           +EPS*EPSO*OMEGA*DCOS(OMEGA*TIME))
c     RETURN
c     END
cC
cC*****************************************************************
cC
c     REAL*8 FUNCTION F1(TIME,R)
cC
```

```
cC  Sinusoidal response
cC
c    IMPLICIT NONE
cC
cC  Computes the incident (TEM)  H-field at feed nodes, given time and
cC  r-coordinate of the feed node.
cC
c    REAL*8 TIME,H_ZERO,FREQ,PI,OMEGA
c    REAL*8 EPSO,MUO,ETA,B_OVER_A,R
c    FREQ=1.14D8
c    PI=DACOS(-1.0D0)
c    OMEGA=2.0D0*PI*FREQ
c    EPSO=1.0D-9/(PI*3.6D1)
c    MUO=4.0D-7*PI
c    ETA=DSQRT(MUO/EPSO)
c    B_OVER_A=1.189D0
c    H_ZERO=1.0D0/(ETA*R*DLOG(B_OVER_A))
c    F1=H_ZERO*DSIN(OMEGA*TIME)
c    RETURN
c    END
cC
cC*****************************************************************
cC
c    REAL*8 FUNCTION F2(TIME,R)
cC
cC  Sinusoidal response
cC
c    IMPLICIT NONE
cC
cC Computes the 2nd. derivative of the incident (TEM) H-field at feed nodes,
cC given time and r-coordinate of the feed node.
cC
c    REAL*8 TIME,H_ZERO,FREQ,PI,OMEGA
c    REAL*8 EPSO,MUO,ETA,B_OVER_A,R
c    FREQ=1.14D8
c    PI=DACOS(-1.0D0)
c    OMEGA=2.0D0*PI*FREQ
c    EPSO=1.0D-9/(PI*3.6D1)
c    MUO=4.0D-7*PI
c    ETA=DSQRT(MUO/EPSO)
c    B_OVER_A=1.189D0
c    H_ZERO=1.0D0/(ETA*R*DLOG(B_OVER_A))
c    F2=-H_ZERO*OMEGA**2*DSIN(OMEGA*TIME)
c    RETURN
c    END
cC
CCCCCCCCCCCCCCCCCCCCCCCCCCCCCCCCCCCCCCCCCCCCCCCCCCCCCCCCCCCCCCCCCCCCCCC
C
     REAL*8 FUNCTION DER(TIME,SIGMA,EPS)
C
C  Unit step response
C
```

```
      IMPLICIT NONE
C
C  Computes contributions to the RHS of the subsytem of diff. eqns.
C
      REAL*8 TIME,E_ZERO,EPS
      REAL*8 SIGMA,B_OVER_A
      B_OVER_A=1.189D0  !2.301D0
      E_ZERO=1.0D0/DLOG(B_OVER_A)
      DER=E_ZERO*SIGMA
      RETURN
      END
C
C*****************************************************************
C
      REAL*8 FUNCTION F1(TIME,R)
C
C  Unit step response
C
      IMPLICIT NONE
C
C  Computes the incident (TEM)  H-field at feed nodes, given time and
C  r-coordinate of the feed node.
C
      REAL*8 TIME,H_ZERO,PI
      REAL*8 EPSO,MUO,ETA,B_OVER_A,R
      PI=DACOS(-1.0D0)
      EPSO=1.0D-9/(PI*3.6D1)
      MUO=4.0D-7*PI
      ETA=DSQRT(MUO/EPSO)
      B_OVER_A=1.189D0
      H_ZERO=1.0D0/(ETA*R*DLOG(B_OVER_A))
      F1=H_ZERO
      RETURN
      END
C
C*****************************************************************
C
      REAL*8 FUNCTION F2(TIME,R)
C
C  Unit step response
C
      IMPLICIT NONE
C
C Computes the 2nd. derivative of the incident (TEM) H-field at feed nodes,
C given time and r-coordinate of the feed node.
C
      REAL*8 TIME,R
      F2=0.0D0
      RETURN
      END
C
CCCCCCCCCCCCCCCCCCCCCCCCCCCCCCCCCCCCCCCCCCCCCCCCCCCCCCCCCCCCC
```

```
      SUBROUTINE DSDIF (NOTR,NN,N,THETA,PRMT,S,T,R,F,
     $  Y,DY,INDEX,EPS,SIGMA,MU,WORKR,WORKI,
     $  TRALPHA,NI,TRID,NOID,P,Q,NP,DONE)
C
C     This subroutine performs a single step algorithm to solve
C     systems of 2nd. order differential equations. The algorithm is
C     described in a paper 'A unified set of single step algorithms,
C     Part 1:General formulation and applications.' by O.C. Zienkiewicz,
C     W.L. Wood, and W. Hine, Int. J. Numer. Methods Eng.,vol.20,
C      pp. 1529-1552, 1984.
C
C     This subroutine will solve the system of differential equations
C     created with the program RADTIDS, however it can be easily
C     adapted to solve in general any system of 2nd order differential
C     equations. All the variables required by RADTIDS are marked with
C      'for RADTIDS'. They are only used for updating the right hand
C      side vector which is time-dependent.
C     For this subroutine to work properly, parameter ORDER needs to
C     be specified. The value of this parameter is the same as the
C     dimension of the right hand side vector, F. Specifying ORDER in the
C     this subroutine reduces the number of variables in the subroutine
C     header. Usually, the value of order is the same as the number of
C     nodes.
C
C
      IMPLICIT NONE
C
      PARAMETER ORDER=379 ! same as number of unknowns (nodes)
      INTEGER  N,NN
      INTEGER  NOTR                                    ! for RADTIDS
      REAL*8   S(NN,NN)
      REAL*8   T(NN,NN)
      REAL*8   R(NN,NN)
      REAL*8   F(NN)
      REAL*8   P(NN)                                   ! for RADTIDS
      REAL*8   Q(NN)                                   ! for RADTIDS
      REAL*8   F_OLD(ORDER)
      REAL*8   F_BAR(ORDER)
      REAL*8   Y(NN)
      REAL*8   DY(NN)
      REAL*8   THETA(2)
      REAL*8   PRMT(7)  ! PRMT(1)=starting time
               ! PRMT(2)=stopping time
               ! PRMT(3)=interval time
               ! PRMT(4)=minimum interval time
               ! PRMT(5)=maximum interval time
               ! PRMT(6)=relative percentage of ERMAX
               !       = 0 if no adjustment of T_DELTA required
               ! PRMT(7)=relative lower bound of ERROR
      REAL*8   MAT(ORDER,ORDER)
      REAL*8   TY(ORDER)
      REAL*8   TDY(ORDER)
```

```
      REAL*8  T1(ORDER)
      REAL*8  ALPHA(ORDER)
      REAL*8  TALPHA(ORDER)
      REAL*8  TRALPHA(NN)
      REAL*8  TRALPHA1(ORDER)
      REAL*8  ERMAX,ERROR
      REAL*8  TIME
      REAL*8  T_DEL_OLD,T_DEL_OLD1
      REAL*8  T_INIT,T_FINAL,T_DELTA,T_MIN,T_MAX
      REAL*8  GAMMA,RELERR
      REAL*8  WORKR(NN)
      REAL*8  NORMA,DIFFY,RCOND
      REAL*8  DER,DERIV,F1,F2,LIM1,LIM2     ! for RADTIDS
      REAL*8  SIGMA(NOTR)                    ! for RADTIDS
      REAL*8  EPS(NOTR)                      ! for RADTIDS
      REAL*8  MU(NOTR)                       ! for RADTIDS
      REAL*8  EPSO                           ! for RADTIDS
      REAL*8  MUO                            ! for RADTIDS
      REAL*8  PI                             ! for RADTIDS
C
      INTEGER FINAL,INDEX
      INTEGER NOID(NOTR)                     ! for RADTIDS
      INTEGER TRID(NOTR)                     ! for RADTIDS
      INTEGER NP(NN)                         ! for RADTIDS
      INTEGER I,J,K
      INTEGER NI(NOTR,3)                     ! for RADTIDS
      INTEGER WORKI(NN)
      INTEGER SUCCESS
      INTEGER COUNT1,COUNT2
      INTEGER DONE                           ! for RADTIDS
C
C*******************************************************************************
C
C
      T_INIT=PRMT(1)
      T_FINAL=PRMT(2)
      T_DELTA=PRMT(3)
      T_MIN=PRMT(4)
      T_MAX=PRMT(5)
      RELERR=PRMT(6)
      GAMMA=PRMT(7)
      LIM1=0.0D0          ! lower limit of the special time interval
      LIM2=1.0D-10        ! upper limit of the special time interval
      PI=DACOS(-1.0D0)
      EPSO=1.0D-9/(PI*3.6D1)
      MUO=4.0D-7*PI
C
        DO I=1,NN
         F_OLD(I)=F(I)    ! First save the previous F
        ENDDO
C
C     Perform the following on first entry to the subroutine.
```

```
C
      IF (INDEX.EQ.1) THEN ! first entry
       DIFFY=1.0D0
       DO I=1,N
        IF (DABS (Y(I)).GT.DIFFY) DIFFY=DABS (Y(I))
       ENDDO
       ERMAX=RELERR*DIFFY
      END IF
C
      DIFFY=0.0D0
      TIME=T_INIT
      COUNT1=0
      COUNT2=0
      FINAL=0
C
C     Loop for the TIME increment
C
      DO WHILE (TIME.LE.T_FINAL.AND.FINAL.NE.2)
C
C     Compute the final point Y(T_FINAL) exactly.
C
      IF (TIME+2.0D0*T_DELTA.GT.T_FINAL) THEN
       IF (FINAL.EQ.0) THEN
        T_DEL_OLD=T_DELTA
        T_DELTA=(T_FINAL-TIME)/2.0D0
        FINAL=1
       ELSE
        T_DELTA=T_FINAL-TIME
        ENDIF
      ENDIF
C
      T_DEL_OLD1=T_DELTA
      TIME=TIME+T_DELTA
       IF (TIME.GT.LIM1.AND.TIME.LT.LIM2) THEN ! special step(s) finished
         DONE=1
       ELSE
         DONE=0
       END IF
C
CCCCCCCCCCCCCCCCCCCCCCCCCCCCCCCCCCCCCCCCCCCCCCCCCCCCCCCCCCCCCCCCCCCCCC
C       Compute,F_BAR
C
C  Compute current value of F using the main subroutines
C  This is the only part which is not mainly resident in this routine
C   and may change according to the nature of problem. This part
C   simply compute the average of the current and the preceding
C   right hand side vector.
C
        DO I=1,NN
         F(I)=0.0D0 !Re-initialize F(I)
        ENDDO
          DO I=1,NOTR
```

```
            DERIV=DER(TIME,SIGMA(I),EPS(I))
          CALL F_ON_BOUNDARY(NN,NOTR,I,DERIV,F,NI,TRID,NOID,P,Q,NP)
          ENDDO
           DO I=1,NN
      IF(NOID(I).EQ.3.OR.NOID(I).EQ.4) THEN
           DO J=1,NN
      F(NP(J))=F(NP(J))-S(NP(J),NP(I))*F1(TIME,P(I))
      &                -R(NP(J),NP(I))*F2(TIME,P(I))
          ENDDO
      END IF
          ENDDO
C
           CALL FCT(ORDER,F_OLD,F,THETA,F_BAR)
C
CCCCCCCCCCCCCCCCCCCCCCCCCCCCCCCCCCCCCCCCCCCCCCCCCCCCCCCCCCCCCCCCCCC
C
       SUCCESS=0
       DO WHILE (SUCCESS.EQ.0)
C
C      Compute TRALPHA.
C
          DO I=1,N
           TY(I)=Y(I)+DY(I)*T_DELTA*THETA(1)
           TDY(I)=DY(I)
          ENDDO
C
          DO I=1,N
            DO J=1,N
            MAT(J,I)=R(J,I)
            ENDDO
          ENDDO
          DO I=1,N
            DO J=1,N
            MAT(J,I)=MAT(J,I)+T_DELTA*THETA(1)*T(J,I)
             ENDDO
          ENDDO
          DO I=1,N
            DO J=1,N
            MAT(J,I)=MAT(J,I)+T_DELTA**2/2.0D0*THETA(2)*S(J,I)
             ENDDO
          ENDDO
C
          DO I=1,N
           TRALPHA1(I)=0.0D0
             DO J=1,N
               TRALPHA1(I)=TRALPHA1(I)+T(I,J)*TDY(J)
              ENDDO
           ENDDO
          DO I=1,N
           T1(I)=0.0D0
             DO J=1,N
               T1(I)=T1(I)+S(I,J)*TY(J)
```

```
        ENDDO
      ENDDO
      DO I=1,N
        TRALPHA(I)=F_BAR(I)-TRALPHA1(I)-T1(I)
      ENDDO
C
C     Computing next TRALPHA=inverse[MAT][TRALPHA]
C
      CALL  DGECO (MAT,NN,N,WORKI,RCOND,WORKR)
      WRITE(*,*) ' TIME',TIME,' RCOND',RCOND
      IF (RCOND.LT.1.0D-10) THEN
        INDEX=10
        WRITE(*,*) 'MATRIX IS VERY ILL-CONDITIONED'
        GO TO 999
      END IF
C
      CALL  DGESL (MAT,NN,N,WORKI,TRALPHA,0)
C
      IF (INDEX.EQ.1) THEN
       INDEX=0
       NORMA=1.0
      ELSE
      NORMA=0.0D0
       DO I=1,N
        IF ( DABS (TRALPHA(I)-ALPHA(I)).GT.NORMA)
     $     NORMA= DABS (TRALPHA(I)-ALPHA(I))
       ENDDO
      END IF
       ERROR=T_DELTA**2/6.0D0*NORMA
C
C     Decide if delta_T must be modified.
C
      IF (ERROR.GT.ERMAX.AND.RELERR.GT.0.0D0.AND.FINAL.EQ.0) THEN
       IF (COUNT2.EQ.0.AND.T_DELTA/2.0D0.GT.T_MIN) THEN
        T_DELTA=T_DELTA/2.0D0
          SUCCESS=5
       ELSE IF (COUNT2.NE.0.AND.T_DELTA/2.0D0.GT.T_MIN) THEN
        SUCCESS=4   !Endless halfing and doubling of T_DELTA
       ELSE
       SUCCESS=2
       ENDIF     ! T_DELTA/2
        ELSE IF (ERROR.LT.ERMAX*GAMMA.AND.RELERR.GT.0.0D0
     $          .AND.FINAL.EQ.0) THEN
        IF (COUNT1.EQ.0.AND.T_DELTA*2.0D0.LT.T_MAX) THEN
         T_DELTA=T_DELTA*2.0D0
           SUCCESS=6
         ELSE IF (COUNT1.NE.0.AND.T_DELTA*2.0D0.LT.T_MAX) THEN
        SUCCESS=4   !Endless halfing and doubling of T_DELTA
       ELSE
          SUCCESS=3
         ENDIF     ! T_DELTA*2
       ELSE        ! no modifications required. Compute new Y.
```

```
      SUCCESS=1
      ENDIF     ! RELERR
C
      ENDDO       ! SUCCESS
       IF (SUCCESS.EQ.5) THEN
        COUNT1=COUNT1+1
        TIME=TIME-T_DEL_OLD1
         GO TO 990
         ELSE IF (SUCCESS.EQ.6) THEN
        TIME=TIME-T_DEL_OLD1
         COUNT2=COUNT2+1
         GO TO 990
         ELSE
    COUNT1=0
    COUNT2=0
       END IF
C    Compute Y(n+1), DY(n+1)
C
      DO I=1,N
       ALPHA(I)=TRALPHA(I)
       Y(I)=Y(I)+T_DELTA*DY(I)+ALPHA(I)*T_DELTA**2/2.0D0
        IF ( DABS (Y(I)).GT.DIFFY) DIFFY= DABS (Y(I))
       DY(I)=DY(I)+ALPHA(I)*T_DELTA
       ENDDO
        ERMAX=RELERR*DIFFY
             DO I=1,NN
               F_OLD(I)=F(I)    ! First save the previous F
             ENDDO
990        IF(TIME.GE.T_FINAL) FINAL=2
         ENDDO  ! TIME
C
     PRMT(1)=TIME
     PRMT(3)=T_DEL_OLD
C
999     RETURN
     END
C
CCCCCCCCCCCCCCCCCCCCCCCCCCCCCCCCCCCCCCCCCCCCCCCCCCCCCCCCCCC
C
            SUBROUTINE FCT(N,F_OLD,F_NEW,THETA,F_BAR)
C
C Works with the differential equation solver. Computes the average
C value of the RHS of the system of differential equation given the
C previous and the current values
C
            IMPLICIT NONE
            INTEGER I,N
            REAL*8 F_NEW(N),F_OLD(N),F_BAR(N)
            REAL*8 THETA(2)
C
            DO I=1,N
             F_BAR(I)= THETA(1)*F_OLD(I)+(1.0D0-THETA(1))*F_NEW(I)
```

```
      ENDDO
      RETURN
      END
C
CCCCCCCCCCCCCCCCCCCCCCCCCCCCCCCCCCCCCCCCCCCCCCC
```

```
CCCCCCCCCCCCCCCCCCCCCCCCCCCCCCCCCCCCCCCCCCCCCCCCCCCC
C
      SUBROUTINE FOUR1(DATA,NN,ISIGN)
C  Replaces DATA by its discrete Fourier transform, if ISIGN is input
C  as 1; or replaces DATA by NN times its inverse discrete Fourier
C  transform, if ISIGN is input as -1. DATA is a complex array of
C  length NN or, equivalently, a real array of length 2*NN. NN must
C  be an integer power of 2. (this is not checked for).
C  (Taken from 'Numerical Recipes, The Art of Scientific Computing',
C   FORTRAN Version, pp. 394-395,by W. H. Press et. al.)
C
      REAL*8 WR,WI,WPR,WPI,WTEMP,THETA
      REAL*8 TEMPR,TEMPI
      REAL*8 DATA(2*NN)
      N= 2*NN
      J=1
      DO 11 I=1,N,2   !bit reversal
        IF (J.GT.I) THEN
          TEMPR=DATA(J)   !exchange the two complex numbers
          TEMPI=DATA(J+1)
          DATA(J)=DATA(I)
          DATA(J+1)=DATA(I+1)
          DATA(I)=TEMPR
          DATA(I+1)=TEMPI
        END IF
        M=N/2
1       IF ((M.GE.2).AND.(J.GT.M)) THEN
          J=J-M
          M=M/2
        GO TO 1
        END IF
        J=J+M
11    CONTINUE
      MMAX=2
2     IF (N.GT.MMAX) THEN
        ISTEP=2*MMAX
        THETA=6.28318530717959D0/(ISIGN*MMAX)
        WPR=-2.D0*DSIN(0.5D0*THETA)**2
        WPI=DSIN(THETA)
        WR=1.D0
        WI=0.D0
        DO 13 M=1,MMAX,2
          DO 12 I=M,N,ISTEP
            J=I+MMAX
            TEMPR=WR*DATA(J)-WI*DATA(J+1)
            TEMPI=WR*DATA(J+1)+WI*DATA(J)
            DATA(J)=DATA(I)-TEMPR
            DATA(J+1)=DATA(I+1)-TEMPI
            DATA(I)=DATA(I)+TEMPR
            DATA(I+1)=DATA(I+1)+TEMPI
12        CONTINUE
          WTEMP=WR
```

```
            WR=WR*WPR-WI*WPI+WR
            WI=WI*WPR+WTEMP*WPI+WI
13        CONTINUE
          MMAX=ISTEP
        GO TO 2
        END IF
        RETURN
        END
```

Bibliography

[1] R. R. Goulette, R. J. Crawhall, and S. K. Xavier, "The determination of radiated emissions limits for integrated circuits within telecommunications equipment," *IEICE Trans. Commun.*, vol. E 75-B, no. 3, March 1992.

[2] C. F. Lee, K. Li, S. Y. Poh, R. T. Shin, and J. A. Kong, "Electromagnetic radiation from a VLSI package heatsink configuration," *IEEE 1991 International Symposium on EMC,* Cherry Hill, New Jersey, 1991.

[3] S. A. Schelkunoff, *Advanced Antenna Theory.* New York: John Wiley and Sons Inc., 1952, pp. 102-109.

[4] H. J. Schmitt, "Transients in cylindrical antennae," *Proc. IEE,* 107 c, pp. 292-298, April 1960.

[5] _____,"Experimental observation of the transient response of linear antennas and loops," *IEEE Trans. Antennas Propagat.,* vol. AP-11, pp. 509-510, July 1963.

[6] H. J. Schmitt, C. W. Harisson, and C. S. Williams, "Calculated and experimental response of thin cylindrical antennas to pulse excitation," *IEEE Trans. Antennas Propagat.*, vol. AP-14, pp. 120-127, March 1966.

[7] R. W. P. King and H. J. Schmitt, "The transient response of linear antennas and loops," *IRE Trans. Antennas Propagat.*, vol. AP-10, pp. 222-228, May 1962.

[8] C. W. Harrison and C. S. Williams, "Transients in wide-angle conical antennas," *IEEE Trans. Antennas Propagat.*, vol. AP-13, pp. 236-246, March 1965.

[9] C. W. Harrison and R. W. P. King, "On the transient response of an infinite cylindrical antenna," *IEEE Trans. Antennas Propagat.*, vol. AP-15, pp. 301-302, March 1967.

[10] A. M. Abo-Zena and R. E. Beam, "Electromagnetic fields at points near pulse-excited linear antenna," *IEEE Trans. Antennas Propagat.*, vol. AP-19, pp. 129-131, Jan. 1971.

[11] R. J. Palciauskas and R. E. Beam, "Transient fields of thin cylindrical antennas," *IEEE Trans. Antennas Propagat.*, vol. AP-18, pp. 276-278, 1970.

[12] Y. -P. Liu and D. L. Sengupta, "Transient radiation from a linear antenna with nonreflecting resistive loading," *IEEE Trans. Antennas Propagat.*, vol. AP-22, pp. 212-220, March 1974.

[13] A. M. Auckenthaler and C. L. Bennet, "Computer solution of transient time domain thin-wire antenna problems," *IEEE Trans. Microwave Theory Tech.*, vol. MTT-19, pp. 892-893, Nov. 1971.

[14] A. J. Poggio and E. K. Miller, in *Computer Techniques for Electromagnetics,* R. Mittra, Ed. Oxford, New York: Pergamon, 1973, ch. 4, pp. 159-261.

[15] E. P. Sayre and R. Harrington, "Transient response of straight wire scatterrers and antennas, *Proc. 1968, International Ant. Prop. Symposium,* Boston, Massachuset, p. 160.

[16] F. M. Tesche, "On the analysis of scattering and antenna problems using the singularity expansion technique," *IEEE Trans. Antennas Propagat.*, vol. AP-21, p. 53, 1973.

[17] K. S. Yee, "Numerical solution of initial boundary value problems involving Maxwell's equations in isotropic media," *IEEE Trans. Antennas Propagat.*, vol. AP-14, pp. 302-307, May 1966.

[18] J. G. Maloney, G. S. Smith, and W. R. Scott, "Accurate computation of the radiation from simple antennas using the finite-difference time-domain method," *IEEE Trans. Propagat.*, vol. 38, pp. 1059-1068, July 1990.

[19] P. A. tirkas and C. A. Balanis, "Finite-difference time-domain method for antenna radiation," *IEEE Trans. Antennas Propagat.*, vol. AP-40, pp. 334-340.

[20] O. C. Zienkiewicz and R. L. Taylor, *The Finite Element Method*, 4th. ed., vol. 2, London: McGraw-Hill, 1988.

[21] P. P. Sylvester and R. L. Ferrari, *Finite Elements for Electrical Engineers,* 2nd. ed.,Cambridge: Cambridge Univ. Press, 1990.

[22] E. Sumbar, F. E. Vermeulen, and F. S. Chute, "Implementation of radiation boundary conditions in the finite element analysis of electromagnetic wave propagation", *IEEE Trans. Microwave Theory Tech.*, vol. 39, pp. 267-273, 1991.

[23] D. C. Chang, "On the electrically thick monopole, part 1: Theoretical solution," *IEEE Trans. Antennas Propagat.*, vol. AP-16, pp. 58-64, 1968.

[24] E. C. Jordan and K. G. Balman, *Electromagnetic Waves and Radiating Systems*, New Jersey: Prentice Hall, 1968.

[25] D. E. Merewether, "Transient currents induced on a metallic body of revolution by an electromagnetic pulse," *IEEE Trans. Electromagn. Compat.*, vol. EMC-13, pp. 41-44, May 1971.

[26] F. M. Tesche, "On the inclusion of loss in time-domain solutions of electromagnetic interaction problems," *IEEE Trans. Electromagn. Compat.*, vol. EMC-32, Feb. 1990.

[27] O. C. Zienkiewicz, W. L. Wood, N. W. Hine, and R. L. Taylor, "A unified set of single step algorithms, part 1: General formulation and applications," *Int. J. Numer. Methods Eng.*, vol. 20, pp. 1529-1552, 1984.

[28] A. C. Cangellaris, C. -C. Lin, and K. K. Mei, "Point-matched time-domain finite element methods for electromagnetic radiation and scattering," *IEEE Trans. Antennas Propagat.*, vol. AP-35, pp. 1160-1173, Oct. 1987.

[29] D. A. Vechinski and S. M. Rao, "A stable procedure to calculate the transient scattering by conducting surfaces of arbitrary shapes," *IEEE Trans. Antennas Propagat.*, vol. AP-40, June 1992.

[30] R. W. P. King, *Tables of Antenna Characteristics.* New York: IFI/Plenum, 1971.